Test and optimization of variance reduction methods in shielding problems with multiplicative media

Matteo Falabino

Advisor: Prof. S. Dulla

Co-advisors: A. Zoia, PhD (CEA Saclay)
D. Sciannandrone, PhD (CEA Saclay)
O. Petit (CEA Saclay)

Dipartimento ENERGIA
Politecnico di Torino

This dissertation is submitted for the
Master Degree in Energetic and Nuclear Engineering

19 July 2019

I would like to dedicate this thesis to all my loved ones, relatives and friends, who have assisted me throughout my studies.

Table of contents

List of figures

List of tables

Chapter 1

Introduction

Nuclear reactor physics is the branch of physics which deals with the study of neutron population in the reactor core. Problems of neutronics, as they are usually called, are commonly solved by two main families of methods: the deterministic ones, that solve the transport equation by adopting approximations and by discretizing the phase space, and Monte Carlo methods. The Monte Carlo approach is based on the stochastic sampling of neutron histories: particle streaming and interactions with matter are sampled according to probability distribution functions derived from physical laws. By recording selected events during the particle flights, it is possible to estimate the magnitude of a given quantity of interest related to particle population. The advantage of this method is the capability of obtaining estimates without introducing any approximation. However, results are characterized by a statistical uncertainty that can be reduced by increasing the number of samples at the expenses of the computational time.

Transport codes based on Monte Carlo methods are mainly applied to core calculation and problems of shielding from radiation and particles. In this second category of problems, the efficiency of the estimate is strongly affected by the small probability of occurrence of the phenomena to be estimated. The lower is the probability of a given event, the higher is the number of histories that have to be simulated in order to achieve acceptable statistical uncertainties. When a problem is too rare to be sampled in a reasonable computational time by a standard Monte Carlo code, the so-called variance reduction methods are generally used in order to accelerate the convergence. These methods modify the probability distribution laws in order to increase the sampling of rare events while preserving the expected values of the estimates. Nowadays, these methods have been widely tested on problems of propagation of neutrons in absence of fissile material.

At the start-up of reactor cores, it is essential to know the counting rate of the detectors located inside and outside the core: the simulation of such scenario by Monte Carlo methods constitutes a real scientific challenge. The number of particles arriving in areas very far from the reactor core is extremely small. Variance reduction techniques are therefore essential.

At present at CEA-Saclay, Monte Carlo calculations having an imposed source and fissile material (generally called "fixed-source criticality problems") are solved using a "Two-step" approach. This method consists in separating the neutron propagation calculation and the calculation of the fission source in two different steps. Thanks to the recent developments, TRIPOLI-4® [1], the reference Monte Carlo code developed at CEA/Saclay, has been endowed with a new variance reduction method: the Adaptive Multi-level Splitting (AMS). Furthermore, the code can be given an external importance function produced with the APOLLO-3® [2] deterministic code (also developed at CEA).

The AMS is a variance reduction method based on the possibility of favouring particle histories approaching the detector, duplicating them during their transport, and penalizing those moving away from it, by eliminating them from the simulation. The coupling with APOLLO-3 is based on the possibility of reading and storing a deterministic adjoint neutron flux: the adjoint flux, being proportional to the importance of the neutrons with respect to the detector, can be used by TRIPOLI-4 to guide the trajectories of the neutrons towards the detector. In principle, the deterministic importance functions can be applied to all variance reduction methods requiring this information. Among them, the exponential transform (with importance sampling), already present in TRIPOLI-4, appears to be the most convenient method for deterministic importance functions.

Both AMS and exponential transform with external importance functions lend themselves in principle to the analysis of systems including fissile media. The aim of this study is to explore core start-up calculations with TRIPOLI-4 Monte Carlo code, by applying the abovementioned variance reduction methods. These techniques will be applied to simplified models. The results thus obtained will be compared to reference calculations in order to assess the quality of the estimates and to quantify the performances. Test results will be extensively discussed putting in evidence the benefits and the characteristics of each method.

Part I

Background

Chapter 2

Neutron transport physics

One of the key issues of nuclear reactor physics is the study of the neutron population inside the reactor core. The physics of such problems is described by the Boltzmann transport equation. Since, due to the enormous number of variables involved, it is impossible to describe the motion of each particle individually, the use of macroscopic parameters is necessary. According to the Boltzmann transport theory, the neutron population can be described making use of a statistical distribution, e.g. the expected number of particles per unit volume present in a given point of the domain, mainly known as neutron density.

One of the most common way to approach this type of problems is the use of the Monte Carlo method. By reproducing the life of a given number of individual particles, it is possible to approximate the behaviour of the whole neutron population with a given accuracy. Another approach consists in the use of deterministic methods. They solve the neutron transport equation by means of numerical integrations and by adopting domain discretizations. The results thus produced are subject to approximations, nevertheless they can be obtained in relatively short calculation times. In this chapter we will present the fundamental concepts of the neutron transport theory and we will summarize the basis of these approaches.

2.1 Neutron transport equation

The neutron transport equation describes the behaviour of neutrons travelling through matter. It has been developed under some fundamental assumptions: particles are treated as point-like, so neglecting their dimensions and the particle population is considered rarefied. Under these hypotheses, collisions between particles of the same species can be neglected. Therefore the behaviour of the neutron population is only given by the interactions between neutrons and the nuclei of the atoms of crossed medium. The present description is limited to the stationary case since the assessment of time-dependency goes beyond the objectives the thesis.

2.1.1 Notations

In the first place, we define the fundamental notations that we will use throughout the document. In transport theory, the neutron population is represented in a 6-dimensional domain called phase-space. Each point in the domain is described by a set of coordinates $(\vec{r},\vec{\Omega},E)$ where:

- $\vec{r}$ is the spatial variable: it is described making use of a set of spatial coordinates, e.g. the Cartesian coordinates x,y,z;
- $\vec{\Omega}$ is the angular coordinate: it represents direction of the motion of the particles. It is identified making use of a unit vector described by two coordinates, e.g. μ,φ;
- E is the energy variable: for particles having mass it is related to the module of the particles speed.

The key concept for neutral particle interactions with matter is the *macroscopic cross section* $\Sigma(\vec{r},\vec{\Omega},E)$ [3–5]. It defines the probability to interact per unit length travelled by a particle having energy E, direction $\vec{\Omega}$ at point $\vec{r}$. In general, except for some particular cases, the medium is assumed to be isotropic, so the cross section dependency on the particle flight direction is not accounted. The macroscopic cross section carries the units of the inverse of a length. In general, the macroscopic cross section of a medium made of N_i different isotopic species can be written as the sum

$$\Sigma(\vec{r},E)=\sum_{i=1}^{N_i}\rho_i(\vec{r})\sigma_i(E) \tag{2.1}$$

where $\rho_i(\vec{r})$ and $\sigma_i(E)$ are respectively the density and the microscopic cross section of isotope i. Conventionally, densities are expressed in term of number of atoms per cm^3, while the microscopic cross sections are measured in *barn* ($1barn=1\cdot10^{-24}cm^2$). Let us now define the cross sections that will be used throughout the thesis:

- $\Sigma_c(\vec{r},E)$, macroscopic capture cross section: probability per unit path of being captured at $(\vec{r},E)$;
- $\Sigma_f(\vec{r},E)$, macroscopic fission cross section: probability per unit path to yield a fission reaction at $(\vec{r},E)$;
- $\Sigma_a(\vec{r},E)$, macroscopic absorption cross section. It expresses the probability per unit path, for a particle with energy E, to be absorbed at point $\vec{r}$. It is defined as

$$\Sigma_a(\vec{r},E)=\Sigma_f(\vec{r},E)+\Sigma_c(\vec{r},E); \tag{2.2}$$

- $\Sigma_s(\vec{r},\vec{\Omega}\rightarrow\vec{\Omega}',E\rightarrow E')d\vec{\Omega}dE$, macroscopic transfer cross section: probability per unit path to undergo a collision in $(\vec{r},\vec{\Omega},E)$ and being re-emitted with energy within the interval $(E',E'+$

dE') and angle $(\vec{\Omega}', \vec{\Omega}' + d\vec{\Omega}')$. It can be also rewritten as the product:

$$\Sigma_s(\vec{r}, \vec{\Omega} \to \vec{\Omega}', E \to E') = \Sigma_s(\vec{r}, E) \cdot f_s(\vec{r}, \vec{\Omega} \to \vec{\Omega}', E \to E'), \tag{2.3}$$

where Σ_s is the scattering cross section, namely the probability per unit path of undergoing a scattering reaction, and f_s the probability density function that rules the neutron re-emission;

- $\Sigma_t(\vec{r}, E)$, macroscopic total cross section: probability per unit path to collide in $(\vec{r}, E)$. It is the sum of the cross sections of all possible interactions:

$$\Sigma_t(\vec{r}, E) = \Sigma_s(\vec{r}, E) + \Sigma_a(\vec{r}, E) = \Sigma_s(\vec{r}, E) + \Sigma_c(\vec{r}, E) + \Sigma_f(\vec{r}, E). \tag{2.4}$$

Moreover we define:

- the multiplicity ν_f: it is average number of particles re-emitted per fission reaction;
- the $\chi(E)dE$ fission emission spectra. It expresses the probability for a neutron produced by a fission reaction to be emitted with energy within the interval $(E, E + dE)$.

Nuclear data such as cross sections and multiplicities are responsible for the behaviour of the particle population. They depend on the isotopic composition of the medium, its temperature and the energy of the incident particles. The effect of the particle population on the nuclear properties of the medium is typically neglected, i.e. nuclear data are considered independent of the particle density. The accuracy of nuclear data libraries is a key point for achieving proper simulation results. Their quality is fundamental and research is still ongoing. All the results that will be presented in this thesis have been obtained using the CEA-V5.12 library based on the European Joint Evaluated Fission and Fusion data (JEFF 3.1.1) [6].

2.1.2 Integro-differential formulation

The mathematical framework of neutral particle transport is described by the linear Boltzmann equation, mainly known as transport equation [4].

$$\begin{aligned}\vec{\Omega} \cdot \vec{\nabla} \phi(\vec{r}, \vec{\Omega}, E) + \Sigma_t(\vec{r}, E) \phi(\vec{r}, \vec{\Omega}, E) = \\ \iint \Sigma_s(\vec{r}, \vec{\Omega}' \to \vec{\Omega}, E' \to E)\ \phi(\vec{r}, \vec{\Omega}', E') d\vec{\Omega}' dE' + \\ \iint \nu \Sigma_f(\vec{r}, E') \frac{\chi(\vec{r}, E)}{4\pi}\ \phi(\vec{r}, \vec{\Omega}', E') d\vec{\Omega}' dE' + Q(\vec{r}, \vec{\Omega}, E)\end{aligned} \tag{2.5}$$

is the steady-state integro-differential formulation of the transport equation. It expresses a balance of the neutron flux ϕ $\left[\frac{\text{neutrons}}{cm^2\ s}\right]$ in the phase-space element $d\vec{r}d\vec{\Omega}dE$ around the point $(\vec{r}, \vec{\Omega}, E)$. The left

hand side of the equation is the "loss" term, while the right hand side represent the "productions". In particular:

- $\phi(\vec{r},\vec{\Omega},E)$ is the neutron flux. It is defined as the product

$$\phi(\vec{r},\vec{\Omega},E) = v(E)N(\vec{r},\vec{\Omega},E), \tag{2.6}$$

  where N is the neutron density, expressed as $\left[\frac{nutrons}{cm^3}\right]$, and v is the neutron speed $\left[\frac{cm}{s}\right]$;

- $\vec{\Omega}\cdot\vec{\nabla}\phi(\vec{r},\vec{\Omega},E)$ is the streaming term. It is defined as the difference between the neutron leaving the domain $d\vec{r}$ and the incoming ones for direction $\vec{\Omega}$;

- $\Sigma_t(\vec{r},E)\phi(\vec{r},\vec{\Omega},E)$ is the collision term. It represents all the particles that, colliding in $(\vec{r},\vec{\Omega},E)$, are absorbed or scattered in another region of the phase-space;

- $\iint \Sigma_s(\vec{r},\vec{\Omega}'\to\vec{\Omega},E'\to E)\phi(\vec{r},\vec{\Omega}',E')d\vec{\Omega}'dE'$ is the transfer term (also known as streaming term). It is the contribution of all the neutrons colliding in $d\vec{r}$ with a different energy E' and direction $\vec{\Omega}'$, that are scattered within $(\vec{r},\vec{\Omega},E)$;

- $\iint \nu\Sigma_f(\vec{r},E')\frac{\chi(\vec{r},E)}{4\pi}\,\phi(\vec{r},\vec{\Omega}',E')d\vec{\Omega}'dE'$ is the fission term. It is non-zero only in fissile material. It accounts for all the neutrons emitted by fission reactions within $(\vec{r},\vec{\Omega},E)$;

- $Q(\vec{r},\vec{\Omega},E)$ is the neutron external source term.

Boundary conditions

A neutron transport physics problem is fully described by the transport equation when accompanied by an appropriate set of boundary conditions (BC's). These are generally expressed by the relation:

$$\phi(\vec{r}_s,\vec{\Omega}_{in},E) = \phi_{in} \qquad \vec{r}_s \in \partial\mathscr{D},\ \vec{\Omega}_{in}\cdot\vec{n} \le 0, \tag{2.7}$$

where $\partial\mathscr{D}$ is the domain boundary, $\vec{n}$ its normal outgoing vector, $\vec{r}_s$ is any spatial coordinate belonging to the boundary, $\vec{\Omega}_{in}$ denotes the directions entering the domain and ϕ_{in} is the imposed incoming flux. Many types of boundary conditions exist: the most common are the vacuum, reflection and rotation conditions. A particularly simple case is represented by the vacuum boundary condition in which the incoming flux is set equal to zero, namely $\phi_{in} = 0$.

2.1.3 Integral formulation

The integro-differential formulation is not the only possible expression of the transport equation. By writing neutron conservation considerations on the neutron paths, it is possible to obtain the integral formulation, a more suitable expression for the Monte Carlo approach [4]. Before going any further it is useful to define:

- the collision density $\psi(\vec{r},\vec{\Omega},E)$, which is the average number of particles undergoing a collision in $(\vec{r},\vec{\Omega},E)$. It is expressed as

$$\psi(\vec{r},\vec{\Omega},E) = \phi(\vec{r},\vec{\Omega},E)\,\Sigma_t(\vec{r},E); \tag{2.8}$$

- the transport kernel $\mathscr{T}(\vec{r}\,' \to \vec{r},\vec{\Omega},E)$, which represents the probability for a neutron emitted in $(\vec{r}\,',\vec{\Omega},E)$ to have the next collision in $(\vec{r},\vec{\Omega},E)$. It is defined as

$$\mathscr{T}(\vec{r}\,' \to \vec{r},\vec{\Omega},E) = \Sigma_t(\vec{r},E)e^{-\int_0^{|\vec{r}-\vec{r}\,'|}\Sigma_t(\vec{r}-s\vec{\Omega},E)ds}; \tag{2.9}$$

- the collision kernel $\mathscr{C}(\vec{r},\vec{\Omega}' \to \vec{\Omega},E' \to E)$, which expresses the probability for a neutron undergoing a collision in $(\vec{r},\vec{\Omega}',E')$ to be re-emitted in $(\vec{r},\vec{\Omega},E)$. Taking into account only the scattering interactions, $\mathscr{C}$ can be expressed as

$$\mathscr{C}(\vec{r},\vec{\Omega}' \to \vec{\Omega},E' \to E) = \frac{\Sigma_s(\vec{r},\vec{\Omega}' \to \vec{\Omega},E' \to E)}{\Sigma_t(\vec{r},E')}. \tag{2.10}$$

  A more complete formulation of the the collision kernel should account for all the reactions with non-zero multiplicity, i.e. that give neutrons re-emission. Therefore, we can write:

$$\mathscr{C}(\vec{r},\vec{\Omega}' \to \vec{\Omega},E' \to E) = \sum_j \frac{\Sigma_{j,t}(\vec{r},E')}{\Sigma_t(\vec{r},E')} \sum_i \frac{\Sigma_{j,i}(\vec{r},E')}{\Sigma_{j,t}(\vec{r},E')} \bar{\nu}_{j,i}(\vec{r},E') f_{j,i}(\vec{\Omega}' \to \vec{\Omega},E' \to E) \tag{2.11}$$

  where Σ_t is the total macroscopic cross section of the medium, $\Sigma_{j,t}$ is the total cross section of nuclide j, $\Sigma_{j,i}$ is the probability per unit path, for a neutron colliding with nuclide j, to undergo the collision of type i. Finally, $\nu_{j,i}$ and $f_{j,i}$ are respectively the multiplicity and the probability density function of reaction i, with the nuclide j;

- the transition kernel $\mathscr{K}(P' \to P)$, which is defined as

$$\mathscr{K}(P' \to P) = \mathscr{C}(\vec{r}\,',\vec{\Omega}' \to \vec{\Omega},E' \to E)\,\mathscr{T}(\vec{r}\,' \to \vec{r},\vec{\Omega},E). \tag{2.12}$$

  It is the probability for a neutron emitted in $P' = (\vec{r}\,',\vec{\Omega}',E')$ to have the next collision in $(\vec{r},\vec{\Omega}',E')$, and being re-emitted in $P = (\vec{r},\vec{\Omega},E)$.

The integral formulation of the transport equation can be written as:

$$\begin{aligned}\psi(\vec{r},\vec{\Omega},E) = &\int \mathscr{T}(\vec{r}\,' \to \vec{r},\vec{\Omega},E)Q(\vec{r}\,',\vec{\Omega},E)d\vec{r}\,' \\ &+ \iiint \mathscr{T}(\vec{r}\,' \to \vec{r},\vec{\Omega},E)\mathscr{C}(\vec{r}\,',\vec{\Omega}' \to \vec{\Omega},E' \to E)\psi(\vec{r}\,',\vec{\Omega}',E')d\vec{r}\,'d\vec{\Omega}'dE',\end{aligned} \tag{2.13}$$

or also, in a more compact formulation:

$$\psi(P) = \int \mathscr{T}(\vec{r}\,' \to \vec{r}, \vec{\Omega}, E) Q(P') dP' + \int \mathscr{K}(P' \to P) \psi(P') dP'. \tag{2.14}$$

In the present formulation, the collision density in a given phase-space coordinate $(\vec{r}, \vec{\Omega}, E)$ is expressed as the sum of the contribution of the sources (external and collisional). The first term is the contribution of the neutrons emitted by the external source Q to the collision density. It is expressed as the number of neutrons emitted in P', times their probability to reach and collide into P. This contribution is then integrated over all possible $\vec{r}\,'$ lying on the path $\vec{r} - s\vec{\Omega}$, where s can be any positive real number larger than zero. In the same way, the second term is the contribution to the collision density of the neutrons scattered along the path. It is defined as the average number of neutrons that have collided in P', namely $\psi(P')$, times the probability ($\mathscr{C}$) of being scattered with the right energy and direction E and $\vec{\Omega}$, times the probability ($\mathscr{T}$) to undergo the next collision in P.

2.1.4 Neumann series expansion

The collision density can be formally decomposed into Neumann series over the collision events, namely,

$$\psi(P) = \sum_{n=0}^{\infty} \psi_n(P), \tag{2.15}$$

where ψ_n is the collision density of particle having undergone n collisions between the source Q and the point P. Each term of the expansion can be expressed as:

$$\psi_0(P) = \int \mathscr{T}(\vec{r}\,' \to \vec{r}, \vec{\Omega}, E) Q(P') dP', \tag{2.16}$$

$$\psi_n(P) = \int \mathscr{K}(P' \to P) \psi_{n-1}(P') dP', \qquad \text{for any } n \geq 1. \tag{2.17}$$

In particular, with ψ_0 we denote the contribution of the neutron emitted from the source and colliding for the first time in P. By summing the ψ_n contributions over the n collisions, it is possible to recover the Equation (2.14), i.e. the integral formulation of the transport equation.

2.1.5 Adjoint transport equation

The equation adjoint to the (direct) transport equation (Eq. (2.5)) reads:

$$\begin{aligned} -\vec{\Omega} \cdot \vec{\nabla} \phi^{\dagger}(\vec{r}, \vec{\Omega}, E) + \Sigma_t(\vec{r}, E) \phi^{\dagger}(\vec{r}, \vec{\Omega}, E) = \\ \iint \Sigma_s(\vec{r}, \vec{\Omega} \to \vec{\Omega}', E \to E') \phi^{\dagger}(\vec{r}, \vec{\Omega}', E') d\vec{\Omega}' dE' + \\ \iint \nu \Sigma_f(\vec{r}, E) \frac{\chi(E')}{4\pi} \phi^{\dagger}(\vec{r}, \vec{\Omega}', E') d\vec{\Omega}' dE' + Q^{\dagger}(\vec{r}, \vec{\Omega}, E). \end{aligned} \tag{2.18}$$

where the unknown is the dimensionless function $\phi^{\dagger}$, known as adjoint neutron flux.

In order to illustrate the meaning of the adjoint flux, it is useful to resort to the definition of "adjoint". Consider $a(P)$ and $b(P)$, two generic functions of the phase-space, and the operator $\mathscr{O}$. The operator adjoint to $\mathscr{O}$, indicated with $\mathscr{O}^\dagger$, is defined by the relation:

$$\langle \mathscr{O} a(P), b(P) \rangle = \langle a(P), \mathscr{O}^\dagger b(P) \rangle \tag{2.19}$$

where $\langle ., . \rangle$ denotes the inner product. Before going any further, it is useful to rewrite the neutron transport equation (Eq. (2.5)) in a more compact formulation. This can be done by relating neutron flux and external source with the Boltzmann operator $\mathscr{B}$, which contains the entire transport physics. The compact formulation of the transport equations reads:

$$\mathscr{B}\phi(P) = Q(P) \tag{2.20}$$

Similarly, the adjoint equation can be written as:

$$\mathscr{B}^\dagger \phi^\dagger(P) = Q^\dagger(P). \tag{2.21}$$

By multiplying $\mathscr{B}\phi(P)$ times the function $\phi^\dagger(P)$, integrating over the whole phase-space, and by using the definition of adjoint (Eq. (2.19)) we can write:

$$\langle \mathscr{B}\phi(P), \phi^\dagger(P) \rangle = \langle \phi(P), \mathscr{B}^\dagger \phi^\dagger(P) \rangle. \tag{2.22}$$

Using Equation (2.20) and Equation (2.21) we can write the relation:

$$\langle Q(P), \phi^\dagger(P) \rangle = \langle \phi(P), Q^\dagger(P) \rangle, \tag{2.23}$$

which is known as *reciprocity relation*.

Let us now consider a generic problem: evaluating a given observable R, called response, related to the neutron population of the system. R can be defined as

$$R = \int_{\mathscr{D}} f(P)\phi(P)dP \tag{2.24}$$

where f is the response function and $\mathscr{D}$ is the detector, i.e. the region of the phase space on which R is defined. The function f correlates the neutron flux in any point $P \in \mathscr{D}$ with its contribution to R. For example, if the observable R is a reaction rate, i.e. the number of occurrences of a given interaction i within a region of the domain per unit of time, f will be defined as the macroscopic cross section of the reaction, namely $\Sigma_i(P)$.

If we now take the adjoint source $Q^{\dagger}(P)$ equal to $f(P)$, with f response function associated to the neutron flux ϕ, we will have:

$$R = \langle \phi(P), f(P) \rangle = \langle Q(P), \phi^{\dagger}(P) \rangle. \tag{2.25}$$

where $\phi^{\dagger}$ is the adjoint flux deriving from the solution of the adjoint transport equation with the present definition of $Q^{\dagger}(P) = f(P)$. In other terms, R can be equivalently calculated by either solving the direct transport equation for ϕ, with the detector response function f, or solving the adjoint transport equation for $\phi^{\dagger}$ and multiplying it by the source Q [7]. In view of these considerations, the quantity $\phi^{\dagger}$ is also called *importance*, i.e., the expected contribution to R, for a neutron emitted at coordinate P from the source Q.

2.2 Monte Carlo particle transport

Monte Carlo methods concern the estimate of physical quantities through the sampling of particle histories from some parent distributions. In the field of neutron transport problems, the Monte Carlo approach evaluates the inner product

$$R = \int_{P \in \mathscr{D}} g(P) \psi(P) dP \tag{2.26}$$

by estimating, instead, the expected value

$$R = \int \eta(\alpha) d\mathscr{P}(\alpha), \tag{2.27}$$

where R is the physical observable of interest, defined on a precise region of the phase-space $\mathscr{D}$, $g(P)$ is the pay-off function associated to the response R, also known as response function, $\eta(\alpha)$ is an unbiased estimator of R and $\mathscr{P}(\alpha)$ is a probability distribution from which a large number N of random variables α_i can be drawn by Monte Carlo sampling. In practice, the expected value is approximated by the sample average

$$\bar{\eta}_N = \frac{1}{N} \sum_{i=1}^{N} \eta(\alpha_i) \tag{2.28}$$

based on the N available Monte Carlo realizations [8].

2.2.1 Convergence of Monte Carlo samples and error estimates

It can be shown that

$$E[\bar{\eta}_N] = E[\eta(\alpha)] = R, \tag{2.29}$$

and furthermore

$$\sigma^2[\bar{\eta}_N] = \frac{\sigma^2}{N}, \tag{2.30}$$

where σ^2 is the variance of the estimator $\eta(\alpha)$. It means that the sample average converges to the response R, and its variance decreases as the magnitude of the particle sample N increases. According to the Central Limit Theorem, if N tends to infinity, the distribution of the sample average tends to the normal distribution with expected value R and variance σ^2/N. As a consequence, the probability that the error committed approximating the expected value R with the sample average lies within a given confidence interval is expressed by the relation

$$P\left(\frac{|\bar{\eta}_N - R|}{|\bar{\eta}_N|} \leq k \, \frac{\sigma}{|\bar{\eta}_N|\sqrt{N}}\right) = \frac{1}{2\pi}\int_{-k}^{k} e^{-t^2/2} dt, \tag{2.31}$$

where $\sigma/|\bar{\eta}_N|\sqrt{N}$ is the relative standard deviation (*RSD*). Throughout the thesis we will express the confidence interval of the Monte Carlo results in terms of percentage relative standard deviation (*PRSD*):

$$PRSD = \frac{\sigma}{|\bar{\eta}_N|\sqrt{N}} \cdot 100 \tag{2.32}$$

2.2.2 Particle track sampling

Each random walk can be represented as a sequence of states in the phase-space, starting at a birth point and ending somewhere in the domain. In particular, each particle in a given state has a probability of reaching the next one which depends only on the coordinates of the state, i.e. position, energy and direction, and on the properties of the crossed medium. This type of random walks are generally described as discrete Markov chains. In the "analog" Monte Carlo transport, neutron histories are sampled according to the laws governing the physics of the problem. More in detail: the starting point is sampled from the source distribution Q, then the flight lengths and the collisions are successively sampled according to the transport and collision kernels shown in Equations (2.9) and (2.11). The particle track ends when an absorption collision is sampled, or when the particle leaks out the domain. If, during the analog transport, the fission collision is selected, a certain number of daughter particles will be sampled and each of them will be simulated individually. For each simulated history, the events of interest are recorded. After simulating a large number of such random walks, the sample average over the recorded observables is computed.

As we can see, the behaviour of the particle tracks sampled in Monte Carlo simulations is fully described by the source distribution, and by the transport and collision kernels. Let us now look more in detail to the collision and particle flight sampling.

Flight length sampling

In a purely homogeneous medium, the cross sections can be considered independent of the spatial coordinate, and therefore influenced just by the energy of the colliding neutrons. Under this assumption, it is possible to write the transport kernel as:

$$\mathscr{T}(\vec{r}' \to \vec{r}, \vec{\Omega}, E) = \Sigma_t(E) e^{-x\Sigma_t(E)}, \tag{2.33}$$

where x is the distance between the coordinates $\vec{r}$ and $\vec{r}'$, namely, the flight length of the particle. We can write the probability density function (pdf) according to which x is sampled as:

$$f(x,E) = \Sigma_t(E) e^{-x\Sigma_t(E)} \qquad x > 0, \tag{2.34}$$

and its cumulative

$$F(x,E) = \int_0^x f(x',E)dx' = 1 - e^{-x\Sigma_t(E)} \qquad x > 0. \tag{2.35}$$

Eq. (2.34) expresses the probability for a particle having energy E to undergo its next collision at a distance x from the previous one. In particular, $e^{-x\Sigma_t}$ is the probability that the particle does not collide between $\vec{r}$ and $\vec{r} + x\vec{\Omega}$, while Σ_t is the probability that it collides within a distance x and $x + dx$. As a result, the particle flight obeys to an exponential distribution whose amplitude is a function of the total cross section Σ_t. Since the cumulative distribution is known, it is possible to sample x by means of the inverse transform method [8]. Let ρ be a random number uniformly distributed over the interval $(0,1]$. The flight length x can be evaluated with

$$x = F^{-1}(\rho, E) = -\frac{1}{\Sigma_t(E)} ln(1-\rho). \tag{2.36}$$

Collision sampling

Using once again the assumption of homogeneous material, it is possible to write the collision kernel as:

$$\mathscr{C}(\vec{\Omega}' \to \vec{\Omega}, E' \to E) = \sum_j \frac{\Sigma_{j,t}(E')}{\Sigma_t(E')} \sum_i \frac{\Sigma_{j,i}(E')}{\Sigma_{j,t}(E')} \bar{\nu}_{j,i}(E') f_{j,i}(\vec{\Omega}' \to \vec{\Omega}, E' \to E) \tag{2.37}$$

It expresses the probability for particle having energy E' and direction $\vec{\Omega}'$, colliding in a given point $\vec{r}$, to have an interaction i with a nuclide j, and to be re-emitted in $(\vec{r}, \vec{\Omega}, E)$. In practice, collision sampling concerns several successive steps:

- In the first place, the nuclide j with which the collision occurs is sampled. The probability distribution is discrete and each nuclide has a probability of being selected equal to

$$P_j = \frac{\Sigma_{j,t}(E')}{\Sigma_t(E')}. \tag{2.38}$$

- Secondly, the sampling of reaction i takes place. The cumulative is step-wise constant and the probability of each reaction is
$$P_i = \frac{\Sigma_{j,i}(E')}{\Sigma_{j,t}(E')}. \tag{2.39}$$

- Subsequently, if the selected reaction i, j is neither a capture ($\nu = 0$) nor a scattering ($\nu = 1$), then its multiplicity must be sampled. This is done according to a distribution having as mean value $\bar{\nu}_{j,i}$.

- For each particle exiting from the collision, energy and outgoing direction are simultaneously sampled from the distribution
$$f_{j,i}(\vec{\Omega}' \to \vec{\Omega}, E' \to E). \tag{2.40}$$

Furthermore, we should consider that the geometries involved in neutron transport problems are in general heterogeneous. It means that the cross sections vary with the spatial position. In order to take this into account, it is common practice to partition the domain into a collection of homogeneous media, where the properties are assumed to be constant.

2.2.3 Scoring process and estimators

The term "score" is commonly used to refer to a precise estimator $\eta(\alpha)$ of a response R, in relation to a given phase-space region $\mathscr{D}$ known as detector. The scoring process consists of counting, for each sampled particle track, the number of events of interest that occur within the detector. This means that the scoring process is responsible for evaluating the "contribution" to the estimate of each particle history. After a large number of tracks, the sample average estimating the response R and the relative uncertainty *PRSD* are computed. By increasing the number of samples, the number of recorded contributions also increases. In this way, the uncertainty of the estimate is expected to decrease, and the sample average is expected to converge to the response R. When computing ensemble averages by the method of independent replicas, for practical reasons particles are collected into sub-samples (i.e., the replicas), which usually take the name of "batches".

Along this brief introduction we referred to a single score. Nevertheless, in general it is possible to define several of them within the same Monte Carlo simulation. In case of multiple scores, the aforementioned scoring procedure will be simply applied as many times as needed. We now want to present more in detail the most commonly used estimators for responses defined on volumes.

Response estimators

Let us take as reference the generic response R, defined as

$$R = \int_{\mathscr{D}} f(P)\phi(P)dP \tag{2.41}$$

where P denote a state in the phase-space, ϕ is the neutron flux and f is a suitable response function. Notice how the estimator can be related to Equation (2.26) by simply defining $f(x) = g(P)\Sigma_t(P)$. Consider any particle track represented as a sequence of states P_i, namely

$$\alpha(P_1, ..., P_k), \tag{2.42}$$

starting at P_1 (the first collision) and ending at a random point P_k. We can thus define two different types of estimators: the track-length estimator and the collision estimator.

In the first one, the particle "contribution" is defined as the length of the path travelled by the particle throughout the detector volume. The estimator is therefore defined as

$$\eta_{track}(\alpha) = \sum_{i=1}^{k} f_i l_i \tag{2.43}$$

where l_i is the length of the i-th flight of the particle path through $\mathscr{D}$, and f_i is the value of the pay-off function along the i-th track.

On the other hand, the collision estimator is defined as the sum of the number of mean free paths travelled by the particles through the detector:

$$\eta_{coll}(\alpha) = \sum_{i=1}^{k} \frac{f(P_i)}{\Sigma_t(P_i)} \mathbb{I}_{\mathscr{D}}(P_i), \tag{2.44}$$

where $1/\Sigma_t$ and $f(P_i)$ are respectively the mean free path of the particle evaluated at the collision point P_i and the related value of the response function. $\mathbb{I}_{\mathscr{D}}$ is the marker function of volume $\mathscr{D}$, i.e.,

$$\mathbb{I}_{\mathscr{D}}(P_i) = \begin{cases} 1 & \text{for } P_i \in \mathscr{D}, \\ 0 & \text{otherwise.} \end{cases} \tag{2.45}$$

The choice between the two estimators depends on the physical problem at hand, and must be guided by the principle of estimating the desired score R with the smallest possible statistical variance, for a given number of simulated particle histories. In general, the collision estimator η_{coll} will have a smaller variance in very large and strongly absorbing regions, while the track length estimator η_{track} will be a wiser choice for thin or weakly absorbing mediums. As the detector region $\mathscr{D}$ shrinks, the variance of η_{coll} rapidly deteriorates, and the use of a track estimator might be a better choice.

2.3 Deterministic approach

The neutron flux, as described by the transport equation, is defined as a function of the continuous phase-space coordinates, namely, energy, direction and spatial position. The deterministic methods

generally deal with this dependence by introducing numerical approximations to discretize the problem [4, 9]. In the following, we want to survey the most common approximations and give a brief description. For the sake of simplicity, we will focus at first on the deterministic resolution of the "direct" transport equation, and then we will draw some conclusion on adjoint calculations.

2.3.1 Classical deterministic approximations

In neutron transport physics problems, neutrons can be found within an extremely wide energy spectrum. For thermal reactors, for examples, it can range from 10^7 eV to 10^{-5} eV. In modern deterministic codes this dependency is accounted by means of the so-called multi-group formalism [3].

Multi-group approximation

The energy spectrum is generally subdivided into N_g energy groups $[E_g, E_{g-1}]$, in which E_{g-1} and E_g are respectively the upper and the lower bound of each interval. By adopting the multi-group approximation, the Boltzmann transport equation can be rewritten as a set of single-group equations:

$$\vec{\Omega}\cdot\vec{\nabla}\phi_g(\vec{r},\vec{\Omega})+\Sigma_t^g(\vec{r})\phi_g(\vec{r},\vec{\Omega})=\sum_{g'=1}^{N_g}\oint d\vec{\Omega}'\,\Sigma_s^{g'\to g}(\vec{r},\vec{\Omega}'\cdot\vec{\Omega})\phi_{g'}(\vec{r},\vec{\Omega}')+ \\ \sum_{g'=1}^{G}\nu^{g'}\Sigma_f^{g'}(\vec{r})\chi^g(\vec{r})\oint\frac{d\vec{\Omega}'}{4\pi}\,\phi_{g'}(\vec{r},\vec{\Omega}')+Q_g(\vec{r},\vec{\Omega}) \quad (2.46)$$

where ϕ_g is the flux of group g, which is defined as the angular flux ϕ integrated over the energy range of the group g, namely,

$$\phi_g(\vec{r},\vec{\Omega})=\int_{\Delta E_g}\phi(\vec{r},\vec{\Omega},E)dE. \quad (2.47)$$

Σ_t^g and $\Sigma_s^{g'\to g}$ are respectively the total cross section of group g and the transfer cross section coupling group g and g', Q_g is the external source, and $\nu^{g'}\Sigma_f^{g'}\chi^g$ is the fission cross section of group g' multiplied by the related multiplicity and group fission spectra. These terms are considered constant in each group and are defined as

$$\Sigma_t^g(\vec{r},\vec{\Omega})=\frac{\int_{\Delta E_g}\Sigma_t(\vec{r},E)\phi(\vec{r},\vec{\Omega},E)dE}{\int_{\Delta E_g}\phi(\vec{r},\vec{\Omega},E)dE} \quad (2.48)$$

$$\Sigma_s^{g'\to g}(\vec{r},\vec{\Omega},\vec{\Omega}')=\frac{\int_{\Delta E_g}dE\int_{\Delta E_{g'}}dE'\,\Sigma_s(\vec{r},\vec{\Omega}'\cdot\vec{\Omega},E'\to E)\phi(\vec{r},\vec{\Omega}',E')}{\int_{\Delta E_{g'}}\phi(\vec{r},\vec{\Omega}',E')dE'} \quad (2.49)$$

$$\chi^g \nu^{g'} \Sigma_f^{g'}(\vec{r},\vec{\Omega}') = \frac{\int_{\Delta E_g} dE \int_{\Delta E_{g'}} dE'\ \nu\Sigma_f(\vec{r},E')\chi(E)\phi(\vec{r},\vec{\Omega}',E')}{\int_{\Delta E_{g'}} dE'\ \phi(\vec{r},\vec{\Omega}',E')} \tag{2.50}$$

$$Q_g(\vec{r},\vec{\Omega}) = \int_{\Delta E_g} Q(\vec{r},\vec{\Omega},E)dE. \tag{2.51}$$

According to the definition, the multi-group cross-sections are evaluated as weighted averages of the cross section values within the group, using the neutron flux ϕ as weight function. The cross sections thus produced are therefore, by definition, dependent on the angular variable. In practice, this dependency is not taken into account. It is generally removed by replacing the neutron flux with the scalar flux Φ, which is defined as:

$$\Phi(\vec{r},E) = \oint d\vec{\Omega}\ \phi(\vec{r},\vec{\Omega},E). \tag{2.52}$$

The angular dependency of multi-group cross sections will no longer be shown in the following.

Furthermore, we should notice that the neutron flux ϕ, which is needed for the cross sections evaluation, is the solution of the problem itself. By assuming the flux to be constant along the energy range of each single group, it is possible approximate the multi-group cross sections with average values. This approximation improves as the amplitude of the energy range considered decreases. Moreover, some nuclides exhibit resonance phenomena, i.e. extremely peaked cross sections for given energy values. In such cases it is essential to take into account the energy dependence of the flux within the group. In modern transport codes, resonances are generally solved by making use of the self-shielding formalism [10].

Legendre polynomials expansion

The scattering term of Equation (2.46) shows a coupling between neutron fluxes coming from different directions $\vec{\Omega}'$. Such dependence is generally taken into account expanding the transfer cross section over Legendre Polynomials, namely,

$$\Sigma_s^{g'\to g}(\vec{r},\vec{\Omega}'\cdot\vec{\Omega}) \simeq \sum_{n=0}^{L} \frac{2n+1}{2} \Sigma_{s,n}^{g'\to g}(\vec{r}) P_n(\vec{\Omega}'\cdot\vec{\Omega}), \tag{2.53}$$

where L is the anisotropy order, P_n is the Legendre polynomial of order n and $\Sigma_{s,n}^{g'\to g}$ is the angular moment of order n of the transfer function. The product $\vec{\Omega}'\cdot\vec{\Omega}$ can be decomposed making use of the associated Legendre functions and then rewriting them in terms of spherical harmonics:

$$\Sigma_s^{g'\to g}(\vec{r},\vec{\Omega}'\cdot\vec{\Omega}) \simeq \sum_{n=0}^{L} 2\pi\Sigma_{s,n}^{g'\to g}(\vec{r}) \sum_{\beta=-n}^{n} Y_n^{\beta}(\vec{\Omega}) Y_n^{\beta^*}(\vec{\Omega}'), \tag{2.54}$$

where Y_n^β is the spherical harmonics of order $n\ \beta$. By inserting the expansion of the transfer function (Eq. (2.54)) into the scattering integral, it is possible to notice how the dependency on the "incident" direction $\vec{\Omega}'$ is limited to the neutron flux and to the spherical harmonics $Y_n^{\beta^*}$. It is therefore possible to write the scattering integral as a function of the moments of angular flux , namely

$$\phi_{g,n}^\beta(\vec{r}) = \oint d\vec{\Omega}'\ \phi_g(\vec{r},\vec{\Omega}')Y_n^{\beta^*}(\vec{\Omega}'). \tag{2.55}$$

The set of single-group transport equations can be rewritten as:

$$\vec{\Omega}\cdot\vec{\nabla}\phi_g(\vec{r},\vec{\Omega}) + \Sigma_t^g(\vec{r})\phi_g(\vec{r},\vec{\Omega}) = \sum_{g'=1}^{G}\sum_{n=0}^{L}\sum_{\beta=-n}^{n}\Sigma_{s,n}^{g'\to g}(\vec{r})\phi_{g',n}^\beta(\vec{r})Y_n^\beta(\vec{\Omega}) + \sum_{g'=1}^{G}\nu^{g'}\Sigma_f^{g'}(\vec{r})\frac{\chi^g(\vec{r})}{4\pi}\Phi_{g'}(\vec{r}) + Q_g(\vec{r},\vec{\Omega}), \tag{2.56}$$

where $\Phi_{g'}(\vec{r})$ is the scalar neutron flux, which is equal to the moment of the flux of order 0 0, namely $\phi_{g',0}^0$.

Discrete ordinates approximation

In order to treat the continuous angular dependence, the most extensively used approach is the discrete ordinates method (S_n). In this method, the flux is calculated for a set of N_d discrete directions and the integral of Equation (2.55) is approximated using quadrature formulae, namely,

$$\oint d\vec{\Omega}\ f(\vec{\Omega}) \simeq \sum_{j=1}^{N_d} w_j f(\vec{\Omega}_j) \tag{2.57}$$

where f is a generic function to be integrated and w_j is the weight related to direction $\vec{\Omega}_j$. w_j and $\vec{\Omega}_j$ are uniquely determined according to the selected quadrature formula.

Iterative resolution scheme

By applying the S_n method, it is possible to express Equation (2.56) in term of a set of $N_d \cdot N_g$ equations coupled by a source term:

$$\vec{\Omega}_i\cdot\vec{\nabla}\phi_k(\vec{r},\vec{\Omega}_i) + \Sigma_t^k(\vec{r})\phi_k(\vec{r},\vec{\Omega}_i) = q_k(\vec{r},\vec{\Omega}_i) \qquad i = 1,..,N_d, k = 1,..,N_g \tag{2.58}$$

where i and k are the indexes denoting the specific angle and energy group for which the flux $\phi_k(\vec{r},\vec{\Omega}_i)$ is calculated. The source q_g is defined as the sum:

$$q_k(\vec{r},\vec{\Omega}_i) = \sum_{j=1}^{N_d} \sigma_{ij}^k(\vec{r})\phi_k(\vec{r},\vec{\Omega}_j) + \sum_{g=1,g\neq k}^{N_g}\left[\sum_{j=1}^{N_d}\sigma_{ij}^g(\vec{r})\phi_g(\vec{r},\vec{\Omega}_j)\right] + \sum_{g=1}^{N_g}\left[\sum_{j=1}^{N_d}\sigma_{fiss}^g(\vec{r})\phi_g(\vec{r},\vec{\Omega}_j)\right] + Q_k(\vec{r},\vec{\Omega}_i). \tag{2.59}$$

The first term is the self-scattering contribution, the second is the scattering contribution from other energy groups, the third term is the fission source and the last one is the external source. With σ_{ij}^g we denote a multiplicative scattering coefficient relating the contribution of angle $\vec{\Omega}_j$ to the source in the i-th direction. It includes the moment of the scattering transfer function, the spherical harmonics and the quadrature formula weight. In the same way, the term of the fission kernel are collected into σ_{fiss}^g.

The practical resolution of the transport equation consists in a fixed-source problem in which the source is iteratively updated [11]. More precisely, we distinguish between 3 nested iterative schemes: outer iterations, thermal iterations and inner iterations. For each single energy group, the Equation (2.58) is solved by keeping constant the fission source and the scattering source from other energy groups. It is therefore computed by iterating over the self-scattering source by means of the so called inner iterations.

In the energy region of down-scattering only, i.e. where scattering reactions can only produce a decrease in neutron energy, the groups are successively calculated, starting from the most energetic one ($g = 1$) and then decreasing in energy. In this way, since the scattering source is a function of only the flux of the groups already calculated, it is possible to update its contribution from group to group. This is valid until reaching the thermal region, that is the energy range in which up-scattering phenomena occurs. In these "thermal" groups, the scattering source is solved iteratively by means of thermal iterations. In practice, once the lowest energy group has been calculated, the scattering source is updated and the groups affected by up-scattering are subsequently recalculated until they reach the convergence. The coupling between the different single-group equations given by the scattering source can also be described by means of the matrix of the system, which is lower triangular for the groups affected by down-scattering only, and becomes approximately complete for thermal groups.

At this point, the fission source, if present, is updated and the calculation is repeated starting from the first group. This last process is known as outer iterations. In general, outer iterations are associated with eigenvalue calculations. Since the eigenvalue we look for is the one related to fissions, the fission source is kept fixed until the flux calculation converges on the scattering sources. Successively, the eigenvalue and fission source are updated, and the process is then repeated. When, as in the case of problems with external source imposed, the eigenvalue calculation is not performed, the process updates just the fission source converging on it.

Spatial resolution

Spatial dependence is generally assessed by dividing the domain into a set of regions. Each region is characterized by a precise nuclide composition and by constant properties. The transport equation, reformulated in the form of a fixed-source problem, is solved at each inner iteration for the entire spatial domain, and for all the directions $\vec{\Omega}_j$. There are several methods that can be applied in the calculation of Eq. (2.58). Among them, we mention: finite differences, finite elements, method of long characteristics, short characteristics and nodal method. The choice of one method rather than another determines the supplementary relations used to solve the system of equations, so the related numerical approximations.

2.3.2 Adjoint flux calculation with deterministic approach

The processes described in previous sections are oriented to the resolution of the direct transport equation. The same methods and approximations are also used is the resolution of the adjoint transport equation (Eq. (2.18)). The main difference between direct and adjoint calculation are the streaming direction, which is inverted, and the multi-group scattering matrix, which is transposed with respect to the one of the direct calculation. As for the directional part, it is sufficient to solve the single-group equation in the opposite direction. Instead, for the scattering part, the predominantly lower triangular coupling (apart from thermal groups) of the direct calculation, becomes a upper triangular coupling in the adjoint formulation, which leads to a reversed resolution scheme: the problem is solved starting from the less energetic groups and ending in the "fast" ones. Obviously, this is slightly more complicated since fission and scattering source for thermal groups need to be updated by means of outer and thermal iterations, which are adapted to the adjoint calculation scheme.

Chapter 3

Variance Reduction methods

The variance reduction methods were born almost simultaneously with the invention of the Monte Carlo method. They are fundamental techniques that allow to speed up the convergence of the simulations and, sometimes, to solve problems that otherwise would not be solvable with available computational resources. Variance reduction methods are compulsory for Monte Carlo simulations wherever the simple analog calculation results to be inadequate and inefficient. We now want to present the variance reduction methods commonly employed in particle transport problems and, more precisely, we will focus on the ones implemented in the TRIPOLI-4 Monte Carlo code. Then, we will present the methods that are the object of study in this thesis, namely: the Exponential transform, the AMS and the "Two-step" method.

3.1 Fundamentals

In Monte Carlo shielding calculations, it is quite common to encounter problems where the event of interest for the score is very rare, i.e. the probability that the event is sampled, according to the probability functions that regulate the physics of the problem, is extremely small. In these cases, in order to record a sufficient number of events at the detector so to produce an estimate of the response with a sufficient accuracy, it is necessary to sample a large number of particle histories. This implies a high computational cost, and very long calculation times. These problems are typically solved by means of variance reduction methods.

The basic idea of variance reduction methods is to favour the sampling of events whose contribution is useful for the score by modifying the statistical laws governing the physics of the problem. In order to keep unchanged the expected value of the estimate R, these variations are accounted for by assigning to each particle a "statistical weight" [12]. By introducing a "modified" probability distribution $\mathscr{P}^*$, the response formulation can be rewritten as:

$$R = \int \eta(\alpha) d\mathscr{P}(\alpha) = \int \eta(\alpha) \frac{d\mathscr{P}(\alpha)}{d\mathscr{P}^*(\alpha)} d\mathscr{P}^*(\alpha) \tag{3.1}$$

where

$$w = \frac{d\mathscr{P}(\alpha)}{d\mathscr{P}^*(\alpha)} \tag{3.2}$$

is the weight of the α particle track. In practice, the weight w is not a constant value, but it is updated along the evolution of the particle track [13]. Every time a collision or a flight length is sampled making use of a modified probability function $\mathscr{P}^*$, w is corrected according to:

$$w' = w \cdot \frac{\mathscr{P}(x)dx}{\mathscr{P}^*(x)dx} = w \cdot \frac{natural\ probability}{modified\ probability}. \tag{3.3}$$

In Monte Carlo parlance, using an abuse of language, we use to refer to variance reduction methods also as biasing techniques. Similarly, the modified probability law is also said to be "biased". However, we stress that correct variance reduction methods do not introduce any bias in the results. They only modify variance of the estimate while preserving the expected values. As opposed to "biased" simulations, we will use the term "analog" to denote simulations without variance reduction, i.e. simulations in which the particle histories are sampled according to original probability distributions.

3.2 Classical variance reduction methods

We now want to provide an overview of the variance reduction techniques that are customary used in Monte Carlo simulations.

3.2.1 Implicit capture

In the practice of Monte Carlo simulations, whenever a particle is absorbed, it is eliminated from the simulation, so the potential contribution that this particle can provide to the detector is lost. In most of the simulations, capture reactions are the main cause of elimination of statistical particles. This phenomenon is generally solved through the use of the implicit capture. This technique consists of a modification of the collision kernel so that capture reactions are no longer sampled. Assuming for the sake of simplicity that the medium is non-multiplying, collisions will therefore be sampled among the scattering interactions only. Each time that a particle will enter a collision in the generic point P_j, its weight will be corrected with the non-absorption probability factor:

$$w' = w \cdot \frac{\Sigma_s(P_j)}{\Sigma_t(P_j)}. \tag{3.4}$$

As a result, the implicit capture allows extending the length of simulated particle tracks. On the other hand, random walk would potentially live forever, unless they are terminated by spatial leakage or energy cut-off. In order to prevent this from happening, the implicit capture is often associated with population control techniques, also known as weight control techniques.

3.2.2 Forced fission

The forced fission technique aims at increasing the sampling of fission events within fissile materials. In each standard simulation with TRIPOLI-4 this technique is automatically applied in conjunction with the implicit capture. Forced fission consists in modifying the probability laws of the reaction sampling. If a particle collides inside a multiplying material, and a fissile isotope is sampled for the collision, the fission reaction is automatically selected. In order to account for this variation and produce unbiased results, the weight of the particles are adjusted, or alternatively the number of particles emitted is reduced. TRIPOLI-4 adopts this second strategy. The average number of particles produced by fission is therefore corrected according to:

$$\bar{\nu}'(P_j) = \bar{\nu}(P_j) \cdot \frac{\Sigma_f(P_j)}{\Sigma_t(P_j)}, \tag{3.5}$$

where $\bar{\nu}$ is the original average number of particles emitted per fission, and the $\Sigma_f(P_j)/\Sigma_t(P_j)$ is the probability of sampling fission reactions. According to this solution, each secondary particle produced will have the same weight as the parent particle before the collision.

3.3 Population control

The purpose of population control methods is to prevent the particle weight from becoming excessively large or small. The idea is that particles having small weights with respect to the average distribution at the detector will provide a negligible contribution to the score, so resulting in waste of computational time and in an increase in the statistical dispersion around the average. Similarly, excessively high weights compared to the average yield an increase of the variance of the sample average, thus producing unwanted statistical fluctuations. In both cases, discrepant weights lead to negative effects on the convergence of the estimate. It is therefore useful that particles having a very small weight are abandoned, and that particles having an excessively large weight are split. The problem is generally addressed by using methods known as Russian roulette and splitting [12].

3.3.1 Russian roulette

The Russian roulette is a population control technique aimed at stopping the sampling of particles histories carrying a small weight. The operating principle requires the particle weight to be monitored along the whole random walk. Each time that the weight w decreases over a given threshold value, namely, $w < w_{min}$, the particle undergoes the Russian roulette. It consists of a simple game that decides whether the particle has to be killed or not. Each particle that undergoes the Russian roulette has a probability of being killed equal to P_{kill}, where

$$P_{kill} = 1 - w. \tag{3.6}$$

More in detail, the game consists in the sampling of a uniform random number ρ from $(0,1]$. If $\rho > w$ the particle is killed, otherwise it survives, and its weight is set equal to 1. This procedure is performed in such a way that the resulting estimate is unbiased, i.e. the average statistical weight is preserved before and after the population control. In TRIPOLI-4 standard simulations, the Russian roulette is automatically activated and the weight threshold w_{min} is set by default to 0.8.

3.3.2 Splitting

The principle of the splitting technique is replacing those particles that carry a large weight w with n equal copies, each with a weight equal to w/n. By splitting particles, we guarantee the global weight to remain constant and, at the same time, we prevent particle weights from diverging. In practice, a threshold value $w_{max} > 0$ is defined. Whenever a particle weight exceed the threshold, namely, $w > w_{max}$, the number n of identical copies of the original particle is determined. n is obtained rounding the weight w up to the next integer value, i.e. $n = \lceil w \rceil$. Each copy takes a weight equal to $w' = w/n$ and is added to the set of particles not yet simulated. The default threshold value of TRIPOLI-4 is $w_{max} = 2$.

3.4 Exponential transform and importance sampling

Shielding problems are generally characterized by a large flux attenuation between source and detector. When the optical distance between the two is large, the probability that a random walk reaches the detector becomes small. This means that simulating this type of problems with analog Monte Carlo is typically not feasible. These problems are generally solved with variance reduction methods able to modify the laws of particle transport, typically with the *exponential transform*. In TRIPOLI-4, the exponential transform is implemented as part of the *importance sampling*, a more systematic approach enabling the construction of non-analog random walks. The exponential transform with importance sampling constitutes the variance reduction method of reference in the code [14].

The importance sampling scheme (or importance biasing) makes use of an arbitrary function $I(\vec{r},\vec{\Omega},E)$ known as *importance*. This function is used to quantify the potential contribution that a particle lying in a given point of the phase-space can give to the score. In other words, it determines whether the particle is of interest or not to the estimate [15, 16]. The purpose of importance sampling is to produce unbiased estimates by modifying the kernels that regulate the entire particle transport. This is done in such a way that the "events" (collision and particle flights) resulting in states of higher importance are sampled more frequently than those with a lower importance.

Importance sampling was born as a practical application of the zero-variance Monte Carlo game theory. It can be shown that by biasing the particle transport using the adjoint flux as importance function it is possible to eliminate the variance associated to the given estimators. Such zero-variance games would carry identical, and identically correct, estimates of the quantity to be computed at each

sampled history [12, 17]. Unfortunately, the zero-variance games can not be used in practice, as they would require the calculation of the adjoint flux, a problem whose computational complexity is at least equal to the one of the original problem. Moreover, the knowledge of the exact adjoint flux would enable us to evaluate directly the response R by means of the reciprocity relation (Eq. (2.25)). Furthermore, even if the adjoint flux were known, the game would require to track the particles for an infinite number of collisions, which is clearly unfeasible in practical applications. Yet despite this, zero-variance games have inspired approximate methods that allow nearly-optimum biasing in Monte Carlo simulations.

A possible way of formulating the importance sampling consists in deriving the biased kernels of the non-analog transport by directly modifying the Boltzmann equation. First of all, we should recall the integral-differential formulation of the transport equation (see Section 2.1.2), but this time using the collision operator (Eq. (2.11)) so as to merge the scattering and fission term:

$$\vec{\Omega}\cdot\vec{\nabla}\phi(\vec{r},\vec{\Omega},E)+\Sigma_t(\vec{r},E)\phi(\vec{r},\vec{\Omega},E)= \iint \Sigma_t(\vec{r},E')\,\mathscr{C}(\vec{r},\vec{\Omega}'\to\vec{\Omega},E'\to E)\phi(\vec{r},\vec{\Omega}',E')d\vec{\Omega}'dE'+Q(\vec{r},\vec{\Omega},E). \quad (3.7)$$

We define the biased flux ϕ^* on the whole phase-space, as the product between the importance function and the neutron flux , namely,

$$\phi^*(\vec{r},\vec{\Omega},E)=\phi(\vec{r},\vec{\Omega},E)I(\vec{r},\vec{\Omega},E). \quad (3.8)$$

We can now rewrite the transport equation in terms of ϕ^* by multiplying each term by the importance function $I(\vec{r},\vec{\Omega},E)$:

$$\begin{aligned}\left[\vec{\Omega}\cdot\vec{\nabla}+\left(\Sigma_t(\vec{r},E)-\vec{\Omega}\cdot\frac{\vec{\nabla}I(\vec{r},\vec{\Omega},E)}{I(\vec{r},\vec{\Omega},E)}\right)\right]\phi^*(\vec{r},\vec{\Omega},E)&=Q^*(\vec{r},\vec{\Omega},E)\\ +\iint\Sigma_t(\vec{r},E')\,\mathscr{C}(\vec{r},\vec{\Omega}'\to\vec{\Omega},E'\to E)\frac{I(\vec{r},\vec{\Omega},E)}{I(\vec{r},\vec{\Omega}',E')}\phi^*(\vec{r},\vec{\Omega}',E')d\vec{\Omega}'dE'.&\end{aligned} \quad (3.9)$$

This formulation allows us to put in evidence the biased kernels. More in detail, we can distinguish:

- the biased total cross section Σ_t^*, defined as

$$\Sigma_t^*(\vec{r},\vec{\Omega},E)=\Sigma_t(\vec{r},E)-\kappa(\vec{r},\vec{\Omega},E)\vec{\Omega}\cdot\vec{\Omega}_0, \quad (3.10)$$

  where $\vec{\Omega}_0$ is the direction of the gradient of the importance function, and κ, known as opacity, is the ratio between its module and the local value of the importance:

$$\vec{\Omega}_0=\frac{\vec{\nabla}I(\vec{r},\vec{\Omega},E)}{|\vec{\nabla}I(\vec{r},\vec{\Omega},E)|}, \quad (3.11)$$

$$\kappa(\vec{r},\vec{\Omega},E) = \frac{|\vec{\nabla} I(\vec{r},\vec{\Omega},E)|}{I(\vec{r},\vec{\Omega},E)}. \tag{3.12}$$

$\vec{\Omega}_0$ is the direction towards which particle flights must be preferentially sampled in order to obtain a reduction of the variance. We should notice that, since κ is by definition always positive, the magnitude of Σ_t^* is influenced solely by the flight direction $\vec{\Omega}$. The explicit formulation of biased transport kernel $\mathscr{T}^*$ can be obtained by simply substituting Σ_t with the biased total cross section Σ_t^* into the analog transport kernel $\mathscr{T}$ (Eq. (2.9)), namely:

$$\mathscr{T}^*(\vec{r}' \to \vec{r},\vec{\Omega},E) = \Sigma_t^*(\vec{r},\vec{\Omega},E) e^{-\int_0^{|\vec{r}-\vec{r}'|} \Sigma_t^*(\vec{r}-s\vec{\Omega},\vec{\Omega},E)ds}; \tag{3.13}$$

- the biased collision kernel $\mathscr{C}^*$, defined as:

$$\mathscr{C}^*(\vec{r},\vec{\Omega}' \to \vec{\Omega},E' \to E) = \mathscr{C}(\vec{r},\vec{\Omega}' \to \vec{\Omega},E' \to E) \frac{\Sigma_t(\vec{r},E)}{\Sigma_t^*(\vec{r},\vec{\Omega},E)} \frac{I(\vec{r},\vec{\Omega},E)}{I(\vec{r},\vec{\Omega}',E')}; \tag{3.14}$$

- the biased external source Q^*, defined as

$$Q^*(\vec{r},\vec{\Omega},E) = Q(\vec{r},\vec{\Omega},E) I(\vec{r},\vec{\Omega},E). \tag{3.15}$$

By means of some substitutions it is possible to rewrite the transport equation as:

$$\vec{\Omega}\cdot\vec{\nabla}\phi^*(\vec{r},\vec{\Omega},E) + \Sigma_t^*(\vec{r},\vec{\Omega},E)\phi^*(\vec{r},\vec{\Omega},E) = \iint \Sigma_t^*(\vec{r},\vec{\Omega}',E')\mathscr{C}^*(\vec{r},\vec{\Omega}' \to \vec{\Omega},E' \to E)\phi^*(\vec{r},\vec{\Omega}',E')d\vec{\Omega}'dE' + Q^*(\vec{r},\vec{\Omega},E). \tag{3.16}$$

The basic principle of exponential transform is to enlarge the mean free path of the particles moving towards regions of the phase-space with an higher importance. According to Equation (3.10), when the flight direction $\vec{\Omega}$ is equal to $\vec{\Omega}_0$, the biased cross section will be reduced, so the flight of the particles will be on average longer. At the same time, when the product $\vec{\Omega}\cdot\vec{\Omega}_0$ is negative, we will have $\Sigma_t^* > \Sigma_t$, so the mean free path of the particle will be shortened. The overall effect of exponential transform on the simulation is therefore moving particles from lower to higher importance regions, typically towards the detector.

As for the collision biasing, in TRIPOLI-4, the kernel $\mathscr{C}$ is left unchanged due to practical reasons: the biasing of the transfer function would require an extensive modification of regular collision routines implemented in the code. In order to ensure unbiased simulation results, the collisions are sampled according to kernel $\mathscr{C}$, but the post-collision particle weights are corrected according to:

$$w' = w \frac{\Sigma_t(\vec{r},E)}{\Sigma_t^*(\vec{r},\vec{\Omega},E)} \frac{I(\vec{r},\vec{\Omega},E)}{I(\vec{r},\vec{\Omega}',E')}. \tag{3.17}$$

By using the importance sampling, the birth point of the random walks is no longer sampled from Q, but according to the biased source $Q^* = Q \cdot I$. The source biasing is taken into account by setting the initial weight of the particles equal to:

$$w_0 = \frac{1}{I(\vec{r}, \vec{\Omega}, E)}. \tag{3.18}$$

Finally the response is calculated as follows:

$$R = \iiint_D \frac{f(\vec{r}, \vec{\Omega}, E)}{I(\vec{r}, \vec{\Omega}, E)} \phi^*(\vec{r}, \vec{\Omega}, E) d\vec{r} d\vec{\Omega} dE \tag{3.19}$$

where the pay-off function f is corrected by a factor $1/I$ in order to account the introduction of the biasing technique. Summarizing, the current version of the importance sampling implemented in TRIPOLI-4 is limited to the biasing of the transport operator (exponential transform) and to the source biasing.

Since, as already mentioned, the exact adjoint flux is generally not available to be used as importance function, it is common practice to bias the particle transport using an approximated adjoint flux. It has been shown that the use of approximated importance can effectively contribute to reducing the variance, therefore increasing the performance of Monte Carlo calculations. In this respect, many different strategies can be adopted to produce adjoint flux approximations. For example, the INIPOND module implemented on TRIPOLI-4 provides approximated importance functions through the use of an algorithm based on the minimization of the optical mean free path. This tool will be discussed further in the next chapter.

3.4.1 CADIS methodology

One of the possible strategies to calculate an importance function suitable for the biasing of single-response Monte Carlo calculations is the use of the Consistent Adjoint-Driven Importance Sampling (CADIS) technique [7, 16, 18, 19]. The method consist in calculating the adjoint flux over a spatial and energetic mesh by means of a deterministic solver. The solution is not exact since many approximations are involved in deterministic calculations (see Section 2.3.1). Moreover, in order to reduce the memory requirements, the angular dependence of the importance is usually eliminated by using only the adjoint scalar flux.

According to the CADIS method, the adjoint source $S^\dagger$ is set equal to the response function of the estimate:

$$Q^\dagger(\vec{r}, \vec{\Omega}, E) = \begin{cases} f(\vec{r}, \vec{\Omega}, E) & \text{for } \vec{r} \in \mathscr{D}, \\ 0 & \text{for } \vec{r} \notin \mathscr{D}. \end{cases} \tag{3.20}$$

The CADIS method should not be used to calculate more than one response simultaneously, since it is oriented to the evaluation of just a single score. The TRIPOLI-4 version of CADIS is coupled with

other variance reduction techniques such as implicit capture and forced fission. Furthermore, in order to control the particle number and to avoid large weight discrepancy, population control techniques are applied [14]. More in detail, the "optimum weight" of the particle being in position $\vec{r}$ with energy E is defined as:

$$\Pi(\vec{r},E) = \frac{1}{I(\vec{r},E)}, \tag{3.21}$$

and its weight discrepancy is calculated as the ratio between the particle weight and its ideal weight:

$$\mathscr{W} = \frac{w}{\Pi(\vec{r},E)}. \tag{3.22}$$

If the particle presents a weight discrepancy lower than 0.5, it will undergo the Russian roulette. If instead $\mathscr{W}$ is greater than 2, it will be split.

For shielding problems, the potentialities of the application of the CADIS method to the TRIPOLI-4 importance sampling have been already tested and extensively discussed in [16]. Nevertheless, the application of CADIS to multiplicative media has not yet been explored with TRIPOLI-4.

3.4.2 FW-CADIS methodology

As we have previously said, the CADIS methodology is meant to solve problems whose goal is to calculate the response on a single detector. In general, in multiple responses simulations, the detector tallies could be placed at different optical distances from the source, and so, they could face different flux attenuations. This means that each detector may have its own importance value and so its own particle "attractiveness". The CADIS methodology, therefore, can not be employed as a whole.

In order to solve multiple-response problems, the method that is customarily used is the Forward Weighted Consistent Adjoint-Driven Importance Sampling (FW-CADIS) [19–22]. In this method, the importance function is computed through an adjoint calculation with a modified adjoint source:

$$Q^{\dagger}(\vec{r},\vec{\Omega},E) = \begin{cases} \dfrac{f(\vec{r},\vec{\Omega},E)}{\iint f(\vec{r},\vec{\Omega}',E')\phi(\vec{r},\vec{\Omega}',E')dE'd\vec{\Omega}'} & \text{for } \vec{r}\in\mathscr{D}, \\ 0 & \text{for } \vec{r}\notin\mathscr{D}. \end{cases} \tag{3.23}$$

In agreement with this formulation, the adjoint source of each detector is weighed by the inverse of the response itself. In this way, a detector placed far from the source, experiencing a small neutron flux, will be characterized by a large adjoint source, so by a large value of importance. A closer detector will consequently experience a larger neutron flux, so it will be "less important" than the first one. By doing so, the FW-CADIS attempts to level out the variance over all responses. Since the definition of the adjoint source is function of the response itself, i.e. the final objective of the calculation, we are not able to evaluate the exact value of $Q^{\dagger}$. The idea behind the method relies on the use of broad

approximation of the direct neutron flux in order to estimate the response at the detectors, and so the adjoint source.

3.5 The Adaptive Multilevel Splitting method

The Adaptive Multilevel Splitting (AMS) is a variance reduction method that does not make use of any modification of the kernels that regulate the particle sampling, but relies on a purely analog Monte Carlo process. The AMS method consists in an iterative process that splits particle histories that are more relevant for the score, thus eliminating and replacing those that are less likely to contribute. AMS was originally theorized for continuous Markov chains [23], then generalized for discrete Markov chains [24, 25], and finally implemented in the TRIPOLI-4 code [15]. For the sake of simplicity, we will just describe how the method works within the Monte Carlo code, therefore without presenting any mathematical details.

The AMS operates individually, which means that AMS iterations are performed on independent particle sets containing a prescribed number of individuals N. For each particle batch simulated with AMS we identify an initialization phase, in which all the random walks are simulated in analog mode, followed by a series of AMS iterations. In each iteration it is possible to distinguish two different steps: a sorting step, whose task is to sort particles histories and to select those to discard, and a splitting step, where particles are re-sampled [15]. The iterative process ends once a given stopping criterion is met. The score is then collected and the sample average is updated.

The sorting step

In order to establish which particle histories are to be split and which are to be eliminated, tracks are sorted according to an importance function. In general, in AMS, the importance function can be any function capable of expressing whether a particle will contribute to the score more likely than another. In AMS, every particle history is seen as a *track*, namely, as an ordered sequence of states in the phase-space. Each state is described by a set of coordinates $(\vec{r}, \vec{\Omega}, E)$ and, by means of the importance function, it is associated with a given importance value. Once a track is sampled, the algorithm evaluates a global track importance, which is defined as the maximum value among the importances of the points of the track itself. In other words, for a generic track α, defined as $\alpha = (P_1, ..., P_{N_s})$ where P_i indicates the i-th state, the track importance is defined as:

$$I(\alpha) = \max_{i \in [1, N_s]} I(P_i), \tag{3.24}$$

where N_s is the number of states of the track.

Let q be the iteration index, and k be the minimum number of tracks to be re-sampled per iteration. At each iteration, the AMS algorithm sorts the tracks in ascending order of importance. Then, it

evaluates the splitting level Z_q, defined as the importance of the k-th track starting from the least important one. All the particle tracks having an importance lower or equal than Z_q will be eliminated from the simulation. If we call K_q the number of particles discarded at iteration q, we will have that $K_q \geq k$ since more than one track may have importance equal to the splitting level Z_q.

According to the algorithm, it is required that the particles arrived at the detector will never be discarded. In this view, when a track reaches the detector, the intersection point between the track and the detector surface is automatically added to the collision points (or states) of the track itself. The importance of the point, and therefore the importance of the track, is automatically set to the numerical infinity. In this way there would never be a trace with greater importance. Moreover, adding to the track the point of intersection with the detector has a twofold advantage: in the first place, it allows enhancing the number of tracks that reach the detector by considering also those that cross it without colliding. Secondly, the tracks that have reached the detector will be at least split starting from their intersection with the detector, and not from points inside it. By adopting this expedient, it is possible to avoid the duplication of the contributions of the tracks to the score (e.g. the length travelled by the particle across the detector, if the track length estimator is used) during the splitting phase.

The splitting step

At each iteration, K_q particles are discarded and then re-sampled. For each deleted particle, one of the $N - K_q$ remaining tracks is randomly selected to be split. The probability distribution that governs this selection is uniform therefore all the tracks have the same probability to be chosen. Let $\alpha = (P_1, ..., P_{N_s})$ be the selected particle. The state in which it will be split is determined according to:

$$P_{split} = \inf\{i \in [1, N_s] : I(P_i) > Z_q\} \tag{3.25}$$

It means that the emission point of the particle history to be re-sampled is defined as the first point of the selected track having importance greater than the splitting level Z_q. Then, starting from the splitting point, the track is sampled according to an analog transport. The working principle of AMS is illustrated in Figure 3.1.

At each iteration, in order to provide an unbiased estimate of the response, the particle re-sampling is taken into account by introducing the weight W_q. In particular, W_q is equal for all the particles, and therefore it can be seen as a global weight associated with the entire particle batch. Considering the generic iteration q, the weight W_q is defined as the probability that a track is not discarded, namely,

$$W_q = 1 - \frac{K_q}{N}. \tag{3.26}$$

Therefore, the weight of the particles at the end of the iterative process will be:

$$w_q = \prod_{i=1}^{q} W_i = \prod_{i=1}^{q} 1 - \frac{K_i}{N}. \tag{3.27}$$

The iteration process will be stopped when, at the q-th iteration, $N - K_q + 1$ particles will reach the detector or, when the splitting level will assume a value equal to the numerical infinity. Finally, the response of interest is estimated by means of the unbiased estimator $\bar{\eta}_{AMS}$, which is defined as:

$$\bar{\eta}_{AMS} = w_q \cdot \bar{\eta}_{MC} \tag{3.28}$$

where $\bar{\eta}_{MC}$ is the value of the sample average evaluated by means of the standard Monte Carlo estimators.

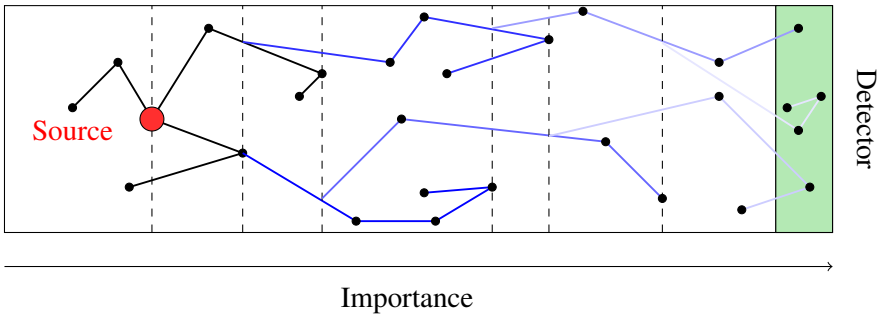

Fig. 3.1 Illustration of the Adaptive Multilevel Splitting algorithm [16]

Branching tracks

The description of the AMS algorithm, for the sake of simplicity, has been focused on "simple" tracks. That is to say that branching like the one produced by fission reactions, has not been accounted for. Nevertheless, AMS is able to solve this type of problems as well. The branching tracks are treated by AMS as single particle histories which are internally divided into several semi-tracks, called branches. In particular, for each track we can distinguish a parent branch, which is originated at the source, and different secondary branches produced by means of interactions with the crossed medium. The importance of the track is defined as the maximum value between the importance of its branches.

When a branching track is selected for splitting, all the branches whose importance is larger than the splitting level Z_q will be duplicated. More in detail, if the selected track has l branches, of which only m of these have $I_{branch} > Z_q$, m splitting points will be defined and consequently, m distinct branches, constituting the new track, will be sampled [15]. Each of the m slitting points, according to Equation (3.25), is defined as the first state of each branch whose importance is larger than Z_q. The other parts of the algorithm remain unchanged respect to what was previously seen for non-branching tracks.

Pros and cons

The main advantage of AMS is its robustness due to the possibility of using any importance function. On the other hand, unlike other variance reduction methods, it requires to keep the track data along the simulation, resulting in a increased memory footprint.

3.6 The Two-step method

The main idea of the Two-step method is to solve "fixed-source criticality calculations" as if they were standard shielding problems, thus handling separately the complexities related to the particles produced by fissions. In this way, it is possible to exploit the potentialities of variance reduction methods already widely tested and optimized for simple propagation problems. More in detail, the Two-step method consists of splitting the simulation in two main stages. The first simulation is devoted to the calculation of the fission source, i.e. the secondary neutrons produced by the fission reaction in the fissile material. While the second stage is responsible for the propagation of the particles from the emission point (both external and fission source) to the detector. This method is currently used at CEA to perform "fixed-source criticality calculations", so we decided to include it in the tests.

The application of this technique leaves the user with a certain degree of freedom since the first step can be carried out using either deterministic and Monte Carlo codes. In the following we will restrict the discussion to the solutions actually adopted in the tests.

First step

The calculation of the fission source has been carried out by using a fixed-source criticality Monte Carlo calculation with the implicit capture, where the source has been defined as the external source of the original problem. The response of the simulation has been required to be equal to $\nu\Sigma_f\Phi$, that is the so called fission particles production density, or rather, the number of fission particle produced per unit time and per unit volume. The production density is defined as a function of the spatial coordinate, thus it has been calculated discretizing the spatial domain with a Cartesian mesh. Since the fission spectrum for the neutron re-emission is known, the production rate has been integrated over the entire energy domain and the dependence of the fission spectrum on the incident neutron energy has been neglected. The production density is clearly non-zero only in the fissile material.

The fission source, needed for the second step, is obtained renormalizing the production density by the product of the external source intensity times the K multiplication factor. K is obtained during the first stage calculation, since TRIPOLI-4 computes this value every time the the fixed-source criticality mode is selected. The K factor is defined as the ratio between the total number of particles produced by fission and the number of particles sampled from the source. We want to stress that the normalization of $\nu\Sigma_f\Phi$ is optional. It has been decided to use it because K, being a global parameter,

is generally estimated with a much better accuracy than the one of the production density (defined on a spatial mesh). In this perspective, we have thought that the normalization may contribute in reducing the uncertainty of the fission source and ensuring particle conservation.

Second step

The second stage consists in a fixed-source calculation in shielding mode with exponential transform (importance sampling). In such simulation, fission reactions are treated simply as captures and no fission particle is sampled. The source of the second step is defined as the sum of the real (external) source plus the fission source previously calculated. We should notice that the importance function needed for the second step has to be representative of the shielding problem only. Therefore, the contribution of fissions has not to be accounted for the importance calculation.

Approximations

One of the main advantages of Monte Carlo with respect to deterministic codes is that the result of the simulation converges precisely to the exact value. Using the Two-step method this is not true anymore. Potential sources of error are related to the uncertainties present in the fission source estimate. In particular we have to take into account the standard deviation of the K multiplication factor, the standard deviation of the production density $\nu\Sigma_f\Phi$, and the approximation involved in the adoption of the domain discretization. It is the user responsibility to insure a sufficient convergence of the first step calculation.

Concerning the simulations performed in this thesis, in order to reduce as much as possible the error introduced by the method, the first step of the simulations has been pushed further until reaching an uncertainty $\sigma\%$ (percentage relative standard deviation) smaller than $1 \cdot 10^{-2}$ in the estimate of the multiplication coefficient K, and smaller than $1 \cdot 10^{-1}$ in the estimate of the fission productions. One possible way to avoid the introduction of sources of error related to the domain discretization is storing the position in the phase space of the particle produced by fission events. This information might be used by TRIPOLI-4 like a fission source. This solution has not been investigated in the tests presented in this document.

Chapter 4

Importance map calculations

With "importance map" we refer to a representation of the importance variable in the whole spatial and energetic domain. The importance, as we have already seen, is a non-dimensional quantity representing the expected contribution that a neutron, at a given point in the phase space, may give to the score. All the variance reduction techniques of interest for the tests that we want to perform, namely the Exponential Transform, the Adaptive Multilevel Splitting method and the Two-step method, need an importance map in order to operate.

For the purpose of our study, we have tested three types of importance maps:

- IDT importance maps, obtained by solving the adjoint transport equation using the deterministic solver IDT (included in APOLLO-3);
- INIPOND importance maps, approximated by using the INIPOND module present in TRIPOLI-4;
- Geometrical importance maps, available only for AMS.

4.1 The IDT solver

IDT is a multidimensional, multi-group solver included in the APOLLO-3 code [11, 26]. It is able to solve the direct and the adjoint transport equations both in fixed-source and in criticality calculations [16]. The angular component of the flux is solved using the discrete ordinates method and the spatial domain is discretized using conformal Cartesian meshes. IDT is able to solve the spatial component of the flux by using nodal, finite difference and the short characteristics method with constant or linear approximation of the volume and surface fluxes. The solver is also equipped with different types of acceleration methods, useful to speed up the convergence of iterative calculations. In particular, we recall DSA, BPA, CMFD [2].

In addition to IDT, APOLLO3 contains other solvers such as TDT, MINARET, MINOS, PASTIS and NYMO [2]. APOLLO-3 provides an effective working environment in which the different solvers

can communicate. Furthermore, thanks to the validation and processing system for evaluated data GALILÉE, it is possible to generate appropriate multi-group libraries [27]. Among the APOLLO-3 functions, we recall:

- capacity to solve resonant cross-sections by means of the self-shielding formalism;
- capacity to relate multiple self-shielding and flux calculations on different geometries in order to optimize the calculation schemes;
- capacity to homogenize/condense fluxes and cross sections on coarser spatial and energetic meshes than the one used for the calculations.

4.2 INIPOND module

INIPOND is a module implemented for the first time in the 90's in TRIPOLI-3 [28]. It has been designed to pre-compute approximated importance maps to be used with the exponential transform method. This module has found large applications in shielding calculations along the years and it is still extensively used today. The advantage of having such a tool is the speed at which the map is computed: it is able to produce approximated solutions of the adjoint problem on a domain discretized in space and energy with a negligible computational time as compared to the simulation time of a Monte Carlo code. This module has been widely discussed in [14]. In AUTO mode, the one that has been tested in our work, INIPOND just requires from the user a spatial and energetic mesh discretization and the definition of one or more detectors. Detectors defined in INIPOND are not necessarily present in the physical model, since they simply act as fictitious particles attractors. They have to be defined in the spatial domain together with a β coefficient, quantifying their attraction strength. The importance in TRIPOLI-4 is approximated as the product of different contributions:

$$I(\vec{r},\vec{\Omega},E) = I_s(\vec{r},E) \times I_e(E) \times I_d(\vec{r},\vec{\Omega},E), \tag{4.1}$$

where $I_s(\vec{r},E)$ represents the contribution of the spatial importance, $I_e(E)$ the energetic contribution and $I_d(\vec{r},\vec{\Omega},E)$ the angular one [14, 15, 29]. The three components are computed using the equations:

$$I_s(\vec{r},E) = \exp\left(-\int_0^{dist(\vec{r},\vec{D})} ds\, K\vec{\Omega}_D \cdot \vec{\Omega}_0(\vec{r}+s\vec{\Omega}_D,E)\right) \tag{4.2}$$

$$I_e(g) = \frac{E^\alpha}{\beta+1}\frac{(E_g^+)^{\beta+1}-(E_g^-)^{\beta+1}}{(E_g^+)-(E_g^-)} \tag{4.3}$$

$$I_d(\vec{r},\vec{\Omega},g) = \frac{\Sigma_t(\vec{r},g)}{\Sigma_t(\vec{r},g)-K(\vec{r},g)\vec{\Omega}\cdot\vec{\Omega}_0} \tag{4.4}$$

where $dist(\vec{r},\vec{D})$ is the distance between the point $\vec{r}$ and the detector D, K is a coefficient that varies with the medium and the energy, $\vec{\Omega}_D$ the unit vector pointing towards the detector, $\vec{\Omega}_0$ the direction

defined by the vector $\frac{\vec{\nabla} I}{I}$. α is a coefficient given for each group, β is a coefficient used to set the strength of the biasing method increasing or reducing the attraction of a detector. (E_g^+) and (E_g^-) are respectively the upper and lower bound of the energy group g. In AUTO mode, the INIPOND module first computes the K coefficient for every material solving a Placzek-like slowing-down equation. Then it computes I_s for the whole spatial and energetic domain. The calculation of $\vec{\Omega}_0 = \vec{\nabla} I_s / I_s$ is performed by estimating the gradient using a finite difference approximation of the spatial importance.

During the first batches of the simulation, TRIPOLI-4 operates by default an adjustment of the importance map calculating some scale factor for each group in order to correct the map. This is done in order to:

- avoid the particle population explosion due to an excessive splitting;
- avoid excessive weight discrepancy between the statistical weights of the particles and the reference weight $\Pi(\vec{r}, \vec{\Omega}, E) = 1/I(\vec{r}, \vec{\Omega}, E)$.

4.3 Geometric importance

The AMS implemented in TRIPOLI-4 has the possibility of using a purely spatial importance function, i.e. an importance produced ignoring the energy dependence. During the simulation, the code is able to calculate on-the-flight the value of the particle importance [15]. The spatial (or geometric) importance is defined as a function of the distance from a given object of interest $\mathscr{S}$. This can be defined in various ways: $\mathscr{S}$ can be a point, a line, a ring, a plane, or a three-dimensional surface (plane, cylindrical or spherical). Given a generic point in the phase space $P = (\vec{r}, \vec{\Omega}, E)$, the importance function can be defined as follows:

- as "attractive": the importance increases as the distance from $\mathscr{S}$ decreases, i.e.

$$I_{\mathscr{S}}(\vec{r}, \vec{\Omega}, E) = \frac{1}{dist(\vec{r}, \mathscr{S})} \tag{4.5}$$

  The particles will therefore be "attracted" to the object;

- as "repulsive": the importance increases with the distance from $\mathscr{S}$, namely

$$I_{\mathscr{S}}(\vec{r}, \vec{\Omega}, E) = dist(\vec{r}, \mathscr{S}) \tag{4.6}$$

  so particles will be "pushed away" from the object.

Furthermore, AMS allows formulating the spatial importance taking into account preferential pathways and weighting the importance differently in different regions of the domain [15]. These solutions, have not been used in the tests presented in this thesis.

Part II

Tests and applications

Chapter 5

Problem and test description

Monte Carlo codes are commonly used in two main classes of problems: criticality simulations, oriented to obtaining the fundamental modes in reactor physics, and fixed-source problems, adopted in shielding calculations for the propagation of neutrons and photons. In this work we will investigate the application of variance reduction techniques to the Monte Carlo simulation of source-driven problems in the presence of fissile material. In order to accurately explore this application, a large number of tests has been performed on several different configurations. This chapter is entirely devoted to the presentation of the models and solutions adopted in the tests. More precisely we will present the models that have been used to perform preliminary studies on single-response problems, discussed in Chapter 6. The models and tests concerning simultaneous estimates on multiple detectors will be discussed later on in Chapter 7. We will present the main ideas and hypotheses under which the models have been designed, the configurations adopted to represent the reactor core, the structure of the work, and the solutions used to produce importance maps. We will often make reference to this section, recalling the models hereby introduced.

5.1 Problem description

5.1.1 Model definitions

The variance reduction techniques have been applied at first to simple toy-models, easy to implement and representative of the problems related to the reactor core loading. Particular attention has been paid in order to develop toy-models sufficiently "hard" to be simulated to require the use of variance reduction techniques. If the event of interest for the problem is not sufficiently rare, it would not be possible to fully appreciate the effectiveness of these methods. On the other hand, in order to be sure of having a reference solution for every tested configuration, the models have to be easy enough to be managed with the available computer resources just using standard Monte Carlo simulations (implicit capture, forced fission and population control techniques).

The models have been designed according to the following ideas:

Table 5.1 Media and isotopes adopted

MEDIA	ISOTOPES	CONCENTRATION [$cm^{-2}barn^{-1}$]
Air	^{16}O	$5.6437 \cdot 10^{-06}$
	^{14}N	$2.1231 \cdot 10^{-05}$
Steel	^{56}Fe	$8.4603 \cdot 10^{-02}$
Water	^{16}O	$3.3290 \cdot 10^{-02}$
	^{1}H	$6.6580 \cdot 10^{-02}$
Fuel	^{16}O	$4.4932 \cdot 10^{-02}$
	^{235}U	$8.4148 \cdot 10^{-04}$
	^{238}U	$2.1625 \cdot 10^{-02}$

- The models have been conceived in order to reproduce the physics of the reactor during the loading phase. Such configurations can be represented as a metal vessel containing water, a small number of fuel assemblies and a detector.

- In order to simplify the calculation of the importance maps, especially for the deterministic solver IDT, we used 2D configurations, i.e., infinite-height geometries. According to this, within the TRIPOLI-4 Monte Carlo simulations, reflective boundary condition have been imposed at top and bottom boundaries. The other boundaries of the domain have leakage boundary conditions.

- For simplicity, the models have been constructed so that they can be described with a 2D Cartesian mesh in which each cell contains an homogeneous medium.

- Each configuration contains a neutron source located within the reactor. The sources that are generally used for the reactor start-up have a high-energy spectrum. Accordingly, in our models we have decided to use sources emitting on the Watt spectrum.

According to this scheme, five different configurations have been produced. The media and the relative isotopic concentrations used for our models are described in Table 5.1. These test cases have been designed with the purpose of exploring the possible configurations that can be encountered during the reactor loading phase. Furthermore, by changing the relative positions of source and fissile media, it will be possible to investigate some peculiar behaviours of the variance reduction techniques. Let us now look more in detail at the toy-models.

Reference Model - Case A

The reference model that we have selected for our investigations is represented in Figure 5.1. It has a single fuel assembly placed in the corner of a square domain and a detector located at the opposite

corner. The domain is made of a water core surrounded by two concentric rings, one 6 cm-thick steel layer, and an outer 3 cm-thick air layer. The fuel assembly is made of a square block having a 6 cm side filled with pure Uranium Oxide at 3.7% enrichment. The detector is a simple square block made of water having 3 cm of side. Assembly and detector are placed respectively at 6 cm and 3 cm from the steel ring. The model has been designed with an overall side of 70 cm.

The source is a square of 2 cm of side placed at the center of the fuel assembly and made of the same fissile material. It is emitting with an isotropic Watt-spectrum and the total intensity is set equal to the arbitrary value $1 \cdot 10^{21}$ $\left[\frac{\text{neutrons}}{s}\right]$. The boundaries of the domain neighbouring with the air layer have leakage boundary conditions. Throughout this report we will refer to this model as to *Case A* or *Reference Model*.

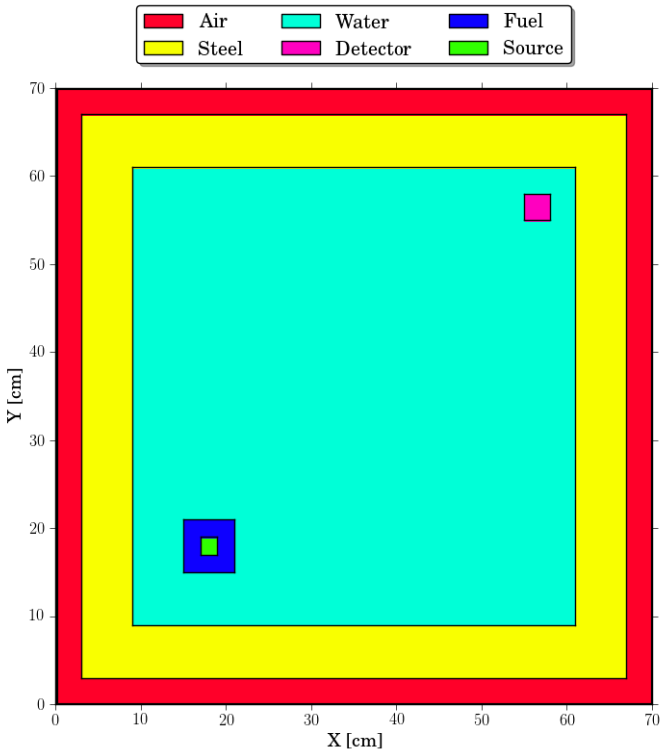

Fig. 5.1 Case A geometry - Reference configuration

Case B

The second model is a slight modification of the reference case. In the attempt of having a larger neutron flux attenuation between source and detector, we have designed the model by taking Case A and increasing the overall side length up to 1 m. The flux attenuation is a useful index in order to quantify the complexity of the model for a Monte Carlo simulation: the lower the neutron flux at the detector as compared to the source intensity, the lower also the number of random walks that

will score at the detector in a conventional Monte Carlo simulation. In order to probe the variance reduction techniques performances, the flux attenuation has been brought from 5 decades in Case A, up to 7 decades, in Case B. Concerning all the other dimensions are kept unchanged with respect to Case A.

Case C

This variant has been thought in order to observe the effect of having a neutron source placed far from the assembly. As compared to the reference case, in this configuration the fuel assembly is placed at the center of the core, while the source position and other dimensions remain unchanged. The model is shown in Figure 5.2. Neutrons must travel a certain distance in water before reaching the fissile material. This should make the model very challenging from the point of view of the variance reduction methods.

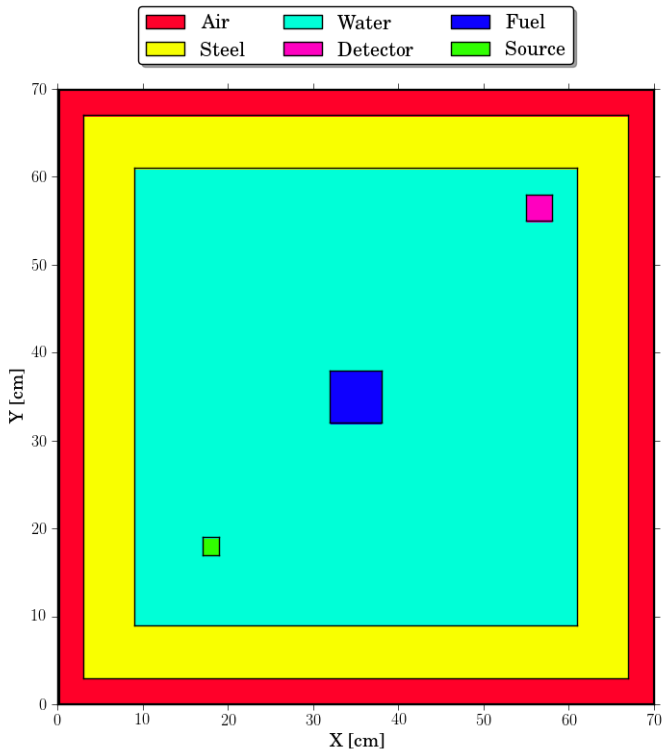

Fig. 5.2 Case C geometry

Case D

This configuration is a variant of the previous one: the assembly is moved near the top-left corner. More precisely, its left face is located 6 cm far from the steel edge and 6 cm under the detector in term of y-coordinate. The model is represented in Figure 5.3. In such configuration, with respect to the

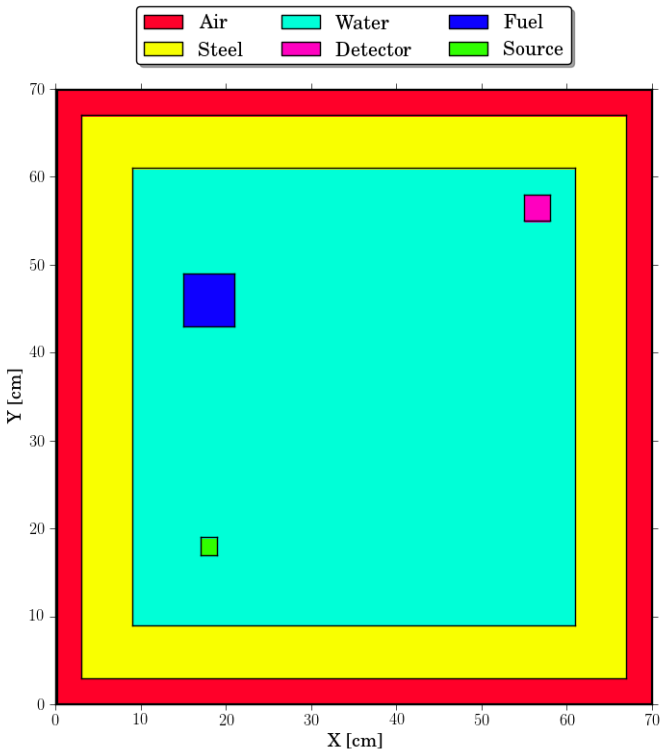

Fig. 5.3 Case D geometry

previous one, the assembly is no more placed along the diagonal, so neutrons emitted by the source must follow a different path with respect to the one connecting the source and the detector in order to induce fissions.

Case E

This model is characterized by a displacement of the source with respect to the reference case. While the assembly position is kept unchanged, the source has been placed inside the water: it has been moved along the main diagonal towards the center of the core. Its center has been placed 6 cm towards the right and 6 cm upward with respect to Case A. This source location has a special significance since, as we will see later, it coincides with a local minimum of the importance maps produced with IDT.

5.1.2 Structure of our analysis

The main objective of the tests is to assess whether the variance reduction methods are able to provide unbiased estimates and to establish whether they succeed in increasing the performances of Monte Carlo simulations. We will study the effectiveness of these methods, and their sensitivity with respect to the quality of the importance map. In this respect, we will perform several simulations monitoring

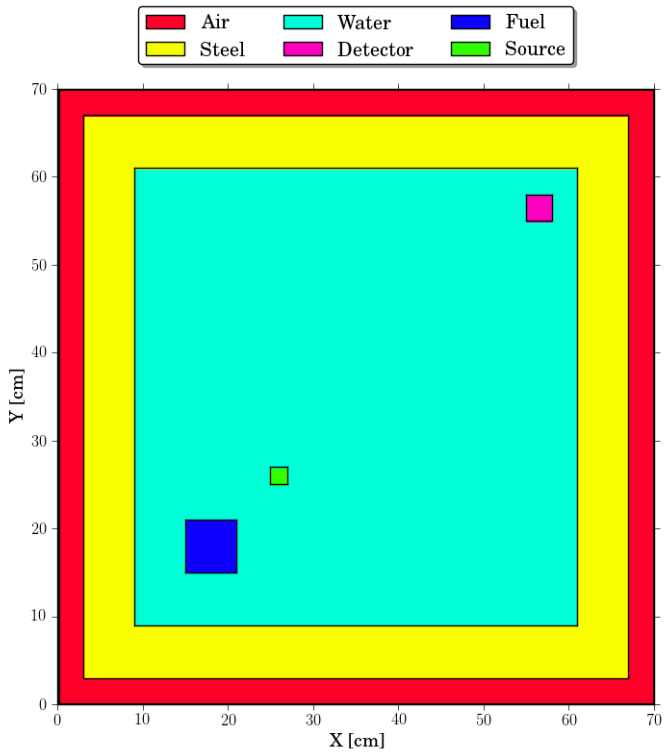

Fig. 5.4 Case E geometry

the neutron flux at the detector and the multiplication factor. In the following we will denote by "Fast flux" the neutrons having energy included in the range $20 - 6.25 \cdot 10^{-7}$ MeV, and by "Thermal flux" the ones in the range $6.25 \cdot 10^{-7} - 1 \cdot 10^{-11}$ MeV. In order to evaluate neutron flux we adopted a Track estimator (based on the length of the trajectories in the crossed medium). This estimator is expected to be more effective in cases where we need to score on a medium with a small optical length, i.e., medium having a characteristic dimension which is small with respect to the mean free path of the particles crossing it (see Section 2.2.3).

The K multiplication factor, which must not be confused with the k eigenvalue, is the average number of neutrons produced by fission per random walk sampled. To estimate this value, it has been decided to adopt "K STEP" as a reference estimator. K STEP is defined as the ratio between the particles emitted by fission over the total number of source particles.

For each of model considered in our study, we used the following general approach:

- A first standard simulation, using implicit capture and population control, is run in order to obtain reference values.
- We run several simulations by adopting the variance reduction methods under analysis, namely the exponential transform, the AMS and the Two-step method. Each has been tested using

different types of importance maps. The choices in terms of importance maps are discussed separately in Section 5.2.

- Whenever one of the previous simulations (with variance reduction) produces unbiased results, it is useful to quantify its performances. For this purpose, the simulations that have given proper results, together with the reference one, are repeated on a single-thread, on the same machine, and in the same identical "environmental" condition. This expedient allows us to evaluate a Figures of Merit (as defined in the following pages), quantifying the simulation performance, which is not influenced by the type of CPU or by other external factors.

In order to compare the results, establish their unbiasedness and quantify the performances, the following guideline has been used:

- The first goal of the test is to demonstrate that the estimate of the neutron flux obtained with the selected variance reduction method is not biased, namely, that the result is coherent with the reference one. For this purpose, we have used a simplified version of the *Welch's t-test*. In order to verify the coherence of two Monte Carlo results, we evaluate the difference between the two estimates, and then we divide this number by its standard deviation. For example, the Welch's t-test for flux estimates can be formulated as:

$$\delta = |\phi_1 - \phi_2|, \tag{5.1}$$

$$\sigma_\delta = \sqrt{\sigma_1^2 + \sigma_2^2}, \tag{5.2}$$

$$\mathrm{Q} = \frac{\delta}{\sigma_\delta}, \tag{5.3}$$

where Q expresses how many times the flux difference δ is contained within its standard deviation. In our application, Q is used to quantify the "quality" of the results estimated with variance reduction methods with respect to reference ones. If Q is smaller that 3, the two results are coherent within 3 standard deviations; if it is larger, we say that the flux estimate of the simulation with variance reduction is "biased". More specifically, the test is considered passed if both thermal and fast flux are coherent.

For the Welch's t-test to be effective, it is essential that the two flux estimates (the reference and the one with variance reduction method) are sufficiently well converged. The σ_δ must be sufficiently small in order to appreciate any bias in the simulation. The smaller is σ_δ, the smaller is the confidence range in which the δ can be accepted. For this reason, it is mandatory to have for each case of study a reference simulation calculated with a sufficiently good precision.

- If the results are coherent, the next stage consists in quantifying the performances obtained by adopting the variance reduction method. For this purpose we define the Figure of Merit (FOM)

as

$$FOM = \frac{1}{\sigma^2 t}. \tag{5.4}$$

FOM is defined as the inverse of the product between the variance of the estimate σ^2 and the computational time t of the simulation. The computational time varies proportionally to N, the number of simulated particle, for N sufficiently large to smooth out the discrepancy between the time needed to simulate a particle history. On the other hand, the variance σ^2 is proportional to the inverse of the number of particle histories N. The Figure of Merit is therefore a quantity independent of the number of histories simulated. The larger the FOM, the better will be the performance of the Monte Carlo simulation. In our evaluations we adopted as variance the square of the relative standard deviation of the total flux estimate. This choice allow us to obtain a FOM value which is independent of the magnitude of the neutron flux. The ratio between the FOM of the simulation with variance reduction and the FOM of the standard simulation expresses how many times the former is faster that the latter. We define this value as FOM GAIN. When, due to the limited computational resources, it has not been possible to evaluate FOM values in the same environmental condition (single-thread, same hardware), the presence of uncertainties has been stressed.

- As last point it is important to analyze the quality of the estimate of the K multiplication factor. The same analysis in term of coherence test and FOM has been performed on the estimates of K.

5.2 Importance maps parameters

Throughout the tests, with the aim of being as much complete and systematic as possible, it has been decided to use several types of importance maps. In particular, the maps have been produced by using the IDT solver, the INIPOND module and the geometrical maps generator of AMS. The purpose of this section is to recall the parameter choices and the settings used to produce the importance maps.

IDT Importance Map

For each toy-models, the deterministic solver IDT has been used to calculate four different types of importance maps:

- Map I: Reference map, produced using an anisotropy order equal to 3 and a relatively high spatial discretization made of about 200×200 cells;
- Map II: The second map has been produced using a less refined mesh (about 100 cells per side) with respect to the previous one;
- Map III: The third map uses the same spatial discretization of Map I but with self-shielded cross sections;

- Map IV: The last map has been obtained increasing the anisotropy order up to 7.

All the maps are produced using a 281-groups energy discretization and a product-type Chebyshev-Legendre quadrature formula with 64 angular directions. The calculation has been carried out using the step short characteristics method [11]. Each map has been calculated imposing a tolerance equal to $1 \cdot 10^{-6}$ on the errors of the iterative process.

INIPOND Importance Map

The INIPOND maps have been calculated using the AUTO mode. They are produced using a uniform grid refinement made by square cells of 1 cm of side, a 4-groups energy discretization, and a detector β factor equal to 0.8 (corresponding to a quite strong particle attraction).

Geometric importance maps

As for the geometric importance maps, these are produced by means of a routine present in the AMS. The maps have been defined as “attractive” with respect to a line passing through the center of the detector. In this way it has been possible to produce a maps representative of the symmetry of the models.

Chapter 6

Single-response tests on toy-models

In the present chapter we want to assess the effectiveness of the variance reduction methods in analysis, namely, the Exponential Transform, the AMS and the Two-step technique. At first, we will test the Two-step technique, which, being the reference method, will be used to perform some benchmark calculations. Successively, by considering the toy-models one by one, we will test the exponential transform and the AMS. Finally, we will summarize the most important results and we will draw the conclusions.

6.1 Two-step method

The Two-step technique is the method currently used at CEA for shielding calculations in presence of fissile material. It is hereby adopted in order to assess its performances and show its main characteristics. It has been decided to test the Two-step technique on some selected cases among the toy models presented in the previous chapter. We have chosen:

- Case A;
- Case B, in order to appreciate the potential of the method in terms of performances;
- Case D, because it presents the assembly in the farthest position from the source.

The obtained results with the Two-step method can be observed in Tables 6.1 and 6.2. FOM values are calculated by considering the computational time spent solving only the second step of the calculation (which is shown in the "time" column).

Looking at the first table we observe that all the results obtained are unbiased. Each Two-step simulation shows a value of the parameter Q lower than 3, that is to say that the neutron flux estimate is consistent with the reference (denoted by "REFERENCE MC" in the table). What is most striking is the magnitude of the performances of this estimate (Table 6.2). The values of the FOM GAIN are so high to make the calculation time of the second stage practically irrelevant respect to the one spent on

Table 6.1 Toy models - Two-step method results - Neutron Flux comparison

Case	Sim.	Fast Flux			Thermal Flux		
		Mean	PRSD [%]	Q	Mean	PRSD [%]	Q
A	REFERENCE MC	6.276E+16	4.91E-01	-	1.450E+17	6.38E-01	-
	TWO-STEP	6.322E+16	4.01E-02	1.49	1.466E+17	4.09E-02	1.72
B	REFERENCE MC	2.541E+14	3.40E+00	-	4.687E+14	4.92E+00	-
	TWO-STEP	2.550E+14	1.39E-01	0.10	4.865E+14	3.35E-01	0.77
D	REFERENCE MC	3.926E+16	6.32E-01	-	9.072E+16	8.10E-01	-
	TWO-STEP	3.937E+16	8.66E-02	0.42	9.038E+16	8.64E-02	0.46

Table 6.2 Toy models - Two-step method results - Figure of Merit comparison

Case	Sim.	Total Flux	PRSD [%]	time [s]	FOM	FOM GAIN
A	REFERENCE MC	2.164E+17	8.73E+00	8771	1.497E-06	-
	TWO-STEP	2.125E+17	9.86E-01	561	1.834E-03	1224.9
B	REFERENCE MC	6.097E+14	2.62E+01	188894	7.707E-09	-
	TWO-STEP	7.287E+14	1.73E+00	543	6.122E-04	79437
D	REFERENCE MC	1.232E+17	9.86E+00	7491	1.373E-06	-
	TWO-STEP	1.276E+17	1.39E+00	532	9.703E-04	706.68

the first step. As it has been already reported in [16], the coupling between IDT maps and TRIPOLI-4 in shielding problems is able to give extremely high performances. The simulations converge quickly in the flux estimate and reach extremely low uncertainty values.

However, we should notice that one of the limiting factor of this method is the need to compute the fission source with a sufficiently good accuracy. This precision is necessary if we do not want to introduce any bias in the simulation. The calculation of the first step turned out to be trivial for the standard Monte Carlo code in cases A and B, where the fissile material is located near the source. In models like case D, having the assembly placed far from the source, the estimate of fission productions becomes much more complicated. In such case, only a small part of the particles emitted from the source is able to reach the assembly. Accordingly, the calculation time of the first step of Case D has been much larger than for cases A and B.

6.2 Tests of the exponential transform

The section is devoted to the tests performed by using the exponential transform variance reduction method. We will simulate each toy-model presented in Chapter 5 individually, and we will discuss the main results.

6.2.1 Case A

The first model that we have studied is Case A. The exponential transform has been tested using as input several types of importance map presented in the previous chapter, namely:

- Four different types of importance map produced with IDT;
- An importance map produced with the INIPOND module.

Figure 6.1 shows the Map I produced by IDT at two different energy groups, the first one corresponding to energies in the range $4.9659 - 4.0657\ MeV$ and the second in the range $2.5 \cdot 10^{-09} - 1.0 \cdot 10^{-11}\ MeV$. The other IDT importance maps will not be shown because presenting no perceptible variations with respect to Figure 6.1.

The fissile assembly gives a non-negligible contribution to the importance map. Figure 6.1(b) shows a increasing trend of the importance in the surroundings of the assembly. It means that thermal neutrons in such region are more important than those that move away from the assembly. In other words, thermal neutrons have a larger probability to reach the detector by giving fission reactions and producing neutrons with higher energy, than directly crossing the reactor and reaching the detector. In Figure 6.1(a) it can be seen how the importance distribution for higher energy neutrons is constantly increasing towards the detector. Consequently, neutrons, independently of their position, are more likely to reach directly the detector, than slowing down and giving fission reactions.

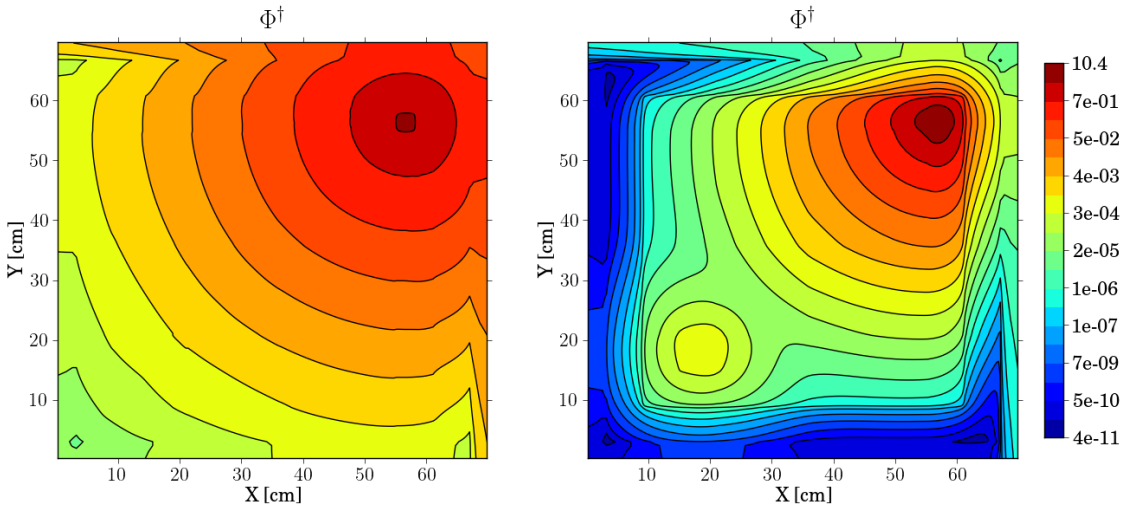

(a) IDT Importance Map I - Energy range $4.9659 - 4.0657\ MeV$

(b) IDT Importance Map I - Energy range $2.5 \cdot 10^{-09} - 1.0 \cdot 10^{-11}\ MeV$

Fig. 6.1 Toy model - Case A - IDT Importance Map I

It can be seen that the INIPOND map represented in Fig 6.2, does not display the contribution of fissions. In none of the energy group it is present any form of peak of importance driving particles

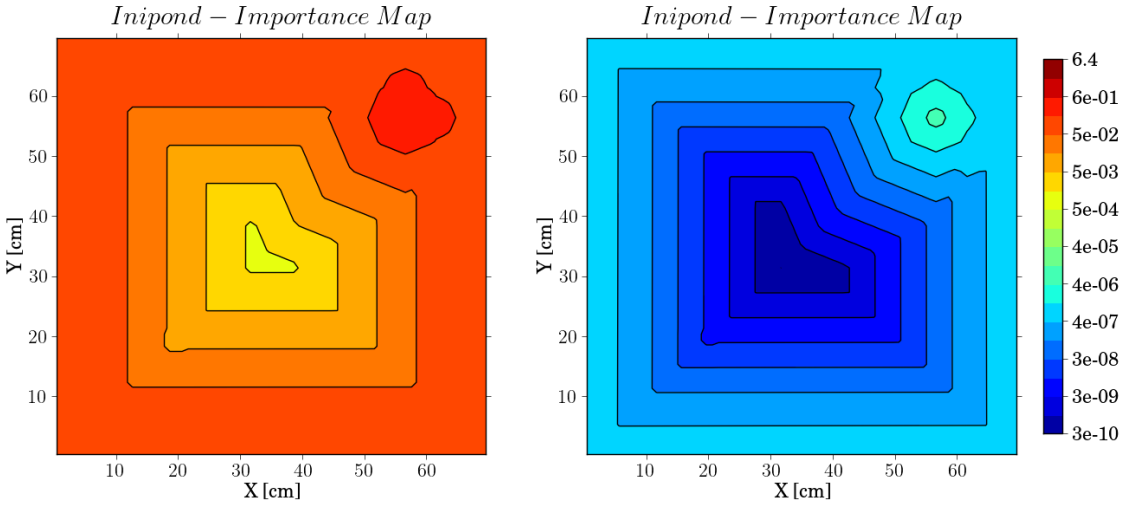

(a) INIPOND Importance map - Energy range $1.0 - 5.0 \cdot 10^{-3}$ *MeV*

(b) INIPOND Importance map - Energy range $6.25 \cdot 10^{-7} - 1.0 \cdot 10^{-11}$ *MeV*

Fig. 6.2 Toy model - Case A - INIPOND Importance map

to the assembly rather than to the detector. Looking at the gradients in the importance maps, IDT and INIPOND maps show two completely different "preferential path" for particles. Except for the fissile zone, the IDT map is similar to a geometrical one: importance grows approximatively with the increasing proximity to the detector. It means that the importance gradient "pushes" the particle directly to the target along straight paths. In the INIPOND map, instead, particle are driven first in the air ring surrounding the reactor, and then to the opposite side passing around the water core. The mean free path of neutrons in air is much larger than 3 cm (air layer thickness), therefore neutrons coming out from the steel, whatever their energy, will leak out from the domain. INIPOND, solving an algorithm based on the optical distances between points and detectors, is not able to properly represent this effect. The importance map thus produced represents the air ring as a viable path for neutrons.

Tables 6.3, 6.4, 6.5 show the results obtained accelerating the simulation of Case A model with the exponential transform method (ET). Table 6.3 contains the main results in terms of neutron flux at the detector. All the Monte Carlo simulations have been run in order to reach a given degree of accuracy in the estimates. The Q values expresses the quality of the results: in all the simulation this value in below the threshold 3, which means that none of them present any type of bias once converged.

Despite the accuracy of the final estimates, the convergence of simulations with the exponential transform is characterized by variance jumps. With "variance jumps" we refer to those rare random walks whose contribution to the final response is considerably different from the other contributions. This kind of event produces a "jump" in the mean value estimate and a steep increase of the variance. This phenomenon has been observed for every type of importance map considered in this work,

Table 6.3 Toy model - Case A - ET results - Neutron Flux comparison

Cases	Fast Flux			Thermal Flux		
	Mean	PRSD [%]	Q	Mean	PRSD [%]	Q
REFERENCE MC	6.276E+16	4.91E-01	-	1.450E+17	6.38E-01	-
ET IDT - MAP I	6.342E+16	1.94E+00	0.52	1.463E+17	1.40E+00	0.58
ET IDT - MAP II	6.291E+16	8.42E-01	0.23	1.459E+17	7.74E-01	0.57
ET IDT - MAP III	6.290E+16	7.43E-01	0.24	1.456E+17	5.62E-01	0.45
ET IDT - MAP IV	6.279E+16	1.00E+00	0.04	1.456E+17	8.37E-01	0.35
ET INIPOND	6.137E+16	2.15E+00	1.03	1.442E+17	9.92E-01	0.49

Table 6.4 Toy model - Case A - ET results - Figure of Merit comparison

Cases	Total Flux	PRSD [%]	time [s]	FOM	FOM GAIN
REFERENCE MC	2.164E+17	8.73E+00	8771	1.497E-06	-
ET IDT - MAP I*	2.098E+17	1.55E+00	3517808	1.177E-07	0.079
ET IDT - MAP II*	2.088E+17	7.88E-01	3516338	4.583E-07	0.306
ET IDT - MAP III*	2.085E+17	6.10E-01	3514084	7.641E-07	0.510
ET IDT - MAP IV*	2.084E+17	8.78E-01	3514966	3.687E-07	0.246
ET INIPOND*	2.056E+17	1.28E+00	2640904	2.310E-07	0.154
(*) FOM values computed on a different hardware configurations					

Table 6.5 Toy model - Case A - ET results - K STEP comparison

Cases	K STEP	PRSD [%]	Q
REFERENCE MC	6.172E-01	7.63E-02	-
ET IDT - MAP I	9.075E-01	7.46E-01	42.77
ET IDT - MAP II	8.706E-01	9.09E-01	31.97
ET IDT - MAP III	9.306E-01	1.21E+00	27.84
ET IDT - MAP IV	9.447E-01	1.47E+00	23.61
ET INIPOND	6.428E-01	6.04E-02	41.98

independently of its quality. The behaviour of these simulations is characterized by an irregular sampling of the fission events along the batches: the majority of them present no or few fission events, while some others contain a large number. In all simulations accelerated with exponential transform, the convergence of the flux estimate is characterized by an underestimation of the flux for many batches, due to the undersampling of the fission neutron contribution. When a batch containing many fission events is sampled, the value of the estimated flux undergoes a sharp increase and so does $\sigma\%$. This behaviour can be observed in Figure 6.3. The figure shows the convergence trend of the fast flux estimate using the exponential transform with IDT Map I. The figure compares the flux estimate at every batch with the result obtained with the reference Monte Carlo simulation once converged

(denoted by “Analog Flux” in the figure label). Each result is represented with its relative error bar corresponding to one standard deviation.

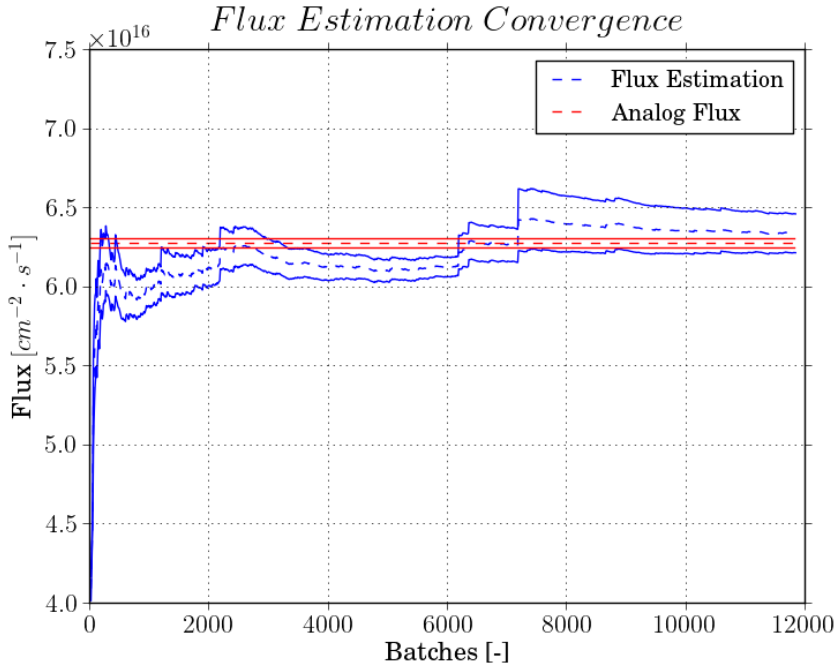

(a) Fast flux estimate - Mean value

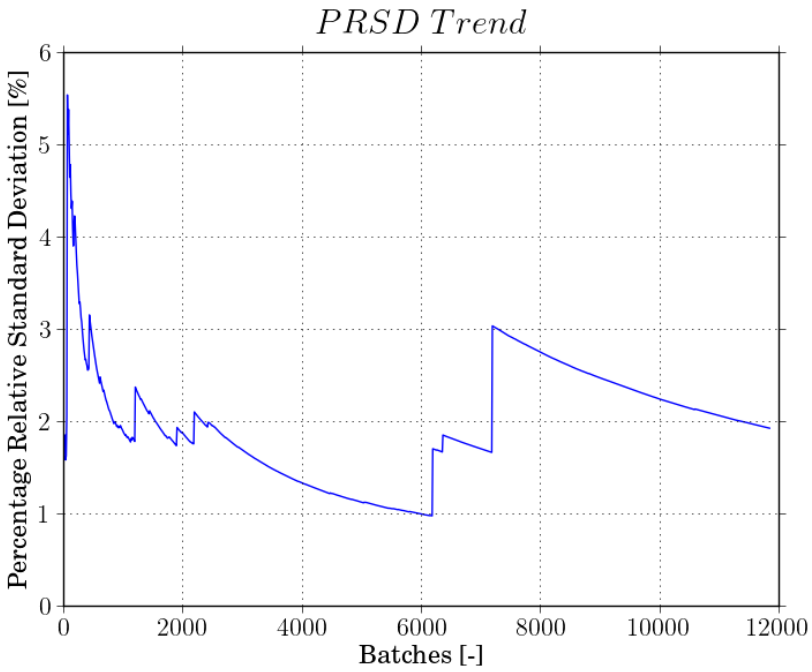

(b) Fast flux estimate - PRSD

Fig. 6.3 Toy model - Case A - ET - IDT Importance Map I - Fast flux estimate convergence trend

From the theory of the Zero-Variance game, we can expect that all particles should provide the same contribution to the score. This is not the case: the neutron flux generally underestimates the correct value and the simulation convergence is affected by extreme events generating variance jumps. In order to have small discrepancies between the particle batches, the correct sampling of fission events is fundamental in this class of problems.

Actually we are not exactly following the ideal zero-variance Monte Carlo game, because the collision kernel is left unbiased in TRIPOLI-4. Furthermore, we are using an importance map that is not the exact adjoint flux, because computed by means of a deterministic solver. We should consider that also small errors could produce artificial gradients in term of importance and thus modify erroneously the length of particle flight and the particle transport. An error in the importance map

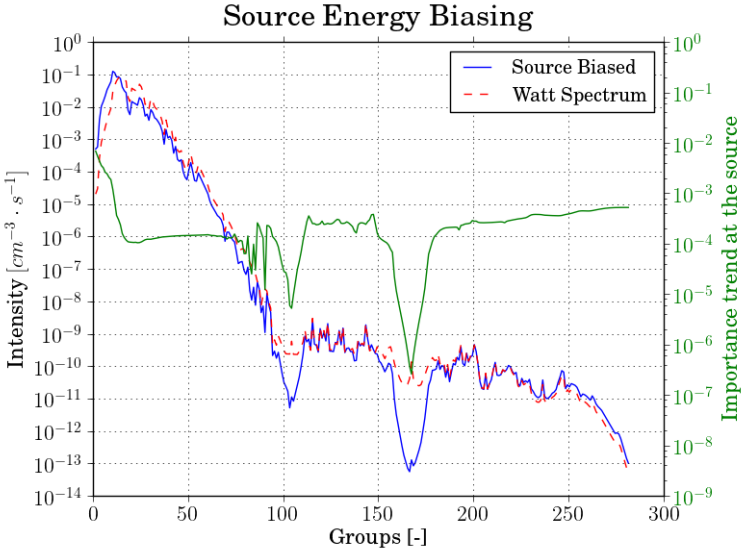

Fig. 6.4 Toy model - Case A - ET Importance Map I - Probability density function of biased source energetic spectrum

could also affect the source biasing, driving to a wrong sampling of particles. This effect can lead to a shift of the source emission spectrum (Watt spectrum) to a more energetic one. High energy neutrons are generally characterized by longer mean free paths, so they might fly too far from the assembly, in regions where it is difficult to come back to give fission reactions.

Figure 6.4 shows the biased source distribution from which particles are sampled. The biased profile is compared for every energy group with the original Watt spectrum distribution. We can see how, where the importance is larger, the biased source turns out to be larger than the original spectrum. When, on the other hand, the importance presents some depressions due to uranium resonances, the biased source spectrum also appears to be depressed. The figure expresses these variations on a logarithmic scale, so that small deviations can actually have large effects on the source energy sampling, thus interfering with the local transport of the particles. Nevertheless, the tests performed

on this class of problems have shown that IDT maps are reliable. We believe that the problem in the simulation is related to the method rather then to the quality of the importance map.

A side effect of the variance jumps can be seen in Table 6.4. We can notice that FOM GAINs are all smaller than the unity. This means that the simulations with exponential transform are slower to converge than the reference case, containing only implicit capture. The erroneous sampling of fissions leads also to a wrong estimate of the K multiplication factor. In Table 6.5 we can see how the value Q of the K estimate with exponential transform are larger than 3, so the estimate are not coherent. We can see that the irregular sampling of fission neutrons affects drastically the multiplication factor estimate.

6.2.2 Case B

The CASE B model has been designed in order to assess the effectiveness of the variance reduction methods on problems with a very strong flux attenuation. For this model we have tested only the IDT importance Map I, shown in Figure 6.5, and the one produced with the INIPOND module. The

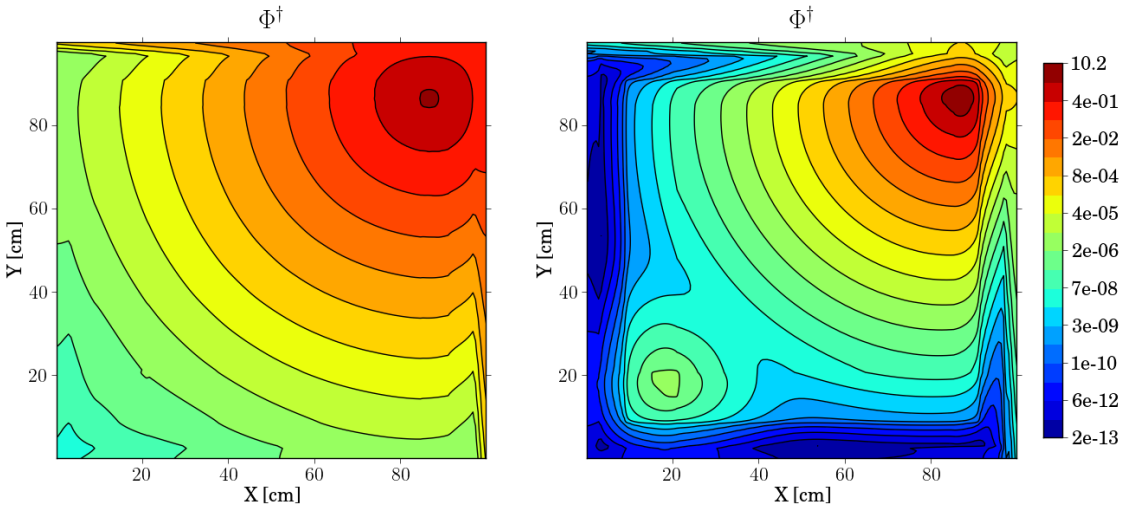

(a) IDT Importance Map I - Energy range $4.9659 - 4.0657\ MeV$

(b) IDT Importance Map I - Energy range $2.5 \cdot 10^{-09} - 1.0 \cdot 10^{-11}\ MeV$

Fig. 6.5 Toy model - Case B - IDT Importance Map I

INIPOND map is not shown since qualitatively identical to the one seen in Case A. The results of the simulations are reported in Tables 6.6, 6.7 and 6.8.

Dwelling on results obtained with the IDT Map I, the estimated flux shows an evident bias. The Q values suggest that the flux results are not coherent, the exponential transform simulation is therefore estimating a result which is different from the reference one. Looking also at convergence profile reported in Figures 6.6, we can see that the exponential transform simulation is still far from

Table 6.6 Toy model - Case B - ET results - Neutron Flux comparison

Cases	Fast Flux			Thermal Flux		
	Mean	PRSD [%]	Q	Mean	PRSD [%]	Q
REFERENCE MC	2.541E+14	3.40E+00	-	4.687E+14	4.92E+00	-
ET IDT - MAP I	1.777E+14	2.97E+00	7.55	3.453E+14	2.98E+00	4.88
ET INIPOND	2.681E+14	3.57E+01	0.15	5.653E+14	3.97E+01	0.43

Table 6.7 Toy model - Case B - ET results - Figure of Merit comparison

Cases	Total Flux	PRSD [%]	time [s]	FOM	FOM GAIN
REFERENCE MC	6.097E+14	2.62E+01	188894	7.707E-09	-
ET IDT - MAP I*	5.230E+14	2.97E+00	3519376	-	-
ET INIPOND*	8.334E+14	3.83E+01	2661386	2.555E-10	0.033
(*) FOM values computed on a different hardware configurations					

Table 6.8 Toy model - Case B - ET results - K STEP comparison

Cases	K STEP	PRSD [%]	Q
REFERENCE MC	6.176E-01	1.71E-02	-
ET IDT - MAP I	6.427E-01	6.01E-02	62.61
ET INIPOND	1.529E+00	5.68E+00	10.50

convergence, although it has been run with a sufficiently large statistics. The convergence trend is similar to the one seen in Case A, but the sampling of batches containing fission particles is much more rare as compared to the previous one. The behaviour is noisy: few particle batches contain huge numbers of fissions particles, while all the others are lacking. The characteristic time between variance jumps is so long that after a simulation time equivalent to 40 days of serial calculation the flux estimate has not yet converged.

The fission neutron spectrum of ^{235}U is quite similar to the Watt spectrum used in source particle sampling. The relatively small dimension of the assembly, its position centred with the source, and its distance from the detector are such that flux attenuation is similar for fission particles and for particles emitted by the source. Until fission have not been simulated, the simulations converge to the results corresponding to fission events being treated as sterile captures. This behaviour can be observed in Figure 6.6(a) since the ratio between the two estimates, with and without exponential transform, in the first batches is approximately the K multiplication factor. Observing the Figure 6.6(b) containing the percent relative standard deviation convergence profile of the fast flux estimate, we can see that the trend starts from a low value. We can state that, at the beginning of the simulation, almost every simulated batch has provided a similar contribution to the estimator of the flux at the detector. This behaviour means that exponential transform is converging fast to a given value, which, in this case,

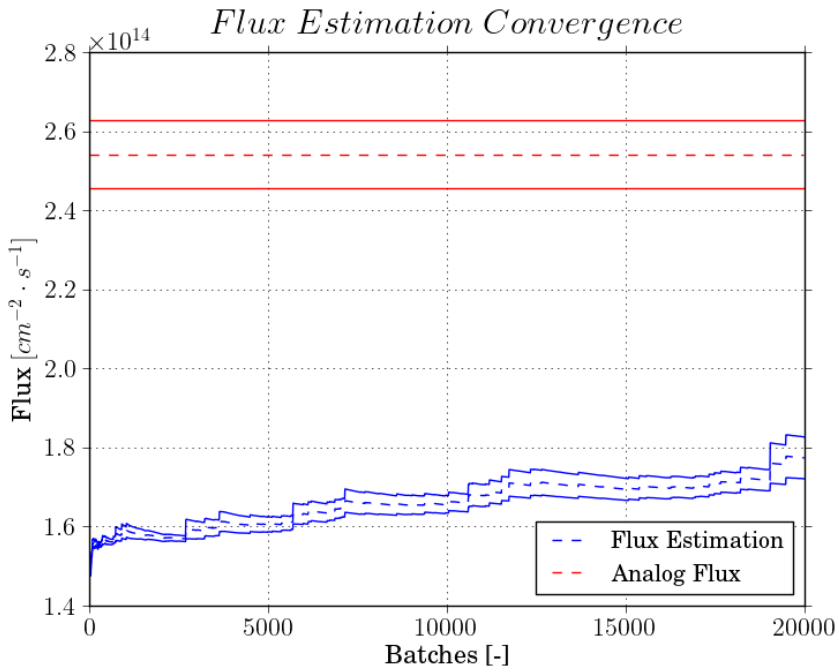

(a) Fast flux estimate - Mean value

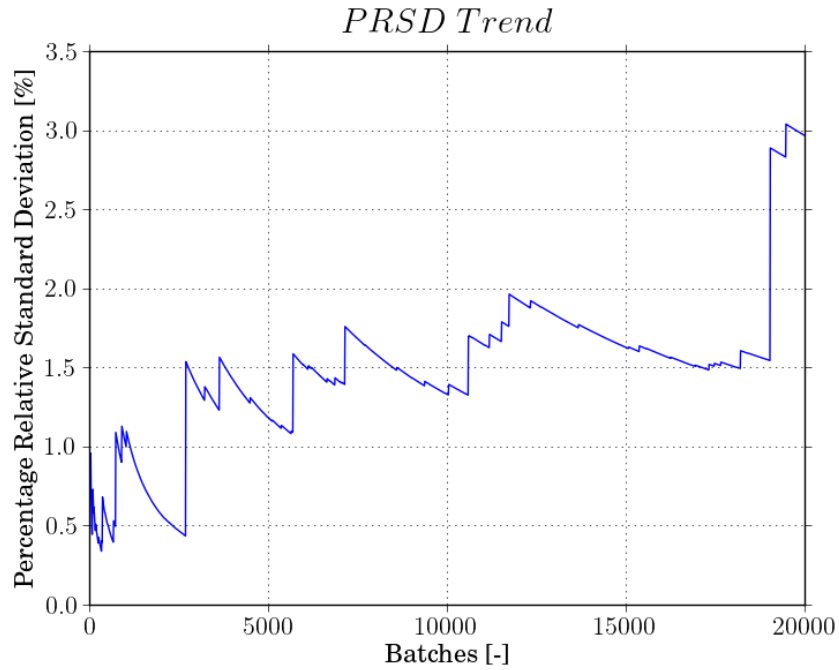

(b) Fast flux estimate - PRSD

Fig. 6.6 Toy model - Case B - ET - IDT Importance Map I - Fast flux estimate convergence trend

corresponds to the result of the simulation without any fission particle sampled. Moreover, the graph

shows that the convergence of the simulation is so deeply affected by variance jumps that the PRSD trend seems to increase rather than decrease.

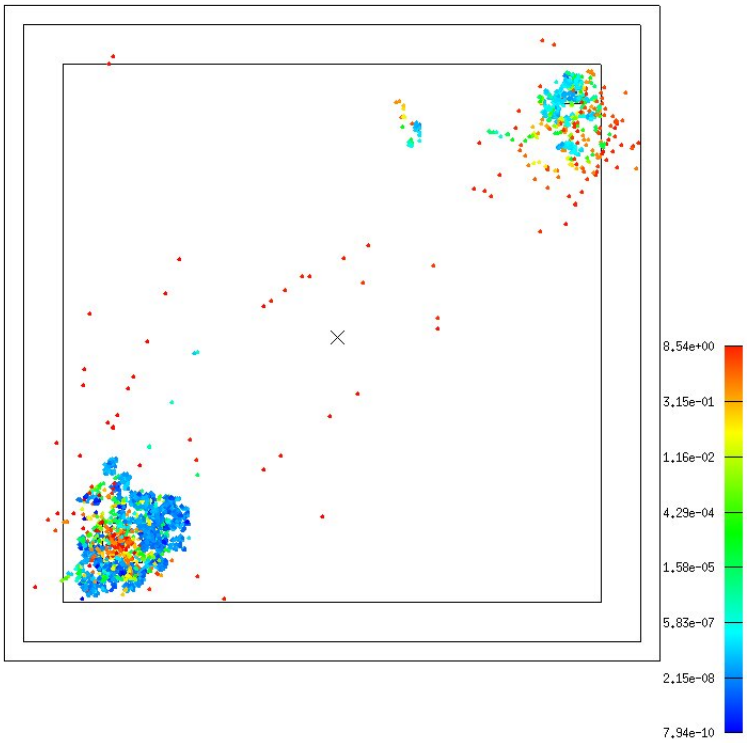

Fig. 6.7 Toy model - Case B - ET - IDT Importance Map I - Collision points and related particle energies [MeV]

Figure 6.7 shows the collision points of 100 neutron histories sampled in the exponential transform simulation using IDT Map I. We can notice that the fissile assembly seems to be populated only by high-energy neutrons. Considering that fission reactions occur almost exclusively with thermal neutrons, this behaviour can explain the undersampling of the fission particles in the simulation. The thermal particles that populate the region surrounding the assembly seem not to be able to come back to the assembly. This behaviour can hardly be explained since the importance gradient should favour their displacement towards the assembly. Secondly, it is interesting to note that neutrons arriving at the detector are those that have high energies, and that thermalize (decrease their energy) on site.

By looking at Table 6.6, we observe that the exponential transform simulation with the INIPOND map, despite the large statistics involved, yields results affected by high uncertainties. Comparing the FOM value of the simulation with the FOM of the reference, we can see that the INIPOND simulation is about 30 times slower. The convergence trend of this simulation presents large variance jumps affecting drastically the performances. INIPOND maps are produced and tuned to work well with

exponential transform but, as seen before, they are not always able to represent the physics of the model. In our current case, as seen in Case A, the INIPOND map is not able to guide particles along the right path. The exponential transform variance reduction method seems to be incapable of giving a regular sampling of the fission reaction, and this leads to a wrong estimate of neutron fluxes and of the K multiplication factors.

6.2.3 Case C

The Case C belongs to a different type of problems in which the source is placed outside the fissile assembly. Neutrons are not emitted in the fissile region, but they must cross part of the reactor to interact with it. In order to have a more complete overview of the problem, we have tested all types of importance map presented. Once again we just show the IDT Map I (Figure 6.8) because the four types of importance map are qualitatively similar.

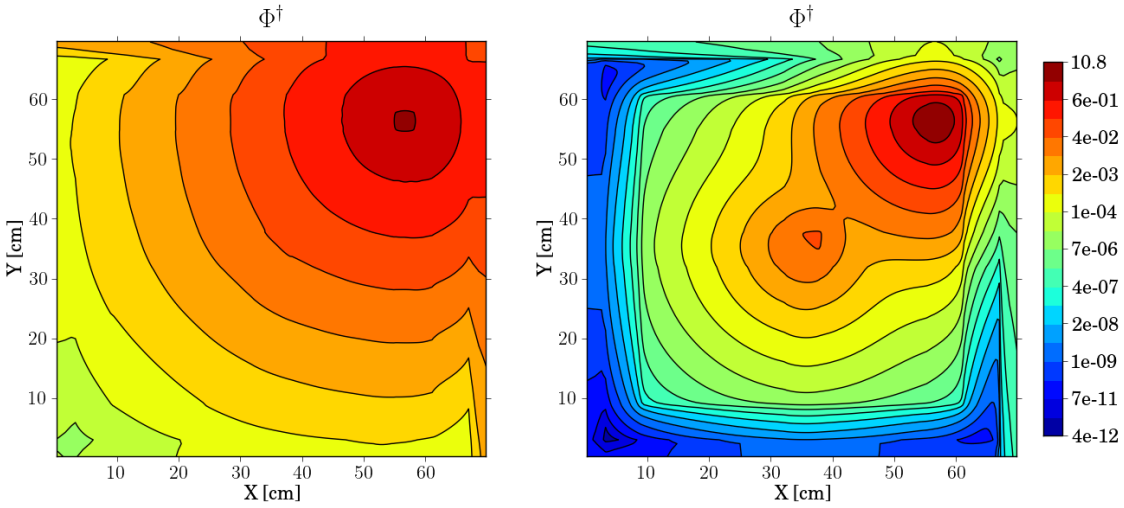

(a) IDT Importance Map I - Energy range $4.9659 - 4.0657\ MeV$

(b) IDT Importance Map I - Energy range $2.5 \cdot 10^{-09} - 1.0 \cdot 10^{-11}\ MeV$

Fig. 6.8 Toy model - Case C - IDT Importance Map I

The results are reported in Tables 6.9, 6.10, and 6.11. From Table 6.9 we notice that none of the results shows any relevant bias. All flux estimates obtained using IDT maps are coherent and the related Figures of Merit are larger that the reference. The convergence trend of the simulations are characterized by few and small variance jumps. Their presence in any case is not deeply affecting the simulation performances. This behaviour coincides with a more regular sampling of the fission events, providing a relatively constant number of secondary particles per batch. In Figure 6.9 we can observe the convergence trend of the thermal flux estimate at the detector using exponential transform and IDT Map I.

Table 6.9 Toy model - Case C - ET results - Neutron Flux comparison

Cases	Fast Flux			Thermal Flux		
	Mean	PRSD [%]	Q	Mean	PRSD [%]	Q
REFERENCE MC	5.255E+16	5.40E-01	-	1.378E+17	6.59E-01	
ET IDT - MAP I	5.218E+16	6.93E-01	0.81	1.353E+17	5.65E-01	2.08
ET IDT - MAP II	5.224E+16	4.69E-01	0.82	1.357E+17	4.12E-01	1.97
ET IDT - MAP III	5.229E+16	4.74E-01	0.69	1.356E+17	4.32E-01	2.01
ET IDT - MAP IV	5.231E+16	7.36E-01	0.51	1.360E+17	6.87E-01	1.42
ET INIPOND	4.983E+16	7.74E+00	0.70	1.233E+17	5.37E+00	2.17

Table 6.10 Toy model - Case C - ET results - Figure of Merit comparison

Cases	Total Flux	PRSD [%]	time [s]	FOM	FOM GAIN
REFERENCE MC	1.839E+17	9.01E+00	7675	1.605E-06	-
ET IDT - MAP I	1.861E+17	3.91E-01	36385	1.793E-04	111.710
ET IDT - MAP II	1.873E+17	4.59E-01	36762	1.292E-04	80.508
ET IDT - MAP III	1.866E+17	4.11E-01	35041	1.690E-04	105.271
ET IDT - MAP IV	1.869E+17	4.30E-01	36778	1.472E-04	91.705
ET INIPOND	2.116E+17	4.85E+01	14480	2.936E-08	0.018

Table 6.11 Toy model - Case C - ET results - K STEP comparison

Cases	K STEP	PRSD	Q	time [s]	FOM	FOM GAIN
REFERENCE MC	1.093E-02	6.26E-01	-	7675	3.321E-04	-
ET IDT - MAP I	1.101E-02	5.99E-01	0.85	36385	7.658E-05	0.231
ET IDT - MAP II	1.115E-02	1.24E+00	1.41	36762	1.776E-05	0.053
ET IDT - MAP III	1.103E-02	5.85E-01	0.98	35041	8.332E-05	0.251
ET IDT - MAP IV	1.107E-02	7.22E-01	1.29	36778	5.209E-05	0.157
ET INIPOND	1.621E-02	6.65E+01	0.49	14480	1.564E-08	4.71E-05

The graph 6.9(a) shows an underestimation of the thermal flux. In terms of Q this is small enough not to be considered as a bias. This behaviour can be observed in all the simulations that we have run using exponential transform. The FOM values of simulations accelerated with IDT maps attain values equal to one hundred times the FOM of the reference simulation. We can see that performances are quite similar for every type of IDT map adopted. Nevertheless, we can appreciate a small increase in terms of FOM passing form a relatively coarse map to more refined ones.

The INIPOND map generated in this case is qualitatively similar to the one of cases A and B, since fission is not taken into account. The effect of the wrong importance map provided by INIPOND results in a unbiased simulation, but having FOM GAIN value smaller than one. The INIPOND simulation converges with variance jumps and, as for previous cases, it shows an irregular sampling

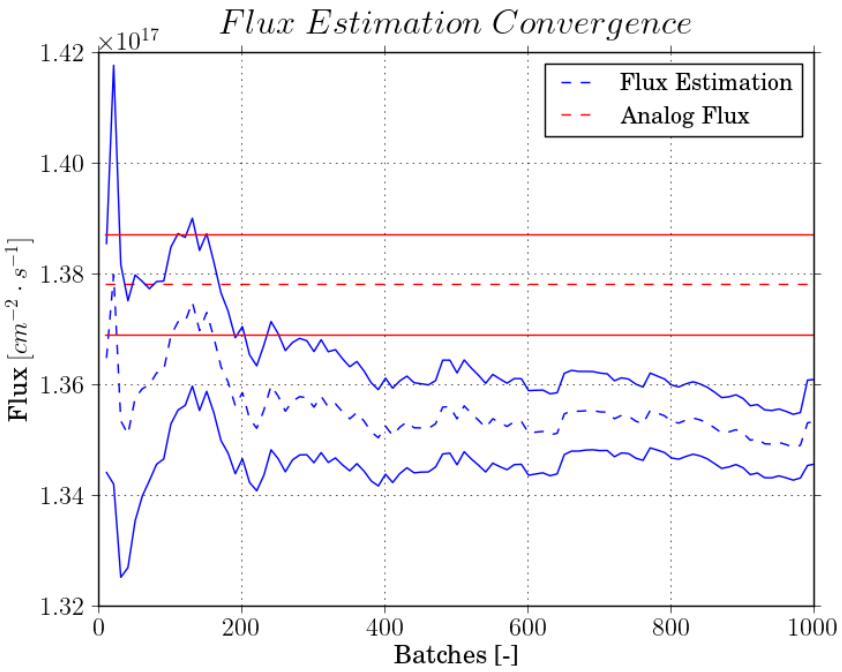

(a) Thermal flux estimate - Mean value

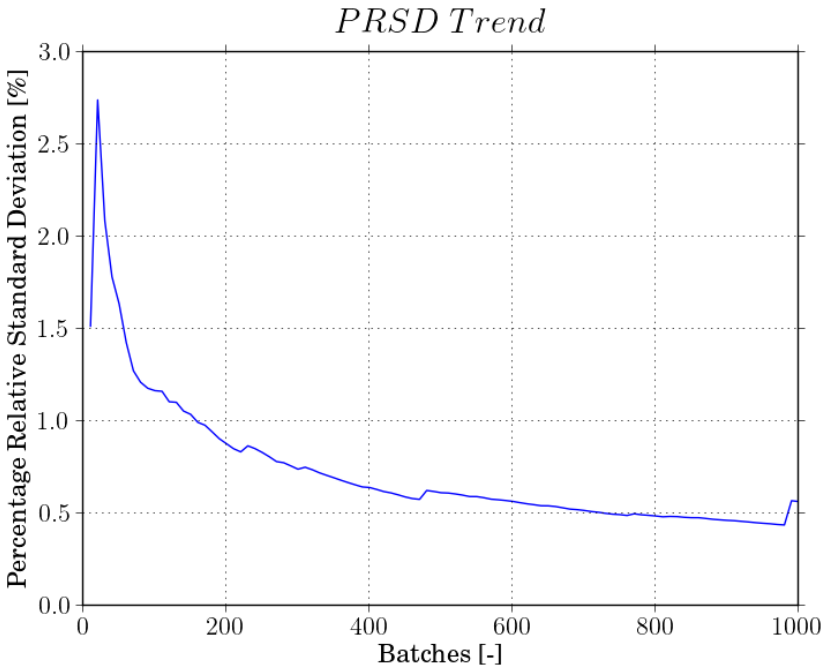

(b) Thermal flux estimate - PRSD

Fig. 6.9 Toy model - Case C - ET - IDT Importance Map I - Thermal flux estimate convergence trend

of fission events. The fission sampling is also relevant in the estimate of the multiplication factor. The regular sampling obtained with the IDT maps provides a good estimate of K. On the other hand, the

INIPOND simulation, having large fluctuations in the number fission particles, provides an estimate of K with a sigma too large to be compared with the reference. In the multiplication factor estimate, FOM values obtained with simulations with variance reduction are however lower than the FOM obtained with the reference simulation. Therefore, exponential transform seems not to be the most effective method to estimate the multiplication factor.

Looking at Tables 6.10 and 6.11, we want to focus on FOM GAIN values of the flux estimates and on the *PRSD* of the K estimates. We should observe a correlation between these values in the simulations run with the IDT maps. The PRSD values of the K estimates are related to the homogeneity of the fission sampling. We notice that when we have a more uniform sampling, thus lower PRSD, we could also observe smaller fluctuations in terms of $\sigma\%$ in the flux estimate, thus better performances. This behaviour suggests that having a number of sampled fissions per batch as uniform as possible is fundamental to obtain a better estimate of the flux and larger performances.

6.2.4 Case D

In the previous case the fissile assembly has been placed in the middle of the reactor. Most of the particles attracted by the detector will then naturally cross the assembly. In order to avoid this geometrical effect, in Case D the assembly has been moved near the top left corner of the domain. Particles providing fission reactions will have to follow a different path from the one joining the source to the detector. Figure 6.10 represents the importance map produced with IDT. The INIPOND map is not shown because almost identical to the one observed in Case A. Looking at Figure 6.10(b)

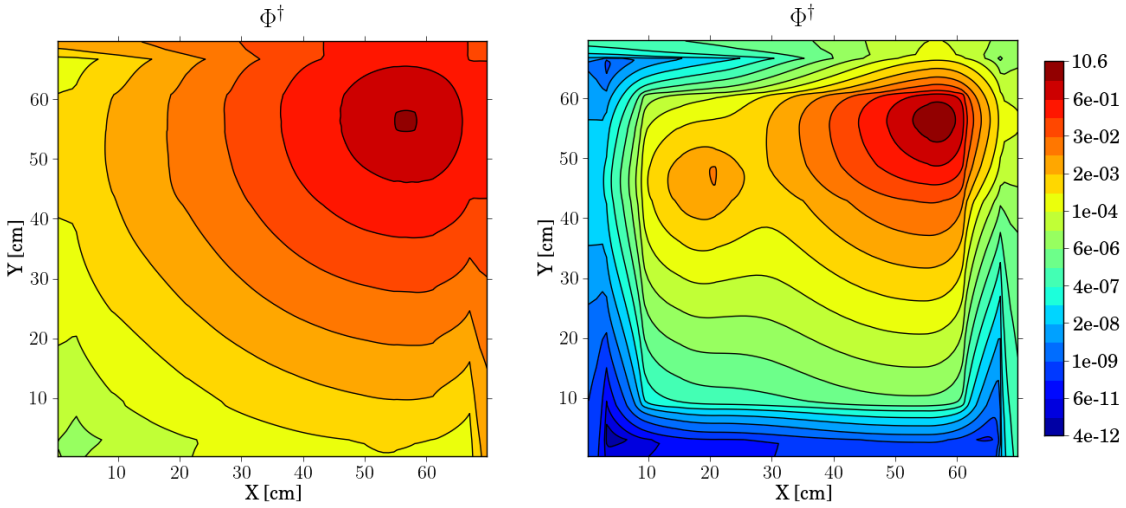

(a) IDT Importance Map I - Energy range $4.9659 - 4.0657\ MeV$

(b) IDT Importance Map I - $2.5 \cdot 10^{-09} - 1.0 \cdot 10^{-11}\ MeV$

Fig. 6.10 Toy model - Case D - IDT Importance Map I

we see that the fissile assembly affects a considerable part of the importance map for thermal neutrons.

This means that fission neutrons provide a non-negligible contribution for the detector. Results are shown in Tables 6.12, 6.13, and 6.14.

Table 6.12 Toy model - Case D - ET results - Neutron Flux comparison

Cases	Fast Flux			Thermal Flux		
	Mean	PRSD [%]	Q	Mean	PRSD [%]	Q
REFERENCE MC	3.926E+16	6.32E-01	-	9.072E+16	8.10E-01	-
ET IDT - MAP I	3.951E+16	4.06E-01	0.84	9.066E+16	2.43E-01	0.08
ET INIPOND	3.923E+16	4.91E+00	0.01	8.972E+16	2.25E+00	0.47

Table 6.13 Toy model - Case D - ET results - Figure of Merit comparison

Cases	Total Flux	PRSD [%]	time [s]	FOM	FOM GAIN
REFERENCE MC	1.232E+17	9.86E+00	7491	1.373E-06	-
ET IDT - MAP I	1.301E+17	5.70E-01	11151	2.764E-04	201.299
ET INIPOND	1.638E+17	3.03E+01	13273	8.187E-08	0.060

Table 6.14 Toy model - Case D - ET results - K STEP comparison

Cases	K STEP	PRSD	Q	time [s]	FOM	FOM GAIN
REFERENCE MC	4.971E-03	9.47E-01	-	7491	1.487E-04	-
ET IDT - MAP I	5.921E-03	1.12E+01	1.43	11151	7.163E-07	0.005
ET INIPOND	4.913E-03	6.33E+00	0.18	13273	1.883E-06	0.013

The flux estimates present a behaviour very similar to the one observed in Case C: the exponential transform simulation with the IDT importance map provides a correct estimate and converges with almost no variance jumps. The simulation is characterized by high performances and an almost uniform sampling of fission events. On the other hand, INIPOND importance map is unable to guide correctly particles along the right path, giving a convergence trend with several variance jumps. This results in a FOM GAIN value of the flux estimate smaller than 1. In Figure 6.11 we show the convergence trend of the thermal flux estimate in the simulation with exponential transform and the IDT importance Map I. We notice that the trend presents only one single variance jump localized in the first batches and than it converges as $1/\sqrt{N}$. The effect of the jump is sufficiently small not to affect the quality of the simulation itself. The flux estimate, in fact, remains coherent with the reference simulation along the whole convergence trend. Nevertheless, this can not ensure a priori that further jumps will not be encountered by pushing further the simulation.

Looking at Table 6.14 we can see that K STEP has been estimated with a low precision by the simulations with variance reduction.Also in this case we notice that the best way for evaluating the

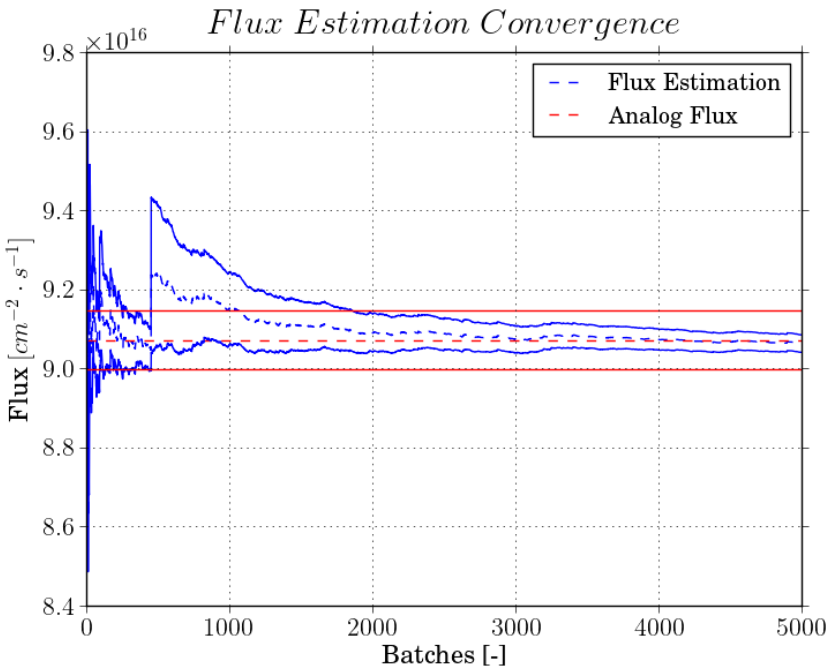

(a) Thermal flux estimate - Mean value

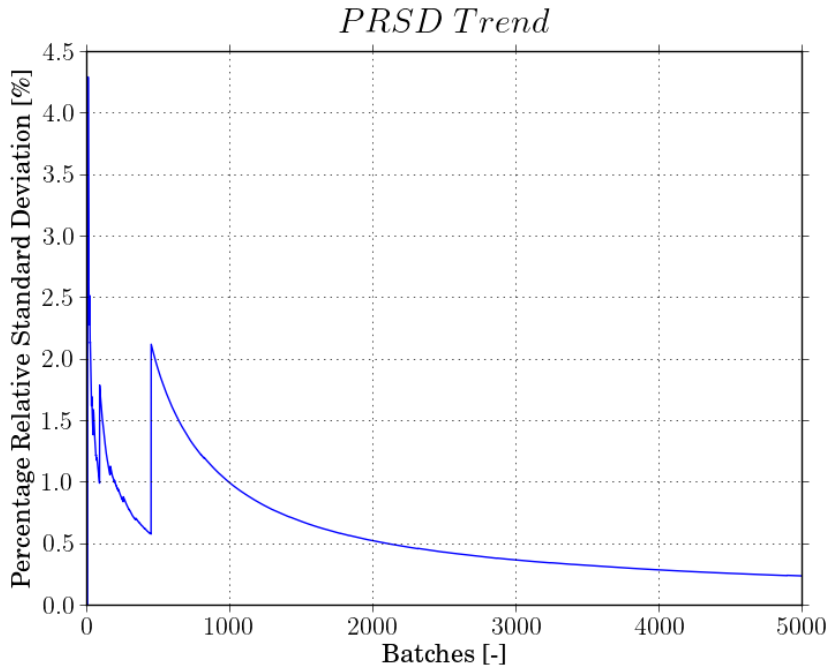

(b) Thermal flux estimate - PRSD

Fig. 6.11 Toy model - Case D - ET - IDT Importance Map I - Thermal flux estimate convergence trend

multiplication factor is the use of Monte Carlo simulations with just population control and implicit capture.

6.2.5 Case E

The Case E model has been proposed to test the limits of exponential transform variance reduction method when the assembly is not in contact with the source. We used the same model of Case A, but source particles have been emitted from a more centred location in the core. Looking at the trend of the importance map along the domain diagonal, represented on Figure 6.12, we notice the presence of a local minimum between the two peaks characterizing fissile assembly and detector. This is located approximatively at 6 cm on the right and 6 cm above the assembly. Its presence suggest a switching behaviour: part of the particles will be attracted by the detector, and the others by the assembly. In this point we have decided to localize the neutron source. The results obtained simulating the model with

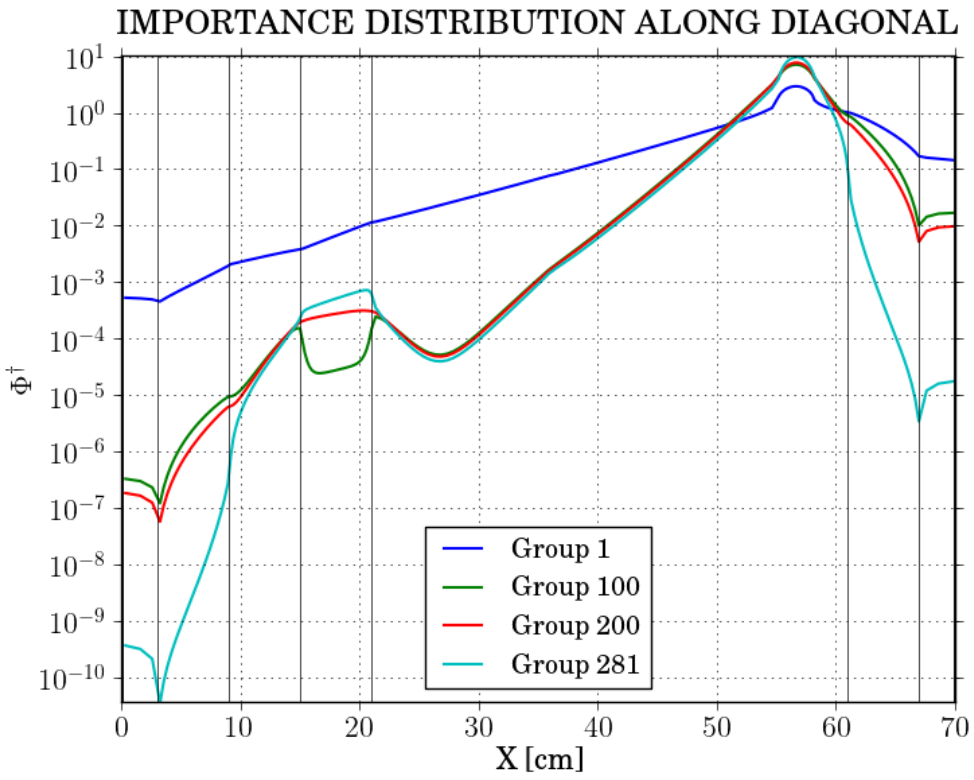

Fig. 6.12 Toy model - Case E - IDT Importance Map I - Distribution along the domain diagonal

the IDT Map I and the INIPOND importance map have been reported on Tables 6.15, 6.16 and 6.17.

We observe that the exponential transform is not able to provide a correct estimate of the neutron flux at the detector using the IDT importance map, while it succeeds to do so using the INIPOND map. The first simulation is affected by an under-sampling of the fission events and the few batches containing fission events are not sufficient to provide an unbiased value. This behaviour is evident in Figure 6.13 (a), where the convergence trend for the fast flux is reported. The variance jumps present in 6.13 (b) are produced by the few batches in which fission particles have been sampled. The

Table 6.15 Toy model - Case E - ET results - Neutron Flux comparison

Cases	Fast Flux			Thermal Flux		
	Mean	PRSD [%]	Q	Mean	PRSD [%]	Q
REFERENCE MC	2.125E+17	4.77E-01	-	5.307E+17	5.80E-01	-
ET IDT - MAP I	2.066E+17	5.79E-01	3.72	5.194E+17	5.70E-01	2.65
ET INIPOND	2.211E+17	4.05E+00	0.95	5.225E+17	5.96E-01	1.86

Table 6.16 Toy model - Case E - ET results - Figure of Merit comparison

Cases	Total Flux	PRSD [%]	time [s]	FOM	FOM GAIN
REFERENCE MC	7.689E+17	4.59E+00	10017	4.74E-06	-
ET IDT - MAP I	7.339E+17	1.11E+00	28522	-	-
ET INIPOND	7.055E+17	3.38E+00	18858	4.63E-06	0.977

Table 6.17 Toy model - Case E - ET results - K STEP comparison

Cases	K STEP	PRSD	Q	time [s]	FOM	FOM GAIN
REFERENCE MC	1.834E-01	1.52E-01	-	10017	4.29E-03	-
ET IDT - MAP I	2.260E-01	1.02E+01	1.85	28522	3.39E-07	0.0001
ET INIPOND	1.908E-01	6.60E-01	5.77	18858	1.22E-04	0.0284

simulation has a behaviour similar to the one seen in case B, where the convergence trend turned out to be irregular. Few batches rich of fission particles carry the whole information of the presence of the assembly, while all the others, having no secondary particles, carry just the information of the particle source.

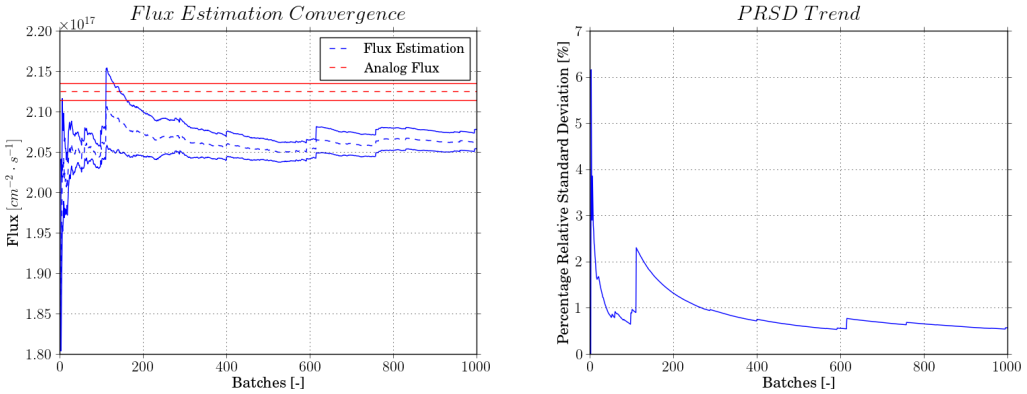

(a) Fast flux estimate - Mean value

(b) Fast flux estimate - PRSD

Fig. 6.13 Toy model - Case E - ET - IDT Importance Map I - Fast flux estimate convergence trend

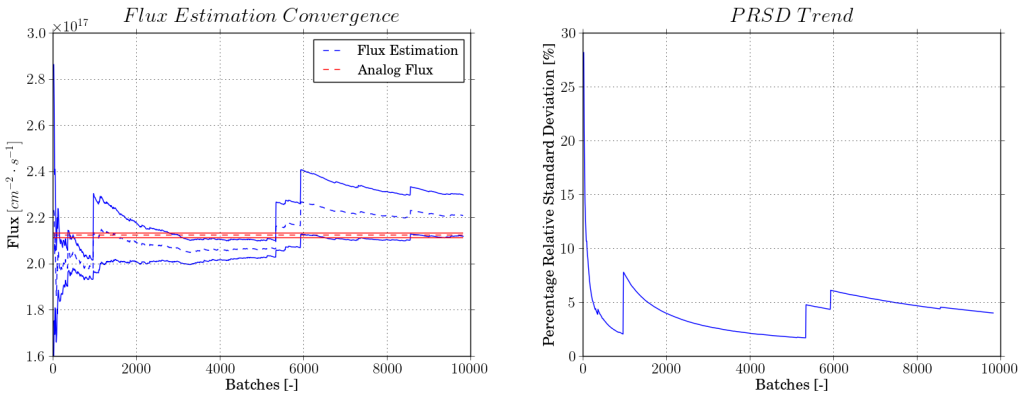

(a) Fast flux estimate - Mean value (b) Fast flux estimate - PRSD

Fig. 6.14 Toy model - Case E - ET - INIPOND Importance map - Fast flux estimate convergence trend

On the other hand, the INIPOND map (Fig. 6.2) is able to provide a good estimate of the flux but with performances worse than the one of the reference simulation. The behaviour of this simulation is surprising because it shows a perfectly regular fission sampling. All particle batches give approximatively the same number of fission particles. A possible explanation can be found by looking at the INIPOND map (Fig. 6.2). We see that due to the erroneous importance gradients of the map discussed in previous sections, all particles sampled in the source are directly driven to the fissile assembly, and then transported to the detector crossing the air layer. According to this hypothesis, the fission sampling may be purely artificial since accidentally produced by the importance map. The variance jump shown in the convergence trend of the flux estimate using the INIPOND map (Figure 6.14 (b)) are of different nature w.r.t. the one seen using the IDT map. While in the latter they are produced by the irregular fission sampling, in the former the variance jumps are due to the erroneous particle transport favoured by the INIPOND map. The effect of these jumps results in a slow convergence for the flux characterized by fluctuating values of PRSD.

Looking at Table 6.17 we observe a behaviour opposite to what it could be expected: the simulation run with the INIPOND map has produced a wrong estimate of the multiplication factor although the fission sampling of this simulation is quite uniform. The few fluctuations in the number of secondary particles result in a small uncertainty of the K factor, underlining a bias in the estimate. Also in this case we can say that the best way to evaluate the multiplication factor is the use of standard Monte Carlo simulations.

Consider now the flux estimate obtained with exponential transform and the IDT map. Particles emitted from the source are sampled preferentially in high energy groups due to the Watt spectrum and due to the source biasing. It means that source neutrons follow the path identified by the blue line in Figure 6.12. These particles are driven directly to the detector and only few of them succeed to thermalize enough in a region sufficiently close to the fissile assembly region so as to be attracted by it. The irregular fission sampling could be therefore explained by the incapability of the method to

reproduce with particle histories all the different paths represented in the importance map, such as the one leading particles to induce fissions in the assembly.

6.2.6 Partial conclusions on the single-step exponential transform method

Exponential transform is a good method for estimating physical quantities in a given response localized in the space. It is well known that this variance reduction technique is not always able to provide good estimate in the rest of the domain. It means that, in our models, the exponential transform may be not able to represent well enough the fission productions in the fissile material. In cases where the fissile material is located too close to the source, like in Cases A and B, the simulation yields non-uniform particle sampling, thus erroneous neutron flux estimate at the detector, erroneous K STEP estimate and convergence trends displaying variance jumps.

On the other hand, the exponential transform is able to give better results in "fixed-source criticality problems" whenever the source is far from the fissile region (Cases C and D). These simulations are characterized by a more regular fission sampling: the flux is estimated with a smaller variance and is not affected by any bias. Care should be taken when using the exponential transform since we are not able to define any region in which its effectiveness is insured. The presence of variance jumps cannot be excluded anyway.

Finally, it is also important to notice the influence of the multiplication factor K on the quality of the flux estimate. It is well established that fissions reactions are sources of additional randomness in every Monte Carlo simulation. With the use of exponential transform the effects of this randomness might become even more relevant, leading in some cases to a bias in the flux estimate. Comparing all the results, we can observe that the worst performances have been obtained in cases having larger K values, so in those models having the source close to the fissile assembly.

6.3 Tests of the Adaptive Multilevel Splitting

In this section we present the results obtained by applying the AMS variance reduction method to the toy models that have been presented in Chapter 5. The analysis of the results will be carried out following the approach already used for the exponential transform.

6.3.1 Case A

The first test has been performed on Case A. The AMS simulation has been run using different importance maps: the IDT ones, the one produced by the INIPOND module and finally a geometrical one. Let us remember that the geometrical map has been produced by setting as attractor the central axis of the detector. The importance map so produced will "push" the neutrons towards the target independently of their energy, and of the medium where they are. As regard the description

and analysis of the main characteristics of the IDT and INIPOND maps, we refer to Section 6.2.1 describing the test of exponential transform on Case A. The results of the tests are reported on Tables 6.18, 6.19 and 6.20.

Table 6.18 Toy model - Case A - AMS results - Neutron Flux comparison

Cases	Fast Flux			Thermal Flux		
	Mean	PRSD [%]	Q	Mean	PRSD [%]	Q
REFERENCE MC	6.276E+16	4.91E-01	-	1.450E+17	6.38E-01	-
AMS INIPOND	6.389E+16	7.69E-01	1.93	1.466E+17	4.51E-01	1.37
AMS GEOM	6.378E+16	9.07E-01	1.55	1.463E+17	4.00E-01	1.14
AMS IDT - MAP I	6.292E+16	8.74E-01	0.26	1.458E+17	5.69E-01	0.65
AMS IDT - MAP II	6.321E+16	9.52E-01	0.67	1.478E+17	6.00E-01	2.13
AMS IDT - MAP III	6.303E+16	1.03E+00	0.37	1.454E+17	5.77E-01	0.29
AMS IDT - MAP IV	6.442E+16	1.73E+00	1.44	1.457E+17	6.43E-01	0.52

Table 6.19 Toy model - Case A - AMS results - Figure of Merit comparison

Cases	Total Flux	PRSD [%]	time [s]	FOM	FOM GAIN
REFERENCE MC	2.164E+17	8.73E+00	8771	1.49747E-06	-
AMS INIPOND	1.601E+17	9.97E+00	2461	4.0876E-06	2.730
AMS GEOM	1.806E+17	1.08E+01	961	8.90929E-06	5.950
AMS IDT - MAP I	1.973E+17	3.58E+00	1408	5.55427E-05	37.091
AMS IDT - MAP II	2.201E+17	4.67E+00	1433	3.20611E-05	21.410
AMS IDT - MAP III	2.062E+17	3.53E+00	1389	5.78073E-05	38.603
AMS IDT - MAP IV	2.062E+17	3.23E+00	1445	6.6259E-05	44.247

Table 6.20 Toy model - Case A - AMS results - K STEP comparison

Cases	K STEP	PRSD [%]	Q	time [s]	FOM	FOM GAIN
REFERENCE MC	6.172E-01	7.63E-02	-	8771	1.96E-02	-
AMS INIPOND	6.162E-01	3.11E-01	0.47	2461	4.21E-03	2.15E-01
AMS GEOM	6.210E-01	1.07E+00	0.58	961	9.15E-04	4.68E-02
AMS IDT - MAP I	6.185E-01	9.13E-01	0.24	1408	8.52E-04	4.36E-02
AMS IDT - MAP II	6.182E-01	8.12E-01	0.21	1433	1.06E-03	5.41E-02
AMS IDT - MAP III	6.137E-01	9.47E-01	0.59	1389	8.03E-04	4.11E-02
AMS IDT - MAP IV	6.151E-01	9.69E-01	0.35	1445	7.38E-04	3.77E-02

From Table 6.18 we see that none of the AMS simulations present any relevant bias. All results, obtained using different importance maps, are coherent with the reference. The FOM values of these simulations are larger than one, so AMS has been effective in all the cases. The coupling between

IDT importance map and AMS is able to improve sharply the performances of the AMS simulation, while the geometrical importance map and the INIPOND one are less efficient.

It is important to verify that the use of AMS does not involve large variance jumps. Such verification is essential since a single jump in variance can affect the outcome of the simulation, leading to a wrong estimate of the expected value. The AMS method, probably because it relies on an analog particle transport, does not present any trace of variance jumps: the sample average converges to the exact result reducing the error approximatively with a $1/\sqrt{n}$ trend. Figure 6.15 shows the convergence of the fast flux estimate in a simulation run with AMS and the IDT Map I. Figure 6.15(a) compares the fast flux estimate at every batch with the result of the reference simulation. The mean values are displayed with their relative error bars corresponding to 1 $\sigma\%$. Figure 6.15(b) shows the PRSD trend along the batches.

All AMS simulations, regardless of the adopted map, are characterized by a uniform fission sampling. A remarkable fact is that AMS is able to provide correct results even with importance maps that contain no information about the fission like for the INIPOND and the geometrical ones. The robustness of the method and its little sensitivity with respect to the quality of the importance map have already been discussed in [15] and they are hereby confirmed for fixed-source criticality problems. In Table 6.20 we can see that the AMS estimates of the multiplication factor K are unbiased. However, the reference simulation is the one characterized by the highest FOM value.

6.3.2 Case B

Tables 6.21, 6.22 and 6.23 show the results of the tests performed on Case B. For simplicity, and because of the little sensitivity of AMS w.r.t. the quality of the IDT map, we have decided to test AMS just with the importance Map I.

Table 6.21 Toy model - Case B - AMS results - Neutron Flux comparison

Cases	Fast Flux			Thermal Flux		
	Mean	PRSD [%]	Q	Mean	PRSD [%]	Q
REFERENCE MC	2.541E+14	3.40E+00	-	4.687E+14	4.92E+00	-
AMS INIPOND	2.547E+14	2.30E+00	0.05	4.836E+14	1.39E+00	0.62
AMS GEOM	2.536E+14	3.45E+00	0.04	4.871E+14	1.66E+00	0.75
AMS IDT - MAP I	2.607E+14	8.48E-01	0.73	4.941E+14	6.85E-01	1.09

We see that none of the flux estimate present any type of bias. The results confirm what it has been seen in the previous case: AMS is able to provide unbiased estimate also with importance map not representative of the whole physics of the problem. The robustness of the method does not ensure good performances with every map. In fact, the discrepancies between FOM values are large. The

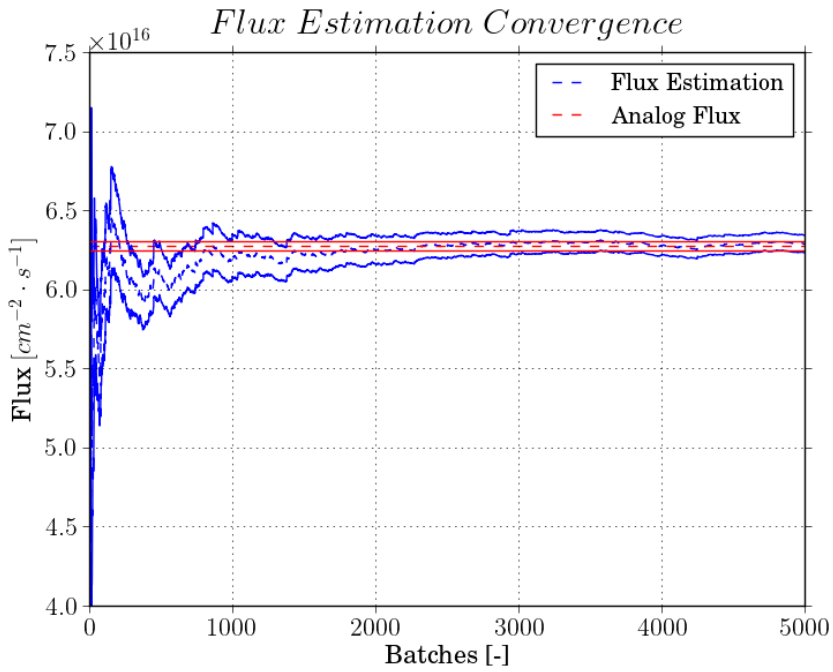

(a) Fast flux estimate - Mean value

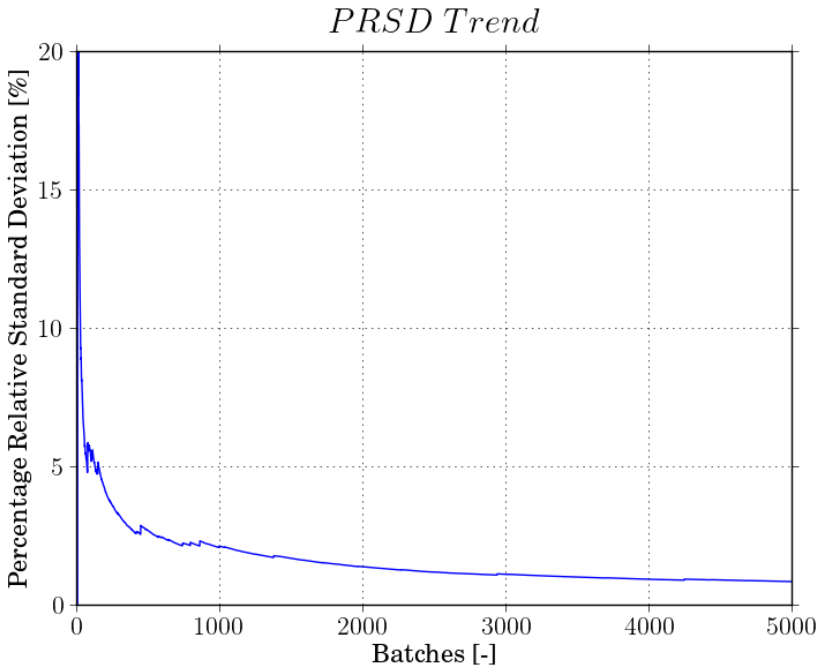

(b) Fast flux estimate - PRSD

Fig. 6.15 Toy model - Case A - AMS - IDT Importance Map I - Fast flux estimate convergence trend

highest performances have been achieved using the IDT map with values two order of magnitude higher than the ones obtained with other maps. We have to remember that the fissile assembly, being

Table 6.22 Toy model - Case B - AMS results - Figure of Merit comparison

Cases	Total Flux	PRSD [%]	time [s]	FOM	FOM GAIN
REFERENCE MC	6.097E+14	2.62E+01	188894	7.71E-09	-
AMS INIPOND*	7.843E+14	7.80E+00	1170512	1.40E-08	1.823
AMS GEOM*	7.407E+14	2.05E+00	8168496	2.91E-08	3.781
AMS IDT - MAP I	7.745E+14	9.24E+00	4030	2.90E-06	376.801
(*) FOM values computed on a different hardware configurations					

Table 6.23 Toy model - Case B - AMS results - K STEP comparison

Cases	K STEP	PRSD [%]	Q	time [s]	FOM	FOM GAIN
REFERENCE MC	6.176E-01	1.71E-02	-	188894	1.80E-02	-
AMS INIPOND*	6.174E-01	1.39E-02	1.75	1170512	4.44E-03	0.2462
AMS GEOM*	6.177E-01	1.35E-02	0.64	8168496	6.68E-04	0.0371
AMS IDT - MAP I	6.270E-01	7.07E-01	2.11	4030	4.96E-04	0.0275
(*) FOM values computed on a different hardware configurations						

centred on the source and emitting fission neutrons on the same spectrum, provides a not negligible contribution to the final score. The use of maps that do not take into account the contribution of fission reactions negatively affects the performances.

The geometrical map leads to the re-sampling of the particles close to the detector at the expense of the more distant ones. The AMS simulation with a geometric map presents a convergence trend without variance jumps, but with a large variance in the flux estimate. This leads to performances comparable to those of the reference simulation. The INIPOND map, as we have already seen, is not able to represent the correct path that the particles should follow to reach the detector. Furthermore, this map does not in any way help particles to induce fission reactions. This explain the large variance of the flux estimates and the very poor performances.

Nonetheless, if AMS is run with an importance map representative of the physics of the problem, it is able to provide large FOM GAIN values. The algorithm performances are intuitively expected to increase with the increasing “difficulty” of the problem to be simulated, i.e., in our cases, with the increasing optical distance between source and detector. The K multiplication factor estimated with AMS is coherent with the one obtained by reference Monte Carlo, but, as seen before, its convergence is slower.

6.3.3 Case C

In Case C the assembly is no more centred on the neutron source, but displaced inside the reactor. The Adaptive multilevel splitting method has been tested using all the available importance maps. The results have been reported in Tables 6.24, 6.25 and 6.26.

Table 6.24 Toy model - Case C - AMS results - Neutron Flux comparison

Cases	Fast Flux			Thermal Flux		
	Mean	PRSD [%]	Q	Mean	PRSD [%]	Q
REFERENCE MC	5.255E+16	5.40E-01	-	1.378E+17	6.59E-01	-
AMS INIPOND	5.210E+16	9.19E-01	0.82	1.349E+17	5.11E-01	2.57
AMS GEOM	5.382E+16	1.48E+00	1.50	1.383E+17	9.69E-01	0.28
AMS IDT - MAP I	5.206E+16	5.41E-01	1.24	1.349E+17	3.75E-01	2.82
AMS IDT - MAP II	5.197E+16	5.52E-01	1.43	1.350E+17	3.85E-01	2.66
AMS IDT - MAP III	5.205E+16	5.59E-01	1.24	1.348E+17	3.85E-01	2.86
AMS IDT - MAP IV	5.200E+16	5.51E-01	1.37	1.351E+17	3.91E-01	2.62

Table 6.25 Toy model - Case C - AMS results - Figure of Merit comparison

Cases	Total Flux	PRSD [%]	time [s]	FOM	FOM GAIN
REFERENCE MC	1.839E+17	9.01E+00	7675	1.605E-06	-
AMS INIPOND	1.755E+17	1.06E+01	2404	3.737E-06	2.328
AMS GEOM	1.782E+17	7.30E+00	996	1.886E-05	11.751
AMS IDT - MAP I	1.905E+17	2.91E+00	1552	7.618E-05	47.458
AMS IDT - MAP II	1.964E+17	2.95E+00	1535	7.503E-05	46.743
AMS IDT - MAP III	1.846E+17	2.35E+00	1555	1.161E-04	72.332
AMS IDT - MAP IV	1.820E+17	3.11E+00	1544	6.700E-05	41.741

Table 6.26 Toy model - Case C - AMS results - K STEP comparison

Cases	K STEP	PRSD [%]	Q	time [s]	FOM	FOM GAIN
REFERENCE MC	1.093E-02	6.26E-01	-	7675	3.321E-04	-
AMS INIPOND	1.049E-02	2.33E+00	1.75	2404	7.651E-05	0.230
AMS GEOM	9.691E-03	7.45E+00	1.71	996	1.811E-05	0.055
AMS IDT - MAP I	1.134E-02	7.51E+00	0.48	1552	1.144E-05	0.034
AMS IDT - MAP II	1.009E-02	7.66E+00	1.09	1535	1.112E-05	0.033
AMS IDT - MAP III	1.043E-02	7.59E+00	0.63	1555	1.117E-05	0.034
AMS IDT - MAP IV	1.143E-02	7.95E+00	0.55	1544	1.025E-05	0.031

The outcome of the simulations once again shows the robustness of the method. For all cases the estimate of the neutron flux appears to be unbiased and consistent with the reference value. In

order to have an adequate fission sampling, the particles must go through the assembly located at the center of the reactor. This path is favoured by the geometric map and by the IDT ones, but not by the one produced with the INIPOND module. In this view, it is rather surprising that AMS yields good estimates of both the neutron flux and the multiplication factor, even using INIPOND map.

Looking at Table 6.25, we see that AMS has given good performance with all the importance maps. The FOM GAIN value obtained with geometrical map is higher than those obtained in previous cases using the same type of map. This could be explained by the position of the assembly, which is is located exactly along the increasing importance path identified by the map. The AMS algorithm, by means of successive particle re-sampling, drives particles along this path, and so it promotes the sampling of fissions. We must also note that the IDT Map II, although less refined, provides performances comparable to those obtained with the others. Therefore, an excessive refinement of the importance map appears to be not required for AMS applications. On the other hand, Map III shows higher performances than those obtained with other IDT maps. This shows how the use of self-shielded cross sections, in some cases, may be beneficial for the AMS.

6.3.4 Case D and Case E

In the following section we discuss the tests carried out on Case D and Case E. In the first case the assembly is placed near the upper left corner of the reactor. In the second, it is placed opposite to the detector with respect to the source. Both cases have been tested with the geometrical, the INIPOND and the IDT Map I. The results are shown in Tables 6.27, 6.28, 6.29 for Case D, and 6.30, 6.31, 6.32 for Case E.

Table 6.27 Toy model - Case D - AMS results - Neutron Flux comparison

Cases	Fast Flux			Thermal Flux		
	Mean	PRSD [%]	Q	Mean	PRSD [%]	Q
REFERENCE MC	3.926E+16	6.32E-01	-	9.072E+16	8.10E-01	-
AMS INIPOND	3.926E+16	1.30E+00	0.00	9.103E+16	6.59E-01	0.33
AMS GEOM	4.199E+16	5.66E+00	1.14	9.300E+16	2.49E+00	0.94
AMS IDT - MAP I	4.034E+16	1.20E+00	1.98	9.165E+16	6.55E-01	0.98

Table 6.28 Toy model - Case D - AMS results - Figure of Merit comparison

Cases	Total Flux	PRSD [%]	time [s]	FOM	FOM GAIN
REFERENCE MC	1.232E+17	9.86E+00	7491	1.37299E-06	-
AMS INIPOND	1.287E+17	1.20E+01	2256	3.09113E-06	2.251
AMS GEOM	1.302E+17	1.50E+01	938	4.71816E-06	3.436
AMS IDT - MAP I	1.289E+17	3.98E+00	1296	4.880E-05	35.540

Table 6.29 Toy model - Case D - AMS results - K STEP comparison

Cases	K STEP	PRSD [%]	Q	time [s]	FOM	FOM GAIN
REFERENCE MC	4.971E-03	9.47E-01	-	7491	1.487E-04	-
AMS INIPOND	4.832E-03	3.76E+00	0.74	2256	3.13742E-05	0.2109
AMS GEOM	4.870E-03	1.17E+01	0.18	938	7.78516E-06	0.0523
AMS IDT - MAP I	4.750E-03	1.13E+01	0.41	1296	6.06715E-06	0.0408

AMS has provided results not affected by any bias in all simulations, even with the geometric maps. This result is not trivial, especially in case E where the assembly, in the geometric map, is placed in a region of lower importance with respect to the source. On the other hand, the performances in the estimate of the neutron flux, although always larger than one, are very small when using geometrical and INIPOND maps. Good FOM GAIN values have been obtained only with the IDT maps.

Table 6.30 Toy model - Case E - AMS results - Neutron Flux comparison

Cases	Fast Flux			Thermal Flux		
	Mean	PRSD [%]	Q	Mean	PRSD [%]	Q
REFERENCE MC	2.125E+17	4.77E-01	-	5.307E+17	5.80E-01	-
AMS INIPOND	2.047E+17	3.16E+00	1.19	5.214E+17	1.57E+00	1.06
AMS GEOM	2.171E+17	3.13E+00	0.68	5.333E+17	1.15E+00	0.38
AMS IDT - MAP I	2.109E+17	7.75E-01	0.81	5.231E+17	4.29E-01	1.99

Table 6.31 Toy model - Case E - AMS results - Figure of Merit comparison

Cases	Total Flux	PRSD [%]	time [s]	FOM	FOM GAIN
REFERENCE MC	7.689E+17	4.59E+00	10017	4.74E-06	-
AMS INIPOND	7.903E+17	4.17E+00	5079	1.13E-05	2.385
AMS GEOM	9.294E+17	1.04E+01	846	1.10E-05	2.313
AMS IDT - MAP I	6.885E+17	3.19E+00	1220	8.07E-05	17.009

Table 6.32 Toy model - Case E - AMS results - K STEP comparison

Cases	K STEP	PRSD [%]	Q	time [s]	FOM	FOM GAIN
REFERENCE MC	1.834E-01	1.52E-01	-	10017	4.29E-03	-
AMS INIPOND	1.811E-01	5.96E-01	2.03	5079	5.55E-04	0.1293
AMS GEOM	1.858E-01	1.71E+00	0.75	846	4.05E-04	0.0943
AMS IDT - MAP I	1.868E-01	1.64E+00	1.12	1220	3.05E-04	0.0710

Performances obtained using the IDT map in case D are coherent with those obtained in other cases. That is to say that the importance map is capable of inducing the resampling of particles along a path different from the diagonal one. In Case E the performances are halved with respect to Case D. This is probably due to the complexity of the information provided by the map (see Section 6.2.5).

6.4 Conclusions on single-response tests

The tests performed on toy models allowed us to compare different variance reduction methods and to assess their qualities. In the first place we have seen that the regularity of the fission sampling along the batches is a fundamental ingredient for a correct estimate of both the neutron flux and the multiplication factor K. Exponential transform is not able to ensure this property in cases where the fissile material is placed near the physical source. On the other hand, a stark improvement in the performance can be observed when the assembly has been placed farther away from the source. However, these cases are also characterized by an large variance in the estimate of the K multiplication factor, an effect that may hide the presence of potential biases. Summarizing, the single-step exponential transform is not always able to give correct estimate of the flux in a given detector.

Concerning the AMS, we have observed the great robustness of the method, which provided proper flux estimates in all the models studied, with any type of importance map. The use of an IDT map for the acceleration of AMS has been seen to be very beneficial and yields much higher performances than other importance maps. However, AMS has not been able to provide, in any case, performances comparable to those of exponential transform when this latter has been effective. Regarding the estimate of the K STEP, none of the methods have provided performances comparable to the one achieved by the reference Monte Carlo simulations run just with the population control and implicit capture.

The AMS algorithm could become very interesting to compute the multiplication factor in configuration where the fissile material is placed far from the source. In models where the optical distance between the two is large enough to challenge the effectiveness of the standard Monte Carlo simulation, the AMS with an appropriate importance map might be an effective solution in estimating the K factor. Nonetheless, we strongly advise against the use of exponential transform for estimates of the K factor because we are not able to define a region of validity within which this method is able to work.

In propagation problems in the presence of fissile materials, the best method in terms of performance to estimate neutron fluxes is the Two-step. The Two-step method can be very expensive as we need to perform different calculations:

- a first simulation for calculating the fission source;

- the production of an importance map for the second step (this can be avoided via the use of INIPOND maps but the same performances obtained with IDT maps are not ensured);
- a second propagation step run with exponential transform.

In order to decrease the error of the flux estimates in the second step, it is necessary to compute the fission source with a sufficiently high accuracy. To do this, it is necessary to:

- have little uncertainty on the estimate of the multiplication factor K and on the distribution of particles produced by fission $\nu\Sigma_f\Phi$;
- have a good spatial discretization of the score in the first step so as to minimize the error on the shape of the fission source.

The Two-step method has various advantages, especially if adopted to study multiple cases with the same fission source. Since the computational time is mostly taken by the first step, once we have calculated the fission source, we can perform studies on multiple detectors in shorter time. The calculation of the fission source also leaves the user with a large degree of freedom as it can be calculated with different approaches depending on the needs. As regards the calculation of the fission source, the possibility of using variance reduction methods or deterministic approaches should be also evaluated. The Two-step methodology can also be used in ex-core propagation calculations in critical reactors. This is because, after obtaining the fission source by criticality calculation, we can then propagate it with exponential transform.

The AMS method is clearly less demanding for the user because it requires just one Monte Carlo calculation and the production of the importance map. The results obtained have shown that IDT maps are able to provide the highest performances, therefore it is recommended to use them. In addition, we expect that AMS will be able to provide good performances even with less converged IDT calculations.

Due to the possible instabilities in the convergence of the exponential transform method, as used in single-step calculations, at the present time we can not recommend this technique for fixed-source calculations in the presence of fissile materials.

Chapter 7

Tests on simultaneous responses on multiple detectors

In this section we want to test the Two-step method and the AMS on a fixed-source criticality problem characterized by the presence of several detectors. We will assess whether these methods are able to provide a proper flux estimate on all detectors within the same simulation. Thereafter, we will evaluate their performances and draw conclusions.

7.1 Test description

7.1.1 The model

For this study we have designed a new toy-model. This has been derived from the model Case A presented in Chapter 5 by adding two detector tallies: one placed near the bottom side of the core, and the other in the upper left corner. We will refer to this model with the name of Multi-detector toy-model. Its geometry is shown in Figure 7.1.

Each detector in made of a 3×3 cm^2 water cell:

- Detector 1: it is the farthest one. It is placed 3 cm far from the top right corner;
- Detector 2: is placed 3 cm far from the top left corner;
- Detector 3: is the closest to the source. Its distance from the bottom steel ring is of 3 cm and its left edge is aligned with the center of the reactor.

With the present choice we want to introduce a strong asymmetry in the model such that the probability for a neutron emitted by the source to reach a detector is significantly different from one detector to another. We believe that in doing so we may better observe the capability of variance reduction methods to bring particles to the detector where they are needed the most.

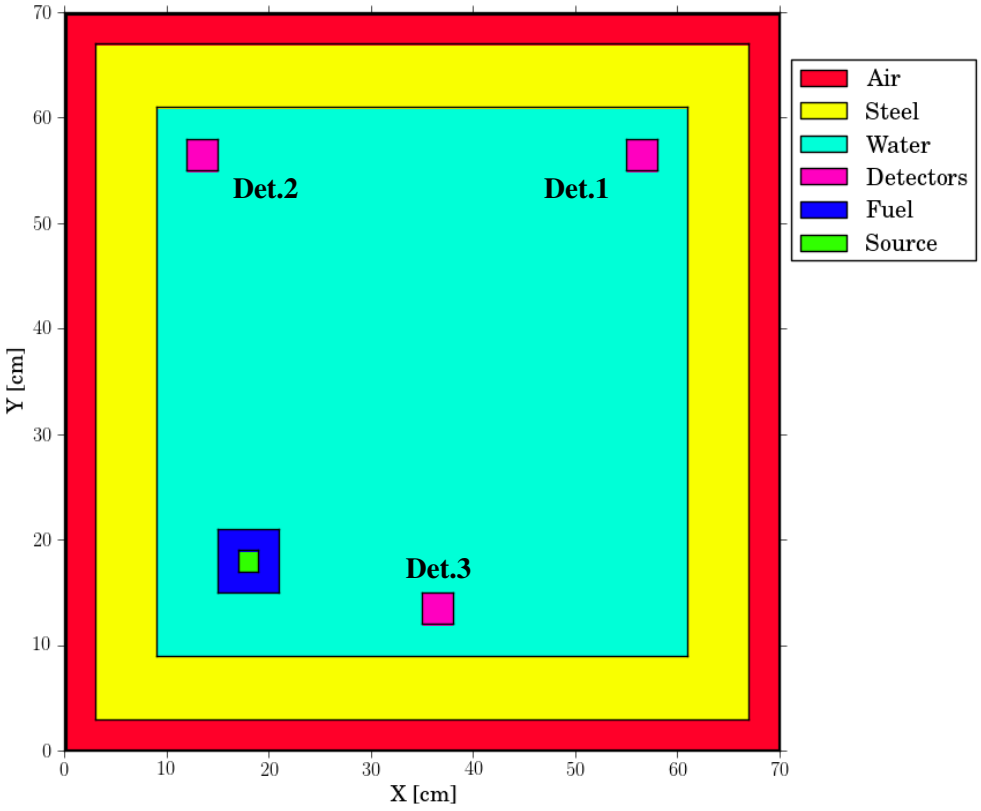

Fig. 7.1 Toy model - Case Multi-detector - Geometry

7.1.2 Importance maps and simulation settings

In order to estimate the neutron flux at the 3 detectors simultaneously, it has been decided to adopt the Forward-Weighted Consistent Adjoint-Driven Importance Sampling technique (FW-CADIS) [20]. The importance map has been calculated by solving the adjoint transport equation with IDT and adopting an adjoint source weighted by the inverse of the direct flux. A first calculation with the IDT solver has been carried out in order to compute approximate values of the direct flux at the 3 detectors. The calculation has been carried out by using a coarse mesh and a low-order angular discretization in order to reduce the computational time. The flux thus evaluated has been spatially averaged on the volume of each detector and the adjoint source has been calculated according to Equation (3.23). After that, a second IDT simulation has been performed in order to compute the importance map. The adjoint flux has been evaluated on a spatial discretization made of 100×100 cells. We used a product-type Chebyshev/Legendre quadrature formula containing 400 directions. In order to accelerate both AMS and Two-step methods, the map has been computed twice: with and

without the contribution of the fissions. The maps produced adopting FW-CADIS method are shown in Figure 7.2 and Figure 7.3.

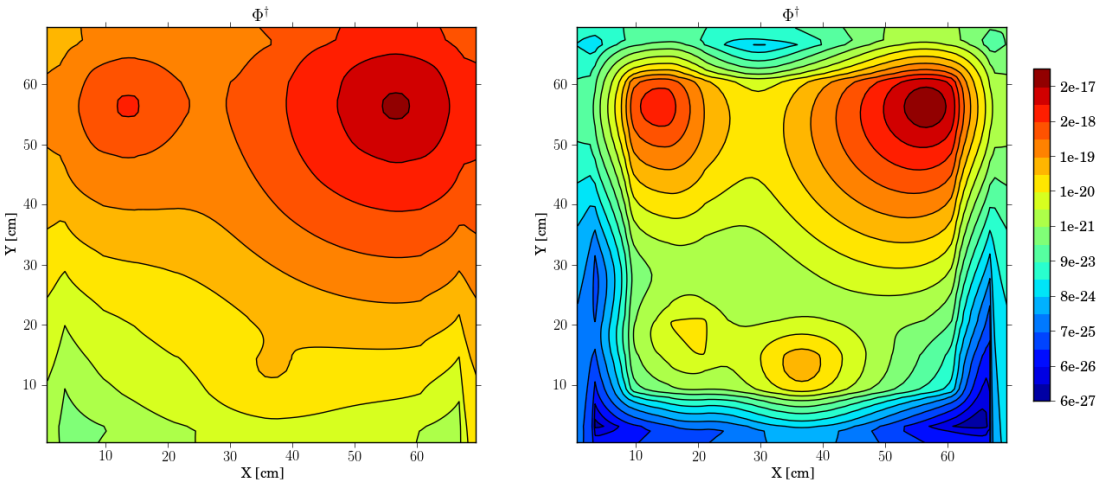

(a) IDT Importance map - Energy range $4.9659 - 4.0657\ MeV$

(b) IDT Importance map - $2.5 \cdot 10^{-09} - 1.0 \cdot 10^{-11}\ MeV$

Fig. 7.2 Toy model Multi-detector - FW-CADIS - with fission contribution

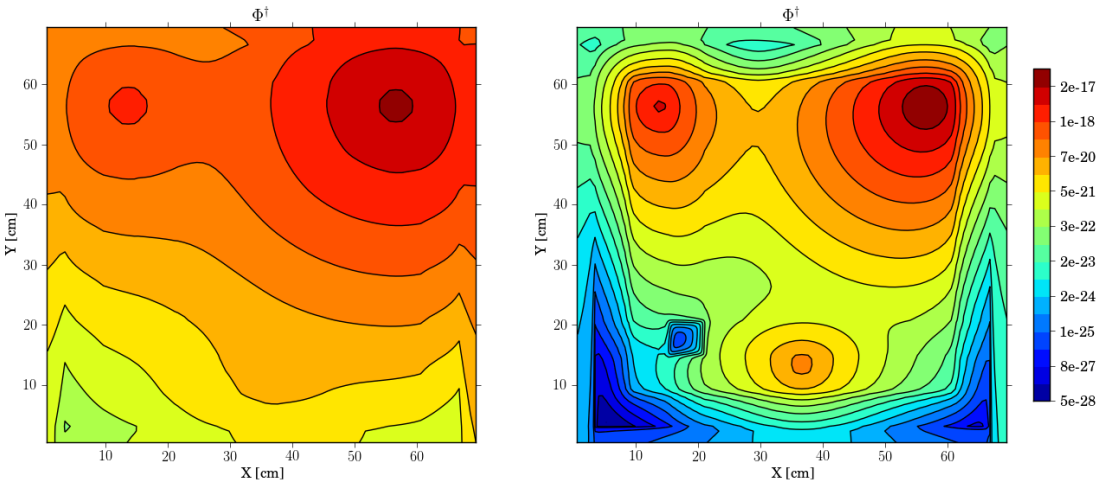

(a) IDT Importance map - Energy range $4.9659 - 4.0657\ MeV$

(b) IDT Importance map - $2.5 \cdot 10^{-09} - 1.0 \cdot 10^{-11}\ MeV$

Fig. 7.3 Toy model Multi-detector - FW-CADIS - without fission contribution

In order to stress the advantages of FW-CADIS we have also run calculations with the CADIS method designed to drive particle to detector 1. The importance map used in this case is the IDT Map I shown in Section 6.2.1 (Figure 6.1).

In AMS simulations, with both CADIS and FW-CADIS importance maps, all 3 detectors have been set as particle targets [15]. Using this setting, when a particle attains one of the detectors, its importance is set artificially to infinity, therefore the related particle track can no longer be discarded. This choice has been made in order to define a proper stopping criteria for the algorithm. Concerning notations, methods of analysis of results and Figures of Merit, we used those already presented in Chapter 5.

7.2 Results

The results of the tests performed by using the FW-CADIS method are shown in Tables 7.1 and 7.2. Tables 7.3 and 7.4 show instead the results obtained by using the single-response CADIS map.

Table 7.1 Toy model Multi-detector - FW-CADIS - Neutron Flux comparison

DET.	SIM.	Fast Flux			Thermal Flux		
		Mean	PRSD [%]	Q	Mean	PRSD [%]	Q
1	REFERENCE MC	6.276E+16	4.91E-01	-	1.450E+17	6.38E-01	-
	AMS - IDT	6.302E+16	4.91E-01	0.58	1.466E+17	5.29E-01	1.31
	TWO-STEP	6.340E+16	1.56E-01	1.98	1.468E+17	9.70E-02	1.90
2	REFERENCE MC	8.400E+17	5.10E-01	-	2.288E+18	6.07E-01	-
	AMS - IDT	8.414E+17	1.87E-01	0.33	2.292E+18	1.57E-01	0.26
	TWO-STEP	8.463E+17	1.99E-01	1.38	2.303E+18	2.32E-01	1.00
3	REFERENCE MC	2.802E+19	8.89E-02	-	1.087E+20	8.86E-02	-
	AMS - IDT	2.803E+19	6.69E-02	0.09	1.087E+20	4.32E-02	0.38
	TWO-STEP	2.804E+19	5.57E-02	0.52	1.085E+20	4.51E-02	1.91

Table 7.2 Toy model Multi-detector - FW-CADIS - Figure of Merit comparison

DET.	SIM.	Total Flux	PRSD [%]	time [s]	FOM	FOM GAIN
1	REFERENCE MC	2.079E+17	2.53E+01	935	1.67E-06	-
	AMS - IDT	2.340E+17	1.38E+01	583	9.04E-06	5.43
	TWO-STEP	2.076E+17	9.82E-01	1682	6.16E-04	370.01
2	REFERENCE MC	3.136E+18	8.20E+00	935	1.59E-05	-
	AMS - IDT	3.094E+18	4.89E+00	583	7.17E-05	4.50
	TWO-STEP	3.176E+18	1.49E+00	1682	2.66E-04	16.72
3	REFERENCE MC	1.372E+20	1.15E+00	935	8.05E-04	-
	AMS - IDT	1.387E+20	1.19E+00	583	1.20E-03	1.49
	TWO-STEP	1.366E+20	6.40E-01	1682	1.45E-03	1.80

From the Table 7.1 we see that, since all the Q values are smaller than 3, none of the flux estimates is affected by any evident bias. The results of the three detectors obtained with both the Two-step methods and AMS are consistent with the one of the reference Monte Carlo simulation. In Table 7.2 we observe that the performances of these calculations are good for all three responses. The Two-step simulation, as already seen, is able to ensure very high performances. The FOM GAIN values obtained in these simulations are higher for the farthest detector, and decrease for detectors near the source. This phenomenon arises from the fact that, as the optical distance between source and detector decreases, the effect of the acceleration method becomes less evident. However, in all cases the FOM GAIN is larger than 1.

As for the AMS, the performances are on the average worse than those obtained with the Two-step method. Unlike the latter, the FOM GAIN values do not vary according to the distance from the source but remain approximately constant. To a first approximation, we can think that the use of FW-CADIS importance map allows the estimate of multiple detectors at the expense of performances on the most distant ones.

Table 7.3 Toy model Multi-detector - CADIS Det.1 - Neutron Flux comparison

DET.	SIM.	Fast Flux			Thermal Flux		
		Mean	PRSD [%]	Q	Mean	PRSD [%]	Q
1	REFERENCE MC	6.276E+16	4.91E-01	-	1.450E+17	6.38E-01	-
	AMS - IDT	6.274E+16	3.18E-01	0.06	1.466E+17	3.61E-01	1.48
	TWO-STEP	6.324E+16	2.10E-02	1.54	1.466E+17	2.21E-02	1.74
2	REFERENCE MC	8.400E+17	5.10E-01	-	2.288E+18	6.07E-01	-
	AMS - IDT	8.395E+17	2.58E-01	0.10	2.299E+18	2.70E-01	0.74
	TWO-STEP	8.380E+17	1.10E+00	0.20	2.276E+18	2.77E+00	0.19
3	REFERENCE MC	2.802E+19	8.89E-02	-	1.087E+20	8.86E-02	-
	AMS - IDT	2.804E+19	6.45E-02	0.66	1.087E+20	5.52E-02	0.50
	TWO-STEP	2.799E+19	2.85E-01	0.42	1.084E+20	5.34E-01	0.52

As regards the tests carried out with the CADIS maps, produced for the estimate on detector 1 only, we can observe that results are not affected by any bias. Table 7.3 shows that all the estimates of the flux, fast and thermal, are consistent with those obtained with the reference Monte Carlo simulation. On the other hand, the simulations performed with CADIS importance map are highly inefficient in terms of performances for the estimate on detector 2 and 3. The Two-step method has given high performances for the estimate on detector 1, while on detectors 2 and 3 FOM GAIN values are much smaller than 1.

AMS tests have shown a similar behaviour: performances on responses 2 and 3, although similar, are worse than the ones of the reference simulation while the estimate at detector 1 is characterized by a FOM GAIN larger than 1. In this detector we can observe a lower FOM value of the flux estimate if

Table 7.4 Toy model Multi-detector - CADIS Det.1 - Figure of Merit comparison

DET.	SIM.	Total Flux	PRSD [%]	time [s]	FOM	FOM GAIN
1	REFERENCE MC	2.079E+17	2.53E+01	935	1.67E-06	-
	AMS - IDT	2.079E+17	1.25E+01	716	8.91E-06	5.349
	TWO-STEP	2.106E+17	5.95E-01	2762	1.02E-03	613.82
2	REFERENCE MC	3.136E+18	8.20E+00	935	1.59E-05	-
	AMS - IDT	3.155E+18	9.52E+00	716	1.54E-05	0.968
	TWO-STEP	3.451E+18	4.88E+01	2762	1.52E-07	0.010
3	REFERENCE MC	1.372E+20	1.15E+00	935	8.05E-04	-
	AMS - IDT	1.421E+20	2.16E+00	716	2.99E-04	0.372
	TWO-STEP	1.279E+20	1.41E+01	2762	1.83E-06	0.002

compared to the one obtained in Case A in Chapter 6. This happens because of the AMS stopping criteria: when a particle reaches one of the targets, it assumes an infinite importance, i.e., it can no longer be discarded. The resulting effect is a progressive resampling of the families of particles already arrived at the nearest detectors that reduces the number of the particles that are moving towards detector 1.

Looking at Tables 7.1 we can see that using exponential transform (Two-step) with a FW-CADIS map all three detectors present similar PRSD values. It means that the flux estimates are obtained with a similar statistics, that is the desired effect of using FW-CADIS maps. On the contrary, looking at Table 7.3, so using a CADIS map, the PRSD values are much worse distributed.

7.3 Comments

Particle histories sampled in simulations with the exponential transform (Two-step method) follow faithfully the paths suggested by the importance map. The high values of PRSD that have been observed when estimating the flux at detectors 2 and 3 with the CADIS map mean that all particles were brought directly to the detector 1. This explains the high FOM values at detector 1 and the small ones at detectors 2 and 3.

Figures 7.4 (a) and (b) represent the PRSD values of the flux estimates over the entire energy spectrum at each point of the domain: the Two-step simulations accelerated with the FW-CADIS importance map on the left (a) and the CADIS one on the right (b). The particles paths behaves exactly according to the importance maps: the figures display very low σ % values, so larger statistics, at the detectors and on the paths connecting them to the source. The rest of the domain, on the contrary, is characterized by high values of uncertainty. This means that points outside these paths have a very low probability of being traversed by particle histories.

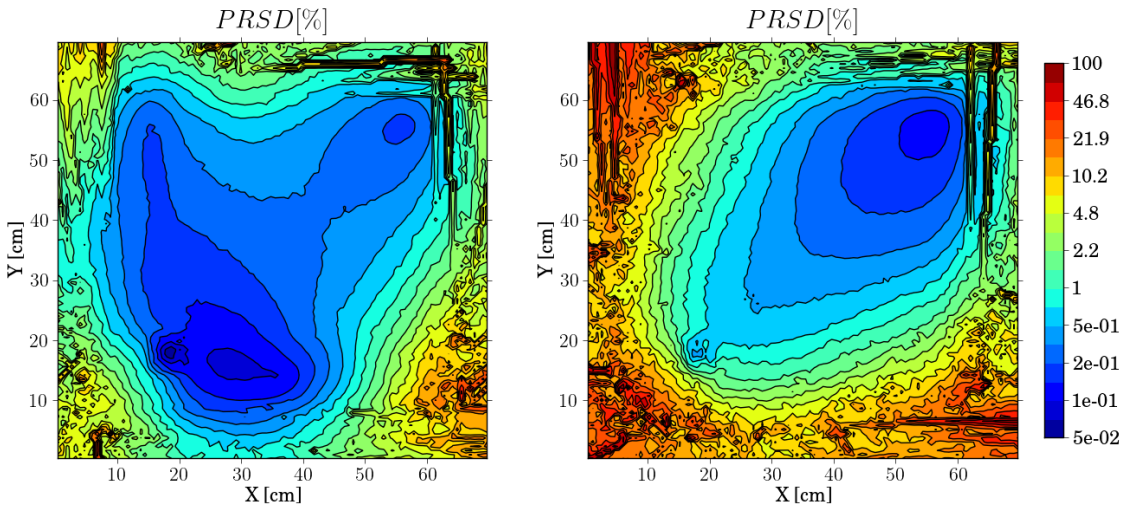

(a) Two-step - FW-CADIS Importance map (b) Two-step - Det.1 CADIS Importance map

Fig. 7.4 Toy model Multi-detector - Two-step - representation of the PRSD of the total flux estimate on the whole domain

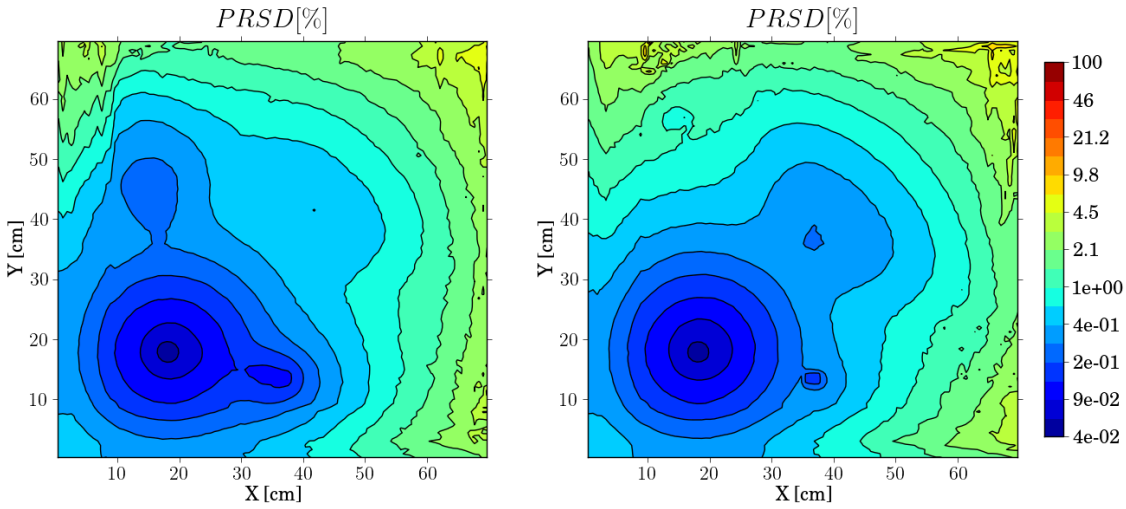

(a) AMS - FW-CADIS Importance map (b) AMS - Det.1 CADIS Importance map

Fig. 7.5 Toy model Multi-detector - AMS - representation of the PRSD of the total flux estimate on the whole domain

Using the same type of PRSD representation for AMS simulations, we observe that the method displays a larger discrepancy between the particle histories and importance map. Figures 7.5 (a) and (b) shows large regions with constant values of variance. It means that the particles are able to travel following various paths, different from the ones indicated by the gradients of the importance maps. The particles will therefore be able to provide a better statistics on the entire domain. This result shows the robustness of the AMS method, but also the reason of smaller FOM GAIN values w.r.t.

the ones obtained with the Two-step method. In Figure 7.5 (b) we see that the PRSD presents local minimums at detectors 2 and 3. This can be explained by the already mentioned resampling of the particles at the closest detectors.

7.4 Conclusions on the Multi-Response Tests

Importance maps produced following the FW-CADIS method are able to accelerate multiple-response fixed-source calculations in the presence of fissile material. In particular, the Two-step method is able to provide high performances even in this type of problems. The AMS performances, instead, are much lower due to the algorithm characteristics. Finally, we have seen that estimating multiple responses using importance maps produced just considering one detector with the CADIS method is not efficient, especially with the Two-step method. Furthermore, we have further confirmation of the robustness of the AMS.

Chapter 8

Tests on reactor-like model

Up to now we have analysed the main features of variance reduction methods and their behaviour in fixed-source criticality problems. By means of toy-models we performed a study on relatively simple geometries representative of the problem considered. In particular, the use of those models allowed us to carry out studies as general as possible, not influenced by any particular reactor design. In order to perform a more specific analysis, we will carry out some tests on a more realistic configuration. The model that we will study in this chapter has been designed to mimic a real reactor core. We have taken as reference a common Pressure Water Reactor (PWR) geometry. With the intent of reducing as much as possible the spatial mesh discretization keeping unchanged the original structure and dimensions, we have simplified and homogenized it where needed. We have studied the model adopting all the variance reduction methods available: the single-step exponential transform, the AMS and the Two-step method. Furthermore, in order to emulate the effect of an increasing quantity of fissile material, we have performed tests on the same reactor model considering different start-up configurations, with different degree of reactor filling. We will present the problem, discuss the main results and then we will draw the conclusions.

8.1 The model

The model used in the following study will not be displayed and no specific detail will be provided. Because of confidentiality reasons, we will just discuss the main characteristics by providing a general description. The reactor, as mentioned earlier, can be identified as a PWR. It consists of a water core surrounded by several shielding layers made of stainless steel, lead and further water. It contains 3 in-core equally spaced detectors and a given number of fuel assemblies arranged according to a square pattern. Each assembly is made of several fuel rods coated by a cladding layer.

For the purpose of producing importance maps with IDT, we have defined the model on a conformal 2D Cartesian mesh. In order to represent the circular shielding layers surroundings the reactor on the spatial grid, we have "voxelized" the model into rectangular voxels using an algorithm

written in Python language. Furthermore, with the purpose of limiting the level of detail of the model, we homogenised the fuel rods content. The same "voxelized" geometry has been used in Monte Carlo simulations in order to avoid geometrical discrepancies between the importance map and the effective reactor model. This expedient is used to refrain from introducing new degrees of freedom in the simulation and creating local effects. As already done in toy-models, we have used the hypothesis of infinite height geometry, therefore reflection conditions have been applied to the top and bottom boundaries. As for the remaining boundaries, leakage conditions have been used. The neutron source is defined as a Watt spectrum emitter and it is located near the bottom-left corner in between the fuel rods. Its intensity is equal to the arbitrary value $1 \cdot 10^{21}$ $\left[\frac{\text{neutrons}}{s}\right]$. In order to better appreciate the performances of variance reduction methods, we have selected as reference detector for the flux measurements the one placed in the opposite corner w.r.t. the source (top-right corner).

In order to be more realistic, the model reactor has been designed so as to be critical when all assemblies are inserted. By means of Monte Carlo criticality calculations, the concentration of absorber nuclides has been calibrated till reaching a k_{eff} equal to 1 with an error smaller that 300 pcm. Once designed, considering different degrees of filling of the reactor, 4 different configuration have been selected. Case G1 refers to the reactor containing just the fissile assembly holding the neutron source centred with it (bottom-left corner of the reactor). The other cases are constructed adding progressively fuel assemblies following a "snail path" along the square pattern. Case G2, G3 and G4 contains respectively 3, 8 and 15 assemblies. As for toy-models tests, the objectives of the simulations is calculating the multiplication factor K and the neutron flux at the selected detector. The study will follow the scheme presented in Section 5.1.2.

8.1.1 Importance map calculation

The importance map has been produced using a more sophisticated and complete approach with respect to the one used in the toy-model tests. Doing this we wanted to emulate what is currently done in advanced core calculations. The importance map has been calculated making use of a fine (tight) spatial mesh (about 250×250 cells) and of a 26-groups energy discretization. In this regard, the calculation of an external library containing the cross sections condensed on such energy discretization is needed. Making use of a simplified 2D model and of the self-shielding formalism, we have pre-computed an approximation of the flux shape. With this, it has been possible to condense the cross sections of the media involved in the model from 281 to 26 groups. A further distinction has been done between the fissile material placed in the outermost region of the reactor core and the one placed at the inside. Such expedient is generally needed since, fuel rods subject to different fluxes will present different condensed cross sections.

Model	Cases	Fast Flux			Thermal Flux			Total Flux - Figure of Metit comparison				
		Mean	PRSD [%]	Q	Mean	PRSD [%]	Q	Mean	PRSD [%]	time[s]	FOM	FOM GAIN
G1	REFERENCE MC	8.773E+14	3.91E+00	-	1.929E+15	5.50E+00	-	3.337E+15	5.76E+01	75255	4.000E-09	-
	AMS INIPOND	8.708E+14	5.49E-01	0.19	1.947E+15	4.24E-01	0.17	3.187E+15	2.11E+01	5447	4.132E-07	103.310
	AMS GEOM	9.061E+14	2.27E+00	0.72	1.973E+15	1.62E+00	0.40	1.990E+15	2.71E+01	8944	1.519E-07	37.980
	AMS IDT	8.870E+14	5.12E-01	0.28	1.980E+15	4.28E-01	0.47	3.055E+15	6.75E+00	7139	3.078E-06	769.449
	ET INIPOND	3.799E+14	4.50E-01	14.49	8.498E+14	3.78E-01	10.16	-	-	-	-	-
	ET IDT	3.913E+14	1.55E+00	13.96	8.824E+14	1.79E+00	9.75	-	-	-	-	-
	TWO-STEP	8.687E+14	2.27E-01	0.25	1.949E+15	1.87E-01	0.19	2.781E+15	1.69E+00	1858	1.895E-04	47368.033
G2	REFERENCE MC	1.955E+15	3.32E+00	-	4.803E+15	4.29E+00	-	1.040E+16	6.06E+01	4051	6.731E-08	-
	AMS INIPOND	1.909E+15	9.55E-01	0.69	4.331E+15	7.05E-01	2.26	6.738E+15	7.64E+00	16717	1.024E-06	15.213
	AMS GEOM	1.942E+15	1.42E+00	0.20	4.362E+15	9.93E-01	2.09	5.726E+15	1.68E+01	16347	2.168E-07	3.221
	AMS IDT	1.913E+15	8.84E-01	0.64	4.344E+15	6.61E-01	2.21	6.007E+15	4.45E+00	16600	3.041E-06	45.175
	ET INIPOND	4.016E+14	6.56E-01	23.91	9.039E+14	5.68E-01	18.90	-	-	-	-	-
	ET IDT	1.354E+15	4.98E+00	6.43	3.232E+15	4.62E+00	6.17	-	-	-	-	-
	TWO-STEP	1.882E+15	7.91E-02	1.13	4.290E+15	6.71E-02	2.48	6.157E+15	2.24E+00	2151	9.264E-05	1376.305
G3	REFERENCE MC	1.779E+16	1.20E+00	-	4.293E+16	1.51E+00	-	5.465E+16	3.11E+01	22480	4.608E-08	-
	AMS INIPOND	1.765E+16	6.71E-01	0.57	4.293E+16	3.34E-01	0.01	6.189E+16	6.61E+00	10043	2.282E-06	49.520
	AMS GEOM	1.790E+16	1.31E+00	0.34	4.356E+16	6.63E-01	0.89	7.364E+16	4.95E+01	4990	8.171E-08	1.773
	AMS IDT	1.766E+16	8.30E-01	0.52	4.318E+16	4.83E-01	0.38	6.238E+16	8.34E+00	17714	8.108E-07	17.596
	ET INIPOND	5.551E+14	1.36E+00	80.84	1.293E+15	1.65E+00	64.16	-	-	-	-	-
	ET IDT	1.665E+16	2.36E+00	2.56	4.104E+16	2.15E+00	1.73	5.967E+16	2.50E+01	87092	1.831E-08	0.397
	TWO-STEP	1.686E+16	2.18E-01	4.32	4.138E+16	1.89E-01	2.37	5.860E+16	1.58E+00	2947	1.362E-04	2956.501
G4	REFERENCE MC	2.887E+17	5.17E-01	-	8.382E+17	6.09E-01	-	1.185E+18	1.64E+01	14810	2.516E-07	-
	AMS INIPOND	2.808E+17	7.16E-01	3.17	8.113E+17	4.32E-01	4.36	1.124E+18	2.98E+00	44449	2.535E-06	10.075
	AMS GEOM	2.876E+17	3.36E-01	0.63	8.326E+17	1.74E-01	1.06	1.127E+18	6.50E+00	8600	7.871E-06	31.283
	AMS IDT	2.896E+17	7.83E-01	0.33	8.373E+17	4.97E-01	0.15	1.006E+18	3.98E+00	4491	1.409E-05	56.000
	ET INIPOND	2.028E+15	6.06E+00	191.53	5.812E+15	6.69E+00	162.59	-	-	-	-	-
	ET IDT	2.895E+17	1.05E+00	0.23	8.336E+17	1.04E+00	0.47	1.138E+18	1.44E+01	64091	7.541E-08	0.300
	TWO-STEP	2.832E+17	2.20E-01	3.38	8.203E+17	1.85E-01	3.37	1.097E+18	1.17E+00	4170	1.751E-04	696.052

Table 8.1 Reactor-like model - Neutron Flux and Figure of Merit comparison

Model	Cases	K STEP	PRSD [%]	Q	time [s]	FOM	FOM GAIN
G1	REFERENCE MC	1.196E+00	7.62E-02	-	75255	2.291E-03	-
	AMS INIPOND	1.219E+00	1.51E+00	1.26	5447	8.038E-05	0.0351
	AMS GEOM	1.197E+00	1.06E+00	0.12	8944	9.891E-05	0.0432
	AMS IDT	1.188E+00	1.27E+00	0.50	7139	8.739E-05	0.0381
	ET INIPOND	2.415E-02	4.81E+01	100.43	-	-	-
	ET IDT	3.216E+00	2.55E+01	2.46	-	-	-
G2	REFERENCE MC	2.109E+00	1.16E-01	-	4051	1.828E-02	-
	AMS INIPOND	2.085E+00	9.62E-01	1.21	16717	6.461E-05	0.0035
	AMS GEOM	2.067E+00	8.47E-01	2.38	16347	8.531E-05	0.0047
	AMS IDT	2.103E+00	8.43E-01	0.34	16600	8.479E-05	0.0046
	ET INIPOND	3.182E-02	5.93E+01	109.18	-	-	-
	ET IDT	4.841E+00	3.31E+00	17.07	-	-	-
G3	REFERENCE MC	4.975E+00	2.69E-01	-	22480	6.143E-04	-
	AMS INIPOND	5.068E+00	2.07E+00	0.88	10043	2.328E-05	0.0379
	AMS GEOM	4.788E+00	2.39E+00	1.62	4990	3.500E-05	0.0570
	AMS IDT	4.970E+00	1.45E+00	0.08	17714	2.675E-05	0.0436
	ET INIPOND	4.823E-01	2.16E+01	42.70	-	-	-
	ET IDT	9.655E+00	1.83E+00	26.41	-	-	-
G4	REFERENCE MC	9.171E+00	6.04E-01	-	14810	1.850E-04	-
	AMS INIPOND	9.186E+00	1.75E+00	0.09	44449	7.373E-06	0.0398
	AMS GEOM	8.939E+00	3.84E+00	0.67	8600	7.871E-06	0.0425
	AMS IDT	7.870E+00	3.73E+00	4.35	4491	1.598E-05	0.0864
	ET INIPOND	3.959E-01	2.16E+01	86.01	-	-	-
	ET IDT	1.288E+01	9.65E-01	27.24	-	-	-

Table 8.2 Reactor-like model - K STEP comparison

8.2 Results

The four configurations of the reactor-like model have been studied following the same approach already used in the previous chapters. The results are presented in Tables 8.1 and 8.2.

8.3 Comments

At first glance, the tests results behave similarly as the ones seen for the toy-models simulations. The neutron flux calculations carried out with the AMS and the Two-step method provide FOM GAIN values larger than 1, so good performances. On the other hand, the single-step exponential transform seems to be not effective since the parameter Q is larger than 3 in most of the simulations.

The AMS has provided correct estimates in all different tests except for case G4 with the INIPOND importance map in which a small bias is present. On average, the use of IDT importance maps has given a beneficial effect to the performance of the AMS simulations. Moreover, we can notice that the AMS performances are significantly higher in case G1 w.r.t. the other ones. This result is reasonable since, adding fissile material, the number of tracks branches, so the effective number of individuals to be split at each iteration increases, and so does the computational cost of the simulation [15]. We should consider that the time that AMS takes to simulate a particle batch, does not always scales with the dimensions of the batch itself. In the presence of multiplying media the number of individuals (branches of the tracks) to be re-sampled changes along the simulation. In particular, this is expected to increase iteration after iteration, since the fissile material is progressively explored by the particles.

Looking at the single-step exponential transform results, it can be seen that quite all estimate present biases. The only exceptions are the simulations performed on cases G3 and G4 with the IDT importance maps, which have provided proper results but with poor performances.

Figure 8.1 shows the convergence behaviours of the relative standard deviation of the flux estimates in the four cases. The trend of G1 and G2 are characterized by two unwanted behaviours: the first one presents large variance oscillations and the second is non-decreasing. Moving from case G2 to G4, so at increasing quantity of fissile material, the convergence progressively becomes more regular. Such behaviour could seems counter-intuitive since fissions, that are a source of randomness, provide a beneficial effect to the convergence. Recalling what we have seen in the previous chapters in the toy-models tests, the single-step exponential transform is not always able to properly describe the fission source. Particularly for those cases where fissile material is located near the source, we have seen that the fission particles sampling could be highly irregular. The resulting behaviour is dual: most of the particle sampled from source are driven directly the detector and the few that remain in the assembly give rise to excessively high numbers of fission events. In this respect, the addition of fissile material, concerning cases G3 and G4, is supposed to smooth out such irregularities between particle histories, and so inducing a more regular convergence behaviour. This is in agreement with the results of Table 8.1.

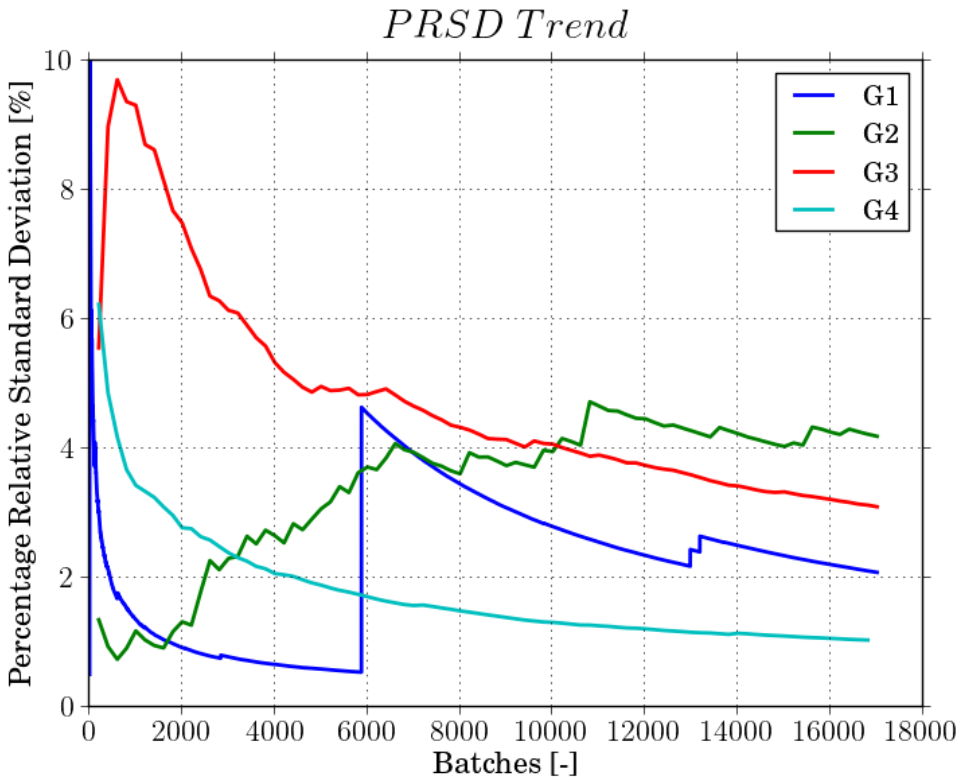

Fig. 8.1 Reactor-like model - ET IDT - Flux estimate - PRSD convergence trend comparison

Concerning the test with the Two-step method, as expected, they have shown high performances and large FOM values. However, we can notice that flux estimates performed for cases G3 and G4 present some mild biases. These mismatches between the reference results and the one obtained with the biasing method are probably due to the errors committed in the fission sources calculation. We can image that the larger is the amount of fissile material in the reactor core, the larger will be the contribution to the score of fission neutrons w.r.t. the ones emitted by the physical source. In particular, considering the geometry of cases G3 and G4, the major contribution to the flux is provided by the neutrons sampled in the assemblies having the highest importance, so the ones closest to the detector. Because of the strategy used in the first-step calculation (Monte Carlo with implicit capture), these assemblies (top-right corner) are also the ones subject to the highest error in the fission source estimate. As a result, the error produced in the fission source calculation is transmitted to the flux estimate, so producing a bias. In conclusion, we must pay attention when estimating the fission source since it is common to incur into this type of problems.

As regards the K-STEP estimates (Table 8.2), we can see that exponential transform is not able to provide proper results. As already observed in the previous tests, this symptomatic behaviour is related to the irregularity of the fission sampling. For what concern AMS, the K estimates have provided correct results except for case G4 with IDT importance map. The performances of this

estimates are really poor anyway. In agreement with what we have already seen, none of the variance reduction methods used is able to provide a K-STEP estimate with performances comparable to the one of a standard Monte Carlo simulation.

8.4 Conclusions on reactor-like model

In the present tests we were able to confirm most of the deductions and observations made in the previous chapters. Once again we observed the robustness of the AMS method. It produced correct results in all cases except for one simulation with the INIPOND importance map. We have seen how the use of importance maps produced with IDT leads, on average, to better performances. We suggest a further investigation of the AMS application in fixed-source calculation, particularly in models rich of localized absorbers and with high multiplication factors. As for the test with the single-step exponential transform, we obtained biased results and low performances. Observing the trends of the PRSD along the simulations, it has been possible to notice how an increasing quantity of fissile material within the reactor core leads to better convergence trends.

We appreciated once again the very high performances of the Two-step method. Furthermore, we have stressed the necessary of calculating the fission source with a sufficiently high accuracy in order to avoid of running into biases. If this is not possible, we should assume a reasonably high relative error in the flux estimate, at least comparable to the one of the fission source. It may be useful to test the possibility of applying other approaches to the calculation of the fission source (first-step), different from the standard Monte Carlo simulation, such as deterministic or Monte Carlo with variance reduction methods.

Chapter 9

Conclusions and perspectives

In this work we explored the application of variance reduction methods on fixed-source Monte Carlo calculations in the presence of fissile material. Three different techniques have been tested:

- The "single-step" exponential transform with the importance sampling;
- The Adaptive Multilevel Splitting (AMS) method;
- The Two-step approach.

Each of these method make use of an importance function, often referred to as "importance map". Different strategies have been adopted in its calculation. We used:

- The IDT deterministic solver with the Consistent Adjoint-Driven Importance Sampling (CADIS) technique;
- The INIPOND automated module implemented on TRIPOLI-4;
- Geometrical importance maps produced by the AMS solver.

Furthermore, the same methods have been used to study the possibility of calculating multiple responses simultaneously by means of the Forward-Weighted Consistent Adjoint-Driven Importance Sampling (FW-CADIS) technique. The tests have been performed on simple toy-models capable of emulating the physics of the reactor in a start-up configuration, and on a more realistic and representative case.

We have seen that the single-step exponential transform is not effective in this type of problems. If the fissile assembly is located relatively close to the source, the importance maps shows a strong "dual behaviour", where particles emitted by the source should either go to the detector or produce fissions in the fissile region. In such cases the exponential transform simulations showed an irregular sampling of fission events, hence large variance fluctuations during its convergence. These oscillations in the flux estimate led in the best cases to performances worse than the one of the reference Monte Carlo

simulations and, in the worst cases, to neutron flux estimates with evident biases. The fission sampling in exponential transform simulations appears to be much more regular in cases having fissile material placed far from the source. This behaviour can be attributed to an incapacity of the method to sample particle histories that faithfully obey to the importance map. It might be interesting to perform further studies focused on this problem.

The AMS method, on the other hand, has shown to be extremely robust. It has provided correct results and good performances in all the test cases. We have seen that the use of IDT maps, rather than INIPOND and geometric maps, is able to greatly increase the performance of the method. A further investigation of AMS in highly multiplicative mediums is anyway suggested.

The Two-step technique is the most effective method in accelerating the performances but also the most expensive for the user. This is because, before propagating particles to the detector using exponential transform, it is necessary to calculate the fission source separately with another simulation. In order to speed up the use of the Two-step method and to remove the approximation involved, in the past years a mode called Multiple Mode has been designed. This mode was present in older versions of TRIPOLI-4. Multiple mode consists of a single stage calculation where the two steps are performed successively for each particle batch. For each batch, the fission source is first calculated in an analog simulation storing the position of the fission reactions. Then, fission points are used in order to define the source of the second step (solved using exponential transform). Remark that fission points are represented with their exact position in the phase-space, therefore, there is no approximation in the representation of the fission source. At present, the Multiple mode can use only mono-kinetic importance maps. This could be limiting since the user is not able to take advantage of external importance maps produced with IDT. Multiple mode could potentially be the most efficient method to accelerate Monte Carlo fixed-source criticality problems.

Regarding simultaneous flux estimates on multiple detectors we appreciated the efficiency of using importance maps produced according to the FW-CADIS method. With this type of maps we have obtained better results both for Two-step method and AMS.

References

[1] E. BRUN, F. DAMIAN, C. DIOP, et al., "TRIPOLI-4®, CEA, EDF and AREVA reference Monte Carlo code", *Annals of Nuclear Energy* **82** (2015), pp. 151 –160.

[2] D SCHNEIDER, F. DOLCI, F. GABRIEL, et al., "APOLLO3 ® : CEA/DEN DETERMINISTIC MULTI-PURPOSE CODE FOR REACTOR PHYSICS ANALYSIS", in: *PHYSOR 2016, at Sun Valley, Idaho (USA)*, 2016.

[3] J. J. DUDERSTADT and L. J. HAMILTON, Nuclear Reactor Analysis, New York : John Wiley and Sons, 1976.

[4] G. I. BELL and S. GLASSTONE, Nuclear Reactor Theory, New York : Van Nostrand Reinhold Co., 1970.

[5] K. M. CASE and P. F. ZWEIFEL, Linear transport theory, Reading, Mass. : Addison-Wesley Pub. Co., 1967.

[6] NUCLEAR ENERGY AGENCY (NEA), Joint Evaluated Fission and Fusion (JEFF) Nuclear Data Library, 2016, URL: https://www.oecd-nea.org/ndata/jeff/.

[7] A. HAGHIGHAT and J. C. WAGNER, "Monte Carlo variance reduction with deterministic importance functions", *Progress in Nuclear Energy* **42**.1 (2003), pp. 25 –53.

[8] I. LUX and L. KOBLINGER, Monte Carlo particle transport methods: neutron and photon calculations, Boca Raton : CRC Press, 1991.

[9] R. SANCHEZ and N. J. MCCORMICK, "A Review of Neutron Transport Approximations", *Nuclear Science and Engineering* **80**.4 (1982), pp. 481–535.

[10] L. MAO and I. ZMIJAREVIC, "A new Tone's method in APOLLO3® and its application to fast and thermal reactor calculations", *Nuclear Engineering and Technology* **49**.6 (2017), pp. 1269 –1286.

[11] I. ZMIJAREVIC, "Résolution de l'equation de transport par des méthodes nodales et des caractéristiques dans les domaines à deux et trois dimensions", PhD thesis, Université de Provence Aix-Marseille I, 1998.

[12] J. SPANIER and E. M. GELBARD, Monte Carlo Principles and Neutron Transport Problems, Reading, Mass. : Addison-Wesley Pub. Co., 1969.

[13] B. MORILLON, Non-analogue Monte Carlo method, application to neutron simulation, Note (CEA-N–2805), CEA/Saclay (France), 1996.

[14] C. M. DIOP, O. PETIT, E. DUMONTEIL, et al., "Tripoli-4: A 3D continuous-energy Monte Carlo transport code", in: *First International Conference on Phisics and Technology of Reactors and Applications (PHYTRA1), at Marrakech (Marocco)*, 2007.

[15] L. HENRI, "Development of an Adaptive Variance Reduction technique for Monte Carlo particle transport", PhD thesis, Université Paris-Saclay, 2017.

[16] M. NOWAK, D. MANCUSI, D. SCIANNANDRONE, et al., "Accelerating Monte Carlo Shielding Calculations in TRIPOLI-4 with a Deterministic Adjoint Flux", *Nuclear Science and Engineering* (2019), pp. 1–16.

[17] J. E. HOOGENBOOM, "Zero-Variance Monte Carlo Schemes Revisited", *Nuclear Science and Engineering* **160**.1 (2008), pp. 1–22.

[18] J. C. WAGNER and A. HAGHIGHAT, "Automated Variance Reduction of Monte Carlo Shielding Calculations Using the Discrete Ordinates Adjoint Function", *Nuclear Science and Engineering* **128**.2 (1998), pp. 186–208.

[19] A. HAGHIGHAT, Monte Carlo Methods for Particle Transport, Boca Raton : CRC Press, 2014.

[20] J. WAGNER, E. BLAKEMAN, and D. PEPLOW, "Forward-Weighted CADIS Method for Global Variance Reduction", *Transactions of the American Nuclear Society* **97** (2007), pp. 630–633.

[21] D. PEPLOW, "Comparison of hybrid methods for global variance reduction in shielding calculations", *Transactions of the American Nuclear Society* **107** (2012), pp. 512–515.

[22] J. WAGNER, D. E. PEPLOW, and S. W. MOSHER, "FW-CADIS Method for Global and Regional Variance Reduction of Monte Carlo Radiation Transport Calculations", *Nuclear Science and Engineering* **176**.1 (2014), pp. 37–57.

[23] F. CÉROU and A. GUYADER, "Adaptive Multilevel Splitting for Rare Event Analysis", *Stochastic Analysis and Applications* **25**.2 (2007), pp. 417–443.

[24] C.-E. BRÉHIER, G. MAXIME, L. GOUDENÈGE, et al., "Unbiasedness of some generalized Adaptive Multilevel Splitting algorithms", *The Annals of Applied Probability* **26**.5 (2016), pp. 3559–3601.

[25] H. LOUVIN, E. DUMONTEIL, T. LELIÈVRE, et al., "Adaptive Multilevel Splitting for Monte Carlo particle transport", *EPJ Nuclear Sciences and Technologies* **3**.29 (2017), pp. 1–10.

[26] K. KOBAYASHI, N. SUGIMURA, and Y. NAGAYA, "3D radiation transport benchmark problems and results for simple geometries with void region", *Progress in Nuclear Energy* **39**.2 (2001), pp. 119 –144.

[27] M. COSTE-DELCLAUX, C. JOUANNE, F. MOREAU, et al., "GALILÉE-1: a validation and processing system for ENDF-6 and GND evaluations", in: *EPJ Web of Conferences, Proceedings of the 4th International Workshop On Nuclear Data Evaluation for Reactor Applications (WONDER-2015), at Aix-en-Provence (France)*, **111**, 2016.

[28] J. BOTH, J. NIMAL, and T. VERGNAUD, "Automated importance generation and biasing techniques for Monte Carlo shielding techniques by the TRIPOLI-3 code", *Progress in Nuclear Energy* **24**.1 (1990), pp. 273 –281.

[29] E. BRUN, F. DAMIAN, E. DUMONTEIL, et al., TRIPOLI-4® Version 8 User Guide, Report (CEA-R–6316), CEA/Saclay (France), 2013.